Doctoral Dissertation
Doctoral Program in Civil and Environmental Engineering
(33rd Cycle)

Self-Healing of Bituminous Binders

A Methodological Framework from Experimental Testing to Advanced Modeling

FABRIZIO MIGLIETTA

Supervisor
Prof. Orazio Baglieri

Co-Supervisor
Prof. Lucia Tsantilis

Politecnico di Torino
2021

This dissertation is presented in partial fulfillment of the requirements for Ph.D. degree in the Graduate School of Politecnico di Torino (ScuDo). I hereby declare that the contents and organization of this dissertation constitute my own original work and does not compromise in any way the rights of third parties, including those relating to the security of personal data.

Fabrizio Miglietta

Torino, June 30th, 2021

ABSTRACT

Self-healing of microcracks has been recognized to play an important role in the overall behavior of bituminous binders. It has been widely observed that the microdamage restoration happening in the field leads to an increase in the lifespan of bituminous pavements. However, self-healing is still debated, and the overall phenomenon requires a more comprehensive understanding. In fact, the evaluation of self-healing of bituminous binders still lacks a universal testing protocol. Several approaches have been proposed by the scientific community, which stems from different ways of studying and modeling the phenomenon. In this background, the present dissertation arises from the comparison of three diverse methods to quantify healing of neat and polymer-modified bituminous binders. Based on the results, the research was furtherly developed by adopting a single testing protocol which included two oscillatory shear loading intervals separated by a single rest period. The methodological approach was focused on the effect of rest time and rest temperature with the purpose of providing simple and effective tools to predict the healing response of the binders. The analysis involved a quantitative assessment of self-healing based on the magnitude of stiffness and fatigue endurance gain, in which biasing time-dependent artefacts were properly quantified and removed. Obtained results were found to be consistent with the kinetics of self-healing phenomena and underscored the importance of multiple testing conditions for a reliable evaluation of true self-healing properties. This is mostly important when the performances of different binders need to be compared. In fact, a single parameter cannot be capable of conveying a reliable ranking between materials, since it is found to be valid only for the specific conditions adopted during testing. Therefore, a new model relying on the generalized logistic function was proposed to describe the self-healing performance of bituminous binders. However, it must be underlined that a comprehensive approach needs to include the evaluation of the overall fatigue performance, not only exclusively based on the relative assessment of self-healing. Advanced modeling also included the application of non-linear viscoelastic constitutive theory which was successfully implemented on the self-healing phenomenon. This allowed the construction of self-healing master curves in the reduced rest time domain which proved the applicability of rest time-rest temperature superposition principle. Such self-healing master curves were found to properly predict the self-healing potentials of bituminous materials.

LIST OF CONTENTS

NOTATION LIST

Acronyms and Abbreviations

BYE	Binder Yield Energy
CAM	Christensen-Anderson-Marasteanu
DCC	Damage Characteristic Curve
DER	Dissipated Energy Ratio
DMR	Dynamic Modulus Ratio
DSR	Dynamic Shear Rheometer
DSR-ER	DSR-based Elastic Recovery
FRF_S	Fatigue-Rest-Fatigue with a Single Rest
FRF_M	Fatigue-Rest-Fatigue with a Multiple Rests
LAS	Linear Amplitude Sweep
LAS-FRF_S	Linear Amplitude Sweep-based Fatigue-Rest-Fatigue (Single Rest)
LVE	Linear Viscoelastic (Viscoelasticity)
NLVE	Non-Linear Viscoelastic (Viscoelasticity)
PP	Parallel Plates Geometry
RSS	Repeated Strain Sweep
t-TS	Time-Temperature Superposition
T-f	Temperature-Frequency
TS	Time Sweep
TS-FRF_S	Time Sweep-based Fatigue-Rest-Fatigue (Single Rest)
TS-FRF_M	Time Sweep-based Fatigue-Rest-Fatigue (Multiple Rests)
$T_{iso\text{-}stiff}$	Iso-Stiffness Temperature
SBS	Styrene-Butadiene-Styrene
SHRP	Strategic Highway Research Program
S-VECD	Simplified-Viscoelastic Continuum Damage
VECD	Viscoelastic Continuum Damage
WLF	William-Landel-Ferry

Main Symbols

a_γ	Non-linear shift factor
a_t	Time-dependent shift factor
a_T	Temperature shift factor

$[A]$	Kernel matrix
A_E	Effectively resisting area
c	Contact points of cracked zone
C	Material integrity
C_1	WLF function parameter
C_2	WLF function parameter
C_{aR}	Material integrity after rest
C_{bR}	Material integrity before rest
C_F	Material integrity immediately before the rest
C_{FRF}	Material integrity immediately after the rest
C_H	Material integrity-based self-healing
C_m	Function of m_h
D_f	Tensile creep compliance
D_h	Compressive creep compliance
e	Exponential function
E_R	Reference modulus
F_t	Surface tension force
F_d	Energy dissipation force
F_g	Gravity force
g	Gravity
$G(t)$	Relaxation modulus
G'	Storage modulus
G''_0	Initial loss modulus
$\|G^*\|$	Norm of complex modulus
$\|G^*\|_0$	Initial norm of complex modulus
$\|G^*\|_g$	Glassy modulus
$\|G^*\|_{LVE}$	Linear viscoelastic norm of complex modulus
$\|G^*\|_{NLVE}$	Non-linear viscoelastic norm of complex modulus
G_i	Prony coefficients
G_R	Reference modulus
h	Gap size
$\dot{h}$	Total healing rate
$\dot{h_1}$	Short-term healing rate
$\dot{h_2}$	Long-term healing rate
h_β	Factor controlling the degree of healing
$h(t)$	Bitumen height within the crack at time t, with respect to the contact point
h_G	Non-linear shift factor
h_p	Distance between the surface and the contact point of cracked area
HI_N	Number of loading cycles-based self-healing index

HI_w	Energy-based self-healing index
H_v	Viscoelastic H-integral
I	Input
I_G	Stiffness-based self-healing index
I_N	Fatigue endurance-based self-healing index
$J(t)$	Creep compliance
J_v	Viscoelastic J-integral
k	Number of element in the Prony series
k_1	Regression coefficient
K_h	Function of m_h
m	CAM model parameter
m_h	Creep compliance in the log scale
M	Torque
n	Number of rest intervals
N_F	Number of loading cycles of first loading in FRF_s test
N_{FRF}	Number of loading cycles of second loading in FRF_s test
N_{RF}	Number of loading cycles of single loading phase in RF_s test
p_1	Material parameter
p_2	Material parameter
p_3	Material parameter
r	Capillary crack radius
r_h	Horizontal direction along the radius
r_m	Function of m_h
R	Response
R_0	Instantaneous healing
R_1	CAM model parameter
R_H	Unit response function
RI_N	Recovery index
RI_S	Damage-based restoration index
R_M	Macroscopic restoration
R_h	Intrinsic healing function
R_{PP}	Radius of the parallel plates
S	Damage parameter
S_{aR}	Damage after rest
S_{bR}	Damage before rest
S_f	Damage parameter to failure
S_F	Cumulated damage measured immediately before rest
S_{FRF}	Cumulated damage measured immediately after rest
S_H	Damage-based self-healing

t	Time
t'_R	Strain-dependent reduced time
t_α	Time of a crack to move of a length α
t_F	Time corresponding to C_F
t_{FRF}	Time corresponding after the rest
t_R	Reduced time
t_{RP}	Rest period
t_{RP_R}	Reduced rest period
T	Temperature
T_F	Temperature of fatigue loading
T_{FH}	Full healing temperature
T_G	Glass transition temperature
T_R	Reference temperature
T_{RP}	Rest period temperature
T_S	Softening point temperature
v_θ	Velocity
w_i	Dissipated energy per unit volume
W^R	Pseudo strain energy
W_r^R	Released pseudo strain energy
W_s^R	Stored pseudo strain energy
W_t^R	Total pseudo strain energy
z	Vertical direction
α	Damage evolution rate
α_1	Regression coefficient
α_2	Regression coefficient
α_3	Regression coefficient
α_4	Regression coefficient
β	Healing zone size
γ	Shear strain
$\dot{\gamma}$	Shear rate
γ_f	Strain amplitude to failure
γ_i	Shear strain amplitude at cycle i
γ_p^R	Peak value of pseudo strain amplitude
$\gamma_{p,NLVE}^R$	Peak value of non-linear pseudo strain amplitude
γ_s	Liquid surface tension
$2\Gamma_f$	Fracture surface energy
$2\Gamma_h$	Healing surface energy
Γ^{LW}	Lifschitz-van der Waals component
Γ^{AB}	Lewis acid-base component

δ	Regression coefficient
δ_C	Regression coefficient
δ_i	Phase angle at cycle i
δ_{LVE}	Linear viscoelastic phase angle
δ_S	Regression coefficient
$\Delta\lvert G^*\rvert$	Damage level
ΔN_i	Endurable number of loading cycles
ΔN_{H_i}	Number of loading cycles ascribable to self-healing
ΔN_T	Number of loading cycles ascribable to thixotropy
Δt	Rest interval between load applications
Δw_F	Dissipated energy due to the first loading phase of FRF_s test
Δw_{FRF}	Dissipated energy due to the rest phase of FRF_s test
Δw_{RF}	Dissipated energy recovered in RF_s test
$\Delta w_{(t=\infty)}$	Asymptotic value of dissipated energy
ε^R	Uniaxial pseudo strain
η	Regression coefficient
η_C	Regression coefficient
η_S	Regression coefficient
θ	Contact angle of the liquid-crack interface
θ_{UP}	Deflection angle
ϑ	Regression coefficient
ϑ_C	Regression coefficient
ϑ_S	Regression coefficient
κ	Regression coefficient
K	Constant of intrinsic healing function
λ	Regression coefficient
ξ	Integration variable of time
π	Archimedes' constant
ρ	Bitumen density
ρ_i	Relaxation time
σ	Uniaxial stress
ς	Additional energy dissipation parameter
τ	Shear stress
τ_i	Shear stress amplitude at cycle i
τ_p	Peak shear stress
$\tau_{p(LVE)}$	Peak shear stress in the undamaged state
υ	Poisson’s ratio
ϕ	Wetting distribution function
φ	Regression coefficient
φ_1	Regression coefficient

φ_2	Regression coefficient
χ	Regression coefficient
ω	Angular frequency
ω_R'	Strain-dependent reduced angular frequency
ω_c	CAM model parameter
ω_k	Angular frequency of k-th element
ω_R	Reduced frequency
Ω	Rotation speed

1. INTRODUCTION

1.1 General Perspective: Fatigue and Crack Healing

Fatigue cracking is one of the major distresses occurring in bituminous pavements. This is mostly caused by repeated vehicular loading, although environmental conditions can contribute to the deterioration process. As the pavement undergoes loading over time, microcracks initiate and later propagate until they finally coalesce into interconnected pieces, which form the so-called alligator-shape cracking. Further deterioration leads to potholes that severely decrease the pavement strength and service life. Among the factors which contribute to the fatigue resistance, such as mixture volumetric characteristics and pavement layer thickness, bituminous binder response is of primary importance. This is motivated by the fact that cohesive microcracks initiate and propagate through the binder phase and/or at the aggregate-binder interface. Thus, the constitutive fatigue behavior of bituminous materials requires to be accurately evaluated for the design of durable pavements.

As luck would it, bituminous materials possess the inherent capability to counteract the damage process and alleviate fatigue cracking. Such a property, referred to as self-healing, contributes toward a prolonged service life of pavements by taking place during recurring rest periods between each axle load application. In fact, the intermittent nature of traffic allows the material to rest, thus promoting the restoration of its functionality to some extent. This is dependent on several intrinsic factors which rely on the bitumen inner characteristics and on different extrinsic factors such as time, temperature, moisture and loading conditions. Therefore, a sound understanding of self-healing phenomenon along with the development of a way to exploit it in service life is certainly needed for the pavement design process.

1.2 Problem Statement

The design of a cost-effective and sustainable flexible pavement requires the behavior of pavement to be understood in different scenarios in terms of loading and environmental conditions. Thus, an accurate evaluation of the material performances is required both with

laboratory testing and in-field testing. This is necessary in order to delay the occurrence of distresses which cause the decay of performances. Among the various distresses affecting bituminous pavements, such as low temperature cracking, rutting and moisture-associated cracking, fatigue cracking is one of the primary modes of failure which needs to be properly addressed in pavement design. However, laboratory setting adopted to test the material is, in a way, different than that on real pavement, thus leading to differences between the laboratory-evaluated fatigue life of bituminous mixture and that of real pavements observed in field. Differences are essentially related to the following factors [1]:

- Difference between calculated versus measured strains;
- Difference between the state of stress in the field and in the laboratory;
- Consideration of the traffic wander area;
- Difference between laboratory-compacted specimens and field compaction;
- Consideration of material healing during rest periods.

For each of these aspects, shift factors are needed to adjust results obtained in the laboratory. The healing effect, which is of interest in this thesis, is responsible for improving the fatigue performance at relatively high temperatures and dominates the laboratory-to-field empirical shift factors in the design process. However, their actual reliability is still unclear and tied to a random choice of a value between 1.5 and 20 [2]. Thus, a more appropriate constitutive model, describing the material behavior, is required to address this problem. However, the complexity of the self-healing physicochemical phenomenon makes it difficult to incorporate this property within a fundamental approach of fatigue cracking. Although several types of intuitive mechanisms have been proposed in the attempt of explaining the process from a theoretical point of view, self-healing characterization of bitumen-based materials still lacks a universal standardized approach.

1.3 Research Objectives and Thesis Outline

The main objective of the present thesis is to provide a sound understanding of the self-healing process through a macroscale characterization at the binder level. The methodological approach relied on three main objectives, related to experimental testing and advanced modeling. The objectives are listed as follows:

I. Comparison between different fatigue-based self-healing protocols;
II. Evaluation of the impact of rest temperature and rest time;
III. Modelling of experimental data by means of a constitutive model.

The structure of this thesis consists of five sections.

Chapter 1 is dedicated to display a general picture of the topic, by introducing the self-healing of pavement materials, occurring as a consequence of deleterious mechanical changes. This section also frames the problem statement and the objectives pursued during the research program.

Chapter 2 is focused on the literature review, thus providing an overview on self-healing of bituminous binders. The major mechanisms describing the self-healing are presented, specifically related to the theories of molecular interdiffusion, surface energy, and capillarity flow. Focus is then placed on screening the factors which influence the healing phenomenon, by differentiating the intrinsic and extrinsic factors. Chapter 2 ends up by presenting the macroscale approaches proposed in the literature to evaluate self-healing on bitumen-based materials at binder level.

Chapter 3 reaches the core of the research program by providing information on the selected materials and the equipment used for testing. This section also provides detailed information on the testing methods adopted during the whole investigation, from the preliminary characterization performed on the binders to the testing approaches adopted to assess self-healing of materials.

Chapter 4 is dedicated to the analysis and interpretation of obtained results. Outcomes are presented based on the three objectives listed above, and in-deep explanations for each of them are provided. Specific models developed during this research program are presented by explaining all the analytical steps followed to calibrate such models to raw data obtained with the testing phase.

The last section concludes this dissertation by summarizing the main conclusions and by suggesting final recommendations for further studies.

2. LITERATURE REVIEW

Preamble

Self-healing of bitumen-based materials is a built-in property related to microstructural rebuilding process, which has been investigated since 1960s. The existence of this phenomenon has been supported by different multi-scale characterization methods and several theories proposed to explain the process. Nevertheless, all the research studies share the cornerstone that self-healing remains a complex, not-fully understood mechanism. This chapter is dedicated to present the most relevant findings, by placing the focus on bituminous binders, which are the materials under study of this thesis. The chapter is basically divided into four sections. In the first section, self-healing of bituminous binders is introduced and discriminated from other biasing phenomena, possibly superimposed to self-healing and fatigue cracking process. The second section presents possible types of mechanism developed to describe the process, based on the concepts of molecular diffusion, surface energy, and capillarity flow. The third section outlines the dependence of self-healing on intrinsic and extrinsic influencing factors. The last section is related to the macroscale methods proposed by the scientific community to characterize the self-healing response of bituminous binders.

2.1 Self-Healing in Bituminous Materials

Several materials such as polymers, ceramics, and metals, possess the capability to heal themselves towards their original state, after being subjected to deleterious structural changes. Among them, bituminous binders are inherently prone to self-repair structural changes in the form of nano/microcracks, which grow and accumulate over time due to repeated vehicular loading and environmental conditions [3]. This holds the promise of designing sustainable pavements because it can considerably decrease maintenance costs, extend lifetimes, and eventually reduce gas emission.

Self-healing in bitumen-based material was first witnessed in 1967 by Bazin and Saunier [4], who observed the beneficial effects of rest periods on damaged specimen of bituminous mixture. They reported that the material healing ability was more pronounced at relatively

high temperatures, although they also noticed this capability to be influenced by other factors. From then on, the self-healing has been a challenging topic interestingly discussed by researcher all over the world.

Although the restoration of material properties is regularly witnessed during rest periods, the driving mechanisms are somehow unclear because self-healing is a complex physico-chemical process made up with different phases untangled to each other. Several attempts have been done to describe the whole phenomenon, but the lack of a clear definition of healing is still required, and consequently a universal evaluation protocol, both at binder and mixture scale. A consensus is that self-healing acts to repair the microcracks, thus bringing to the restoration of material initial properties. However, it is worth underlining that it has no effect with respect to open cracks unless there exist external forces able to promote the closing of macrocrack [5]. For the sake of clarity, it is underlined that, in this thesis, microcracks formation and propagation, leading to detrimental structural changes, refers to as damage. Such damage is the consequence of defects in the binder matrix [6], that trigger microcrack initiation and consequent propagation, when the material undergoes the so-called fatigue loading characterized by cyclic mechanical loading. Microcracks can grow cohesively in the binder medium (cohesive cracking) or occur at the binder-aggregate interface (adhesive cracking) [7]. Thus, the healing process which comes down to the binder medium, must be also considered within the mixture.

Manifold experimental studies have underlined that the fatigue life of bituminous mixture is extended when rest periods are introduced between successive loading pulses [8,9]. It is believed that this is mostly due to the healing process occurring during these rest periods, thus empirical shift factors are needed to adjust the laboratory-evaluated fatigue life when compared to that measured in field [10]. This helps the mechanistic pavement design procedures to account for healing, although a clear consensus is not achieved in the scientific community about this.

2.1.1 Healing versus Viscoelastic Response

It is recalled that self-healing of bituminous binders refers to the intrinsic capability which leads to the restoration of original properties, by diminishing the micro-damage accumulated within the material [3]. However, biasing effects come into play during both the damaging process and the consequent restoration, due to the time/temperature-dependent nature of bitumen [7]. These undesired reversible effects lead to the loss and restoration of mechanical properties being overestimated, as pictured in Figure 2.1.

In fact, the bitumen viscoelastic response can similarly lead to increment of mechanical properties, thus making it difficult to discriminate healing-related restoration from other time-dependent phenomena. This is specifically true in viscoelastic materials, in which the variable of time is extremely important because the relationship between stress and strain depends on time. For this reason, they are also called time-dependent materials. Viscoelastic behavior, upon sufficiently rapid stress input, is depicted through an initial elastic response followed by a continuous increasing strain at decreasing rate. Whenever the input is interrupted, the response is characterized by an instantaneous elastic recovery followed by a continuous decreasing strain over time [11]. This is due to the molecular chains' rearrangement within the bituminous matrix, which includes the linear and non-linear viscoelastic responses (hereafter denoted as LVE and NLVE, respectively). The former comprises the elastic response and the viscous dissipated energy, whether the latter includes also other phenomena such as non-linearity and thixotropy [12].

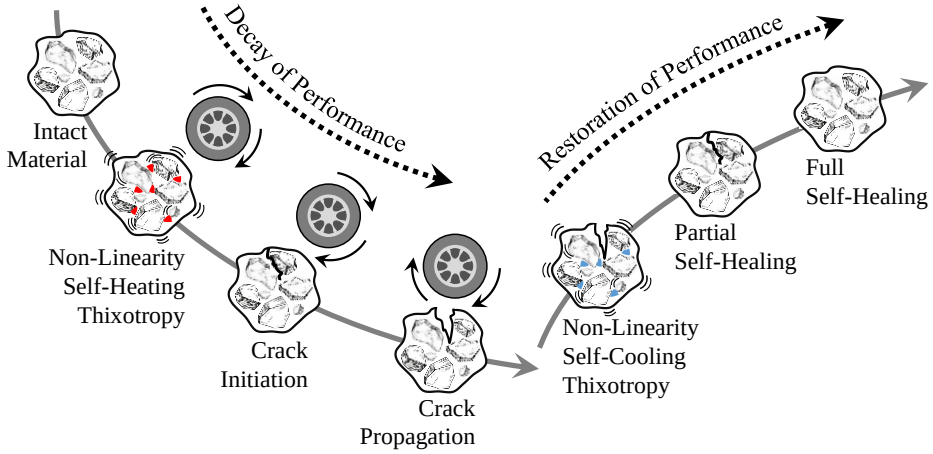

Figure 2.1 – Pictorial representation of factors occurring in the damage-restoration phenomenon [7].

When referring to cyclic loading imposed over time to the material, changes in its mechanical characteristics are mostly the result of non-reversible components ascribed to the initiation and propagation of fatigue microcracks, which eventually leads to failure by coalescing to macrocracks. However, part of the performance decay is imputed to parasitic effects such as local self-heating, non-linearity and thixotropy [13]. Self-heating is associated to the viscous dissipated energy which determines an increase in the internal temperature of the fatigued material, thus consequently causing a reduction in stiffness [14,15]. Non-linearity occurs if the load amplitude is high enough to determine a deviation of the behavior from the linear viscoelasticity, and it generally vanishes when the stress or strain amplitude tends to zero [16]. However, it must be underlined that even though the strain amplitude imposed

to the overall mixture is low, the strains generated within the interspaces among aggregates can be significantly higher, thus involving non-linear effects [7].

Whether the material is left idle after deleterious microstructural changes, local cooling, thixotropy and self-healing begin to act in favor of the restoration of the original state. The part of restoration associated to reversible parasitic effects has been suggested to be referred as recovery. Instead, the reverse of structural damage is defined as self-healing [7]. Self-healing and thixotropy co-exist during rest periods and loading application phases, although healing is imparted by the viscous nature of material whether detrimental microstructural changes are present, whereas thixotropy is not related to damage [17,18].

Thixotropy is defined as a reversible phenomenon characterized by time-dependent softening, i.e. continuous decrease of viscosity, when the material is subjected to shearing/shaking, followed by the time-dependent recovery of viscosity when the flow is interrupted [19]. In other words, it is related to material microstructural changes, from the disruption of the microstructure when the material is shaken, and subsequent restructuring process due to Brownian motion when the material is at rest [7,20,21]. Interpretation of this phenomenon relies on the sol-gel picture of bitumen, with gel structure formation occurring during rest periods. Thus, when subjecting the material to loading phases, part of the stiffness loss can be ascribed to thixotropy. On the other hand, part of the stiffness gain during the unloading conditions can be imputed to thixotropy as well [13]. However, thixotropic mechanism needs to be differentiated from linear viscoelasticity of creep and relaxation since it occurs only when high levels of inputs, outside the linear viscoelastic domain, are involved [22]. In fact, viscoelastic materials do not necessarily exhibit thixotropic behavior. Such a difference can be understood when subjecting the material to a step-down in shear rate history. Normal viscoelastic bodies would respond with a monotonically decreasing stress upon reaching a plateau value, whereas the most general thixotropic behavior would be depicted by an instantaneous drop in viscosity, followed by a fast relaxation and a subsequent increase in stress [19].

Steric hardening is also associated to the thixotropic nature of the material. In fact, thixotropy and steric hardening are both related to microstructural rearrangement of molecules, although generated by different causes [12]. Steric hardening is defined as a time-dependent behavior occurring in isothermal conditions at intermediate to low temperatures [23]. This phenomenon initially takes place from the ordering process of asphaltenes during the bitumen cooling phase from its melted state [24]. Continuous reorganization of molecules over time during isothermal storage leads to the building up of stronger networks of asphaltenes with a concomitant increase of bitumen stiffness [25]. This increase in binder consistency with time, not ascribable to chemical aging, was firstly observed by Traxler *et al.* [26] who underlined the reversibility of the phenomenon by heat or mechanical work. For such rea-

sons, it is also referred to as reversible aging. In particular, the occurrence of steric hardening, within the region of intermediate temperatures, relies on the formation of secondary bonds among the polar components of the bituminous matrix. These secondary associations arise over time from the mutual interaction between adjacent molecules. In fact, the bitumen molecules, characterized by different degree of polarity, possess regions with both positive and negative charges, which tend to attract oppositely charged regions of molecules nearby. Due to the weakness of the secondary bonds, which can be easily disrupted, the phenomenon is completely reversible [27]. In the case of polymer modified binders, the presence of styrene-butadiene-styrene (SBS) hinders the ordering capability of alkanes and alkyl aromatics, as demonstrated by Collins *et al.* [28]. It can be concluded that the magnitude of steric hardening is bitumen and temperature dependent [29] and it generally affects healing tests by leading to an overestimation of the true material healing property when prolonged rest times are imposed [30].
Some attempts to incorporate these biasing effects within the fatigue-healing context of bituminous binders have been successfully carried out. Santagata *et al.* [30] uncoupled the steric hardening effects from those ascribable to self-healing by subjecting the material to fatigue-based healing test with the insertion of a rest period, coupled with test in which a single loading phase was applied after a prolonged rest. Canestrari *et al.* [31] took into account the thixotropic phenomenon occurring in fatigue-based healing test with multiple rest times. Shan *et al.* [22] proposed the use of thixotropic model correlated with measurements obtained through fatigue and healing tests.

2.2 Theoretical Perspective on Self-Healing

Interpretation and understanding of the self-healing phenomenon require models, capable of describing the process. Due to the analogy between polymeric system and bituminous material, it is instructive to recall the healing definition in polymers. In the case of two fractured surfaces, if there exists the possibility of them to be brought into contact at a temperature above the glass transition, then the crack interface tends to disappear and a consequent increase in the mechanical strength develops until achieving the properties of the virgin material [32,33]. In the context of bituminous binders, three main theoretical mechanisms have been proposed in the literature, based on the concepts of molecular diffusion, surface energy, and capillarity flow. However, although the theory on this topic looks sound, the complexity of the physicochemical process of self-healing is still debated.

2.2.1 The Molecular Interdiffusion Concept

In the context of polymeric systems, explanation of the self-healing mechanism has arisen from the molecular interdiffusion theory proposed by Wool and O'Connor [34]. Crack healing is described as a subsequential multi-stage process, triggered by initial surface rearrangement, which leads to approach of micro-crack surfaces, followed by wetting and completed by diffusion and randomization processes. These stages are schematically presented in Figure 2.2. The whole mechanism is intended to lead to the strength restoration of the material by re-establishing secondary associations among microstructural components, and subsequent formation of mechanical bridges at the crack interface by Rouse diffusion or by reptation [18,35,36]. The first two stages of the process are related to the rearrangement and approach of crack surfaces, respectively. In particular, the first stage, which includes inward migration, relaxation, and chains' chemical reactions, generally reduces the strength achievable through cohesive bonds due to inhomogeneity at the crack surface [37,38]. The second stage refers to the approach of surfaces which firstly leads to partial mechanical bonds, occurring due to molecular flow [39]. This process is facilitated in polymeric system characterized by lower viscosity, whereas in high viscosity systems the interpenetration of the cracked surfaces and the concomitant uniform contact are hindered [40].

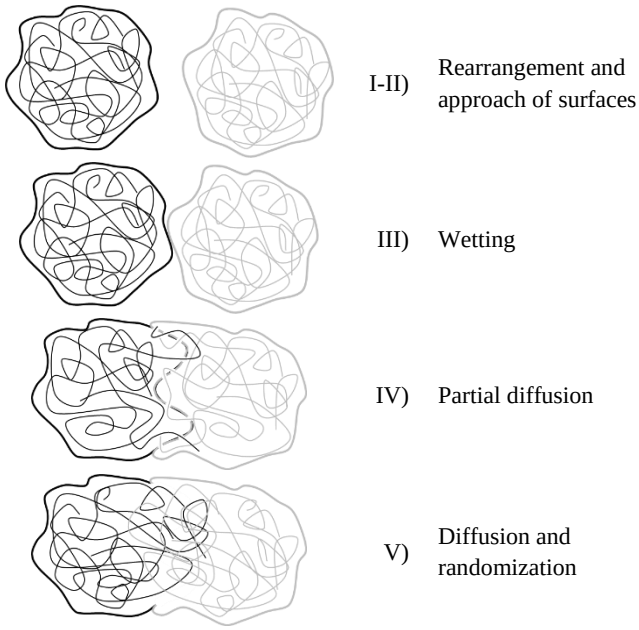

Figure 2.2 – Schematic representation of crack healing via a multi-stage process made up with: (I-II) rearrangement and approach, (III) wetting, (IV) diffusion and (V) randomization [34].

The third stage is related to wetting of crack interfaces, which represents the preparatory step towards the diffusion of molecular chains across the crack once the intimate contact between the microcrack faces is achieved. This is promoted by the absence of inhomogeneities which potentially represent barriers in achieving cohesive strengths [33]. The final stages of diffusion and randomization lead to the pristine molecular configuration through entanglement and interpenetration of molecular minor chains with random Gaussian conformations. This mechanism was defined by Kim and Wool [38,39] in their minor chain model, presented in Figure 2.3, based on the reptation model proposed by De Gennes [35,41]. Such a model basically pictures a random molecular chain confined in a tube-like region, representing the constrains imparted by other chains in the bulk. The chain progressively untangles itself from the initial tube (minor chains), finally diffusing among the obstacles and across the interface towards new conformations.

It is concluded that the diffusion stage is responsible of the restoration of mechanical properties during healing, whereas the randomization stage leads to complete loss of memory of the crack interface.

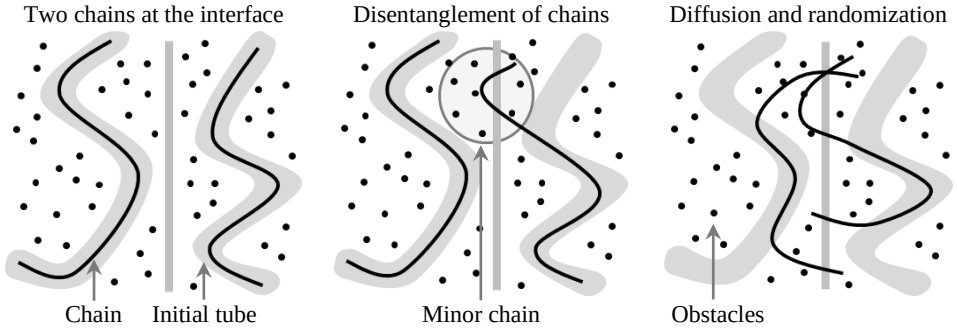

Figure 2.3 – From left to right, schematic representation of two chains in their initial conformations nearby the interface towards their conformation due to diffusion and randomization phenomena [39].

The macroscopic restoration, R_M, was proposed in the form of a convolution integral, in which an intrinsic healing function, $R_h(t)$, for wetting and diffusion, and a wetting distribution function, $\phi(\tau)$, were defined as indicated in Eq. (1) [34].

$$R_M = \int_{-\infty}^{t} R_h(t-\xi)\frac{d\phi(\xi)}{d\xi}d\xi \qquad \text{(Eq. 1)}$$

$$R_h(t) = R_0 + \mathrm{K}\cdot t^{1/4}\cdot\phi(t) \qquad \text{(Eq. 2)}$$

In which ξ is a variable of time, t is the actual time and K is a constant. Eq. 2 expresses the time dependence of $R_h(t)$, through the summation of the instantaneous healing, R_0, driven by cohesion, and the time-dependent healing due to wetting, $\phi(t)$, and interfacial diffusion.

Based on the multi-stage model for polymeric system, Phillips [42] reduced the multi-stage concept to three steps for fatigue cracking and healing, due to the similarity between bitumen and polymers. Fatigue and healing can be imagined as two competitors acting in pavement during its service life. Fatigue cracking process starts with the crack initiation (first step), which propagates over time due to loading (second step), eventually leading to material failure (third step). The first step is the slowest whereas the last is the fastest. The consequence of this process within the material is the loss of its characteristics, such as modulus and strength. On the other hand, self-healing counteracts the fatigue phenomenon leading to restoration of modulus and strength. Self-healing process, according to Phillips, is triggered by the initial closure of crack (first step), promoted by consolidation of stress and material flow. This is followed by wetting phenomenon (second step), encouraged by thermal actions, which eventually leads to the gain of the pristine material structure after diffusion and randomization of asphaltene molecules (third step). The material flow is thought to be the fastest step compared to the following two steps which are believed to require more time to fully occur. A schematic representation of the model is given in Figure 2.4, which represents a corrected reproduction of the original representation published by Phillips, in which the restoration of strength was inconsistently presented to happen before the modulus gain.

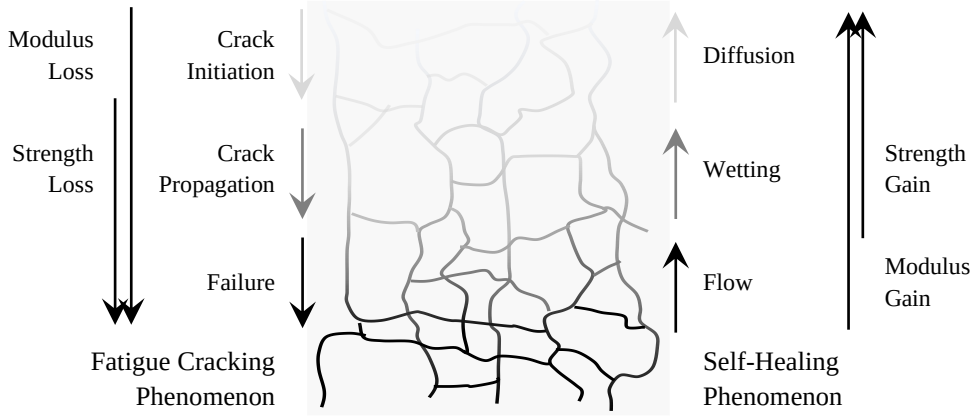

Figure 2.4 – Schematic representation of the three-step model [42].

Based on the findings of Wool and O'Connor, Bhasin and co-workers [43,44] developed a novel testing procedure based on two-pieces sample to determine the intrinsic healing function of Eq. 1. Basically, they assumed that the wetting distribution function can be reduced to the Dirac-delta function by bringing the two pieces of the sample into intimate contact. Thus, the macroscopic restoration is reduced to the intrinsic healing functions, expressed by the Avrami-like equation of Eq. 3:

$$R_h(t) = R_0 + p_1\left(1 - e^{-p_2 t^{p_3}}\right) \quad \text{(Eq. 3)}$$

Where t is the time, R_0 denotes the instantaneous healing due to intimate contact of sample faces and p_1, p_2 and p_3 are material parameters.

2.2.2 The Surface Energy Concept

The surface energy concept takes hold from the fracture mechanics of a viscoelastic body developed by Schapery [45]. The theory provides insights on the mechanical work required for crack growth in the material, namely the fracture energy (Γ_f) introduced as surface energy, $2\Gamma_f$, which is thermodynamically defined as the energy needed to develop a new unit area of surface. Such an energy is counterbalanced by the energy stored in the material for the formation of new additional cracked area [46]. This is expressed in Eq. 4, where E_R is the arbitrary reference modulus, D_f is the tensile creep compliance over the time t_α, and J_v is the J-integral, namely the energy release rate which represents a crack-growth parameter.

$$2\Gamma_f = E_R D_f(t_\alpha) J_v \quad \text{(Eq. 4)}$$

Thus, newly created cracks can occur in those cases in which the work of adhesion is overpassed by the released energy. It follows that low values of $2\Gamma_f$ and high values of D_f accelerate the crack growth rate [47].

The theory was developed for crack growth, but it is also applicable to crack closure due to healing. In fact, a reduction in crack surface energy allows the healing process to be triggered and developed [12]. The healing surface energy ($2\Gamma_h$) derived for a crack zone is reported in Eq. 5, where D_h is the compressive creep compliance over the time t_α, and H_v is the H-integral [48]. Similarly to the microcrack growth, the microcrack healing is promoted by low values of $2\Gamma_h$ and high values of D_h [47]. Moreover, it is worth noting that both Eq. 4 and Eq. 5 refer to viscoelastic materials because pseudo parameters are introduced to isolate viscoelasticity.

$$2\Gamma_h = E_R D_h(t_\alpha) H_v \quad \text{(Eq. 5)}$$

The surface energy approach was applied to the wetting of aggregate-binder systems, offering quantification of adhesive bonding by means of parameters adopted for surface energy derivation [46,49,50]. However, differently from the surface energy and compliance of Eq. 4 and Eq. 5 that are measurable, measuring the adhesive surface energy is not a trivial task. Fowkes [51,52] defined the surface energy for a single phase (either bitumen or aggregate) as the summation of two components, represented by the Lifschitz-van der Waals non-polar component (Γ^{LW}), proven to control the healing rate in the short term ($\dot{h_1}$), and the Lewis

acid-base polar component (Γ^{AB}), impacting on the long-term healing rate ($\dot{h_2}$) [50]. Based on these two components of the surface free energy, the overall healing rate, $\dot{h}$, is determined as expressed in Eq. 6-8 [12,53]:

$$\dot{h} = \dot{h_2} + \frac{\dot{h_1} - \dot{h_2}}{1 + \frac{\dot{h_1} - \dot{h_2}}{h_\beta}\Delta t} \quad \text{(Eq. 6)}$$

$$\dot{h_1} = \beta \left[\frac{K_h E_R D_h H_v}{2\Gamma^{LW}}\right]^{\frac{1}{m_h}} \quad \text{(Eq. 7)}$$

$$\dot{h_2} = \beta \left[\frac{2 r_m {E_R}^2 D_h H_v \Gamma^{AB}}{(1-\upsilon^2) C_m^{1/m_h} H_v}\right] \quad \text{(Eq. 8)}$$

Where:

- Δt is the interval of rest between successive load applications;
- h_β is a factor controlling the degree of healing of material;
- β refers to size of the healing area;
- m_h is the slope of the creep compliance in the logarithm scale;
- K_h, r_m and C_m are functions of m_h;
- υ is the Poisson's ratio.

2.2.3 The Capillarity Flow Concept

The theory described above provides reasonable basis to explain the healing process that occurs in repairing the microcracks. However, when fresh open cracks come into play, the multi-stage and the surface free energy concepts cannot hold, because the visible gap between the crack faces hinders the wetting and diffusion phenomena, due to the lack of fully intimate contact. Despite this consideration, the effect of healing is still observed in those cases in which advantageous conditions exist, in terms of proper rest duration and adequate environmental temperature. In fact, above certain values of temperature, bitumen behaves as a viscous Newtonian fluid [54], being capable of flowing through the crack. Thus, in order to provide explanations to such observations, the capillarity flow theory was introduced by Garcia *et al.* [5], who experimented it by simulating open cracks through a set of capillarity tubes.

The capillarity penetration of a fluid within the interspaces of a medium is generally allowed by spontaneous movements triggered by differences in the interfacial pressure. At some point, this pressure will be counterbalanced by the hydrostatic pressure, due to the

presence of gravity, thus interrupting the capillarity flow [55]. The forces acting on the bitumen within an open crack are combined in Eq. 9, deducted from the Lucas-Washburn equation, and pictured out in Figure 2.5.

$$F_t = F_d - F_g \quad \text{(Eq. 9)}$$

Where the force F_t is exerted by the surface tension, the dissipation force F_d accounts for the energy dissipation, such as that due to friction occurring at the crack faces during the bitumen movement, and F_g is imparted by the gravity. Such forces are made explicit in Eq. 10-12 [56]:

$$F_t = 2\pi r \gamma_s cos\theta \quad \text{(Eq. 10)}$$

$$F_d = 2\pi\varsigma \frac{dh(t)}{dt} \quad \text{(Eq. 11)}$$

$$F_g = \rho g \pi r^2 \left[h_p - h(t)\right] \quad \text{(Eq. 12)}$$

Where:

- r is the radius of the capillary crack;
- γ_s is the liquid surface tension;
- θ is the contact angle of the liquid-crack interface;
- ς is a parameter accounting for additional dissipation of energy;
- t refers to time;
- ρ is the density of bitumen;
- g represents the gravity;
- h_p is the distance between the surface and the contact point of the cracked area;
- $h(t)$ is the height reached by the bitumen within the crack at time t.

Thus, Eq. 9 can be rewritten by substituting Eq. 10-12:

$$2\pi r \left[\gamma_s - \varsigma \frac{dh(t)}{dt}\right] = \rho g \pi r^2 \left[h(t) - h_p\right] \quad \text{(Eq. 13)}$$

By assuming that the speed of the bitumen, during the capillarity movement, is constant, and by considering the analytical solution of Eq. 13, presented in Eq. 14, the area effectively resisting, $A_E(t)$, after the time t of healing is given as [5,56]:

$$h(t) = \left(h_p + \frac{2\gamma_s}{\rho g r}\right)\left(1 - e^{-\frac{\rho g r t}{2\varsigma}}\right) \quad \text{(Eq. 14)}$$

$$A_E(t) = c\frac{\rho g r t}{2\varsigma}\left(h_p + \frac{2\gamma_s}{\rho g r}\right)^2 \int_0^t \left(1 - e^{-\frac{\rho g r t}{2\varsigma}}\right) e^{-\frac{\rho g r t}{2\varsigma}} dt \quad \text{(Eq. 15)}$$

Where *c* is the value of contact points. However, it must be underlined that the validity of such a model is restricted by the assumption that the bituminous binder exhibits near-Newtonian behavior, which is known to occur above certain values of temperature [54].

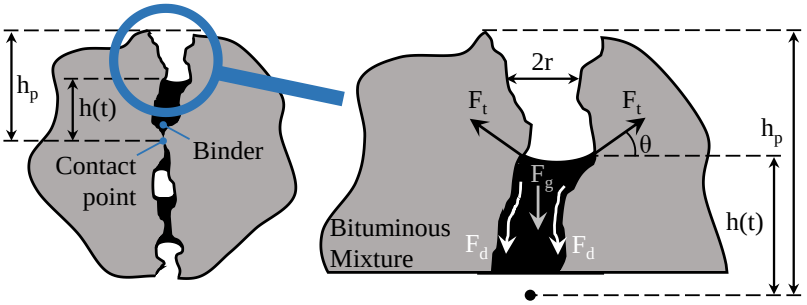

Figure 2.5 – Schematic representation of the capillarity flow during healing phenomenon [56].

2.3 Factors Influencing Self-Healing

The self-healing process is influenced by several factors. At both the micro- and macro-scale level, these factors are represented by the inner characteristics of bitumen which include physical properties, chemical composition, molecular structure, surface free energy, and the presence of modifiers. Although the propensity to self-repair is strongly dictated by the inherent material properties, extrinsic factors come into play by promoting or hindering the healing phenomenon. The main factors of this category are represented by rest time, temperature, moisture, and loading conditions.

2.3.1 Intrinsic Factors

The composition and morphology of bituminous binders play a substantial role in determining the healing aptitude. Several experimental studies demonstrated that bituminous binders characterized by a low viscosity, low softening point, and high penetration grade are more prone to self-repair structural damage. This is due to the fact that the material easily flows through the microcrack channels, thus encouraging wetting and diffusion phenomena to occur [10,57,58]. However, the material properties from a macroscale perspective are in turn dictated by the binder chemical composition. In fact, the presence of low molecular weight compounds with a high aromatic fraction [59,60] promote the healing process because this imparts a lower viscosity with a higher aptitude to interpenetrate the interstices of the microcracks [61,62]. Moreover, the presence of longer chains and fewer branched microstruc-

tures promotes the molecular mobility and consequently the aptitude of the material to diffuse at crack interfaces [63,64]. Correlation between self-healing and surface free energy was demonstrated by Little *et al.* [65] and Lytton [50]. A lower quantity of Lifschitz-van der Waals components is desirable to have good healing response, since they hamper short-term healing. Instead, a higher amount of Lewis acid-base components promotes the healing phenomena prevailing in the long-term.

As the material microstructure determines the intrinsic aptitude to self-heal, the incorporation of chemical agents within the bituminous matrix, used as bitumen modifiers, plays a large part in determining the binder ultimate healing response. However, with specific emphasis placed on Styrene-Butadiene-Styrene (SBS) polymers, the effects of the mutual interactions occurring between the polymeric system and bitumen, in terms of healing performances, remain still unclear and debated. In fact, Qiu [17] underlined that the healing potential of SBS-based systems need to be appropriately evaluated, based on the fact that, from one end, rupture within the polymeric network compromises the healing phenomenon; from the other end, at lower damage level, the elastic recovery of the polymeric network results in a confinement to accelerate the self-healing-related stages. Nevertheless, several studies highlighted the positive contribution of SBS on the healing-related gain [66,67]. When crosslinked polymer network is widespread within the neat bituminous matrix, Shen *et al.* [68] and Sun *et al.* [69] reported enhanced restoration of the polymer-modified binders, via constant stress loading-based healing tests and fluorescence microscope, respectively. Also Santagata *et al.* [70] indicated that the healing potential was enhanced by the presence of the polymer, during fatigue-based healing test with a single rest period. Similarly, Canestrari *et al.* [31] witnessed increasing self-healing capabilities with the increase in SBS content, during oscillatory loading interrupted with the insertion of multiple rest periods. The general explanation of such results relies on the molecular motion promoted by the polymeric long chains which are more likely inclined to rearrangement and diffusion processes [31,68].

The opposite view indicates the negative contribution provided by the SBS to the inner self-healing potential of base bitumen. Lv *et al.* [71] adopted different modifiers, such as SBS, gilsonite, High Density Polyethylen (HDPE) and crumb rubber, underlining that regardless the type of additive, the healing aptitude was more deteriorated the higher the content of the modifier. In agreement with that, Qiu *et al.* [72] observed that the addition of SBS reduced the healing potential of the base binder mastic. Moreover, regardless of the wet or dry conditions of the specimen during the test, the SBS detrimental effect was also underlined by Lv *et al.* [71] via CT-scanned images. Explanation to this outcome relies on the building-up of polymeric networks arising from the incorporation of polymer molecules into base binders. In fact, SBS molecules partially absorb saturates and aromatics bitumen components,

whereas the unaffected presence of asphaltenes leads to increased viscosity [73]. This hinders the material flow, which eventually elicits the reduction of healing ability [74].
An additional factor impacting on the healing capability is related to the aging process of bituminous binders. It was demonstrated that the molecular oxidation phenomenon, progressively increasing over time, inevitably hampers the inherent ability of material to self-repair [75–78]. Exceptions can be found when considering polymer modification in the long-term aging state, as indicated by Canestrari *et al.* [31] who observed overall positive effect to the healing process. This was suggested to be driven by the favorable interaction between the oxidated shorted polymeric chains and the unaged chains of the virgin binder.
The intrinsic factors discussed above are summarized in Table 2.1.

Table 2.1 – Summary of intrinsic factors contributing to self-healing of bituminous binders.

Intrinsic Factor	Propensity to healing
Penetration grade	High value
Softening point	Low value
Viscosity	Low value
Microstructural compounds	Low molecular weight, high aromaticity
Microstructural conformation	Long chains, few branches
Surface energy: Lifschitz-van der Waals component	Low value
Surface energy: Lewis acid-base component	High value
Aging level	Low value
Modifiers	Debated

2.3.2 Extrinsic Factors

The time-dependence of the self-healing process, with specific focus on wetting and molecular interdiffusion phenomena, determines the importance of rest period duration, as first extrinsic factor to be considered [30,34]. In fact, prolonged rest time between successive vehicular loading applications allows the abovementioned phenomena to take place to a greater extent, thus leading to increased magnitude of stiffness and strength restoration [67,79,80]. Moreover, it is implicit that the impact of rest period on the magnitude of restoration depends on its length, and this is believed to contribute to extend the actual fatigue life of pavement structure [57,80–82]. Castro *et al.* [83] suggested that rest period duration of ten times the loading time can be sufficient for a full restoration.
By referring to the temperature, its strong impact on the self-healing performances is essentially due to the temperature dependence of the bitumen viscosity and molecular mobility [54]. At low temperatures corresponding to the glassy region, the self-healing potential dramatically vanishes due to the impossibility of material flow and interdiffusion of mole-

cules to occur at microcrack faces. In this regard, Sun *et al.* [84] witnessed that temperatures lower than -5 °C completely impedes the healing response to take place. With increasing temperature, the concomitant increase in molecular mobility promotes the bitumen flow, thus triggering the process of structural damage repair. Several authors investigated the optimal temperature in re-establishing the pristine binder functionality, arguing that it depends on the bituminous binder viscoelastic response [56,85–87]. Tang *et al.* [87] acknowledged that the optimum healing temperature corresponds to the softening point temperature, that increases with aging of binders. Zhang *et al.* [85] introduced the concept of self-healing threshold temperature based on an index, which gives indication of the bitumen flow behavior. In those cases in which this index reaches value of 0.9 or greater, bituminous binders exhibit near-Newtonian fluid characteristics, thus healing faster the crack. Sun *et al.* [88,89], instead, revealed that the optimal healing temperature ranges between 40.3–48.7 °C, based on the phase transition temperature window of bituminous binders.

Another extrinsic factor affecting the healing response of bitumen is related to the presence of water. Several studies underlined the detrimental effect of moisture which results in decreasing the healing rate and preventing the thermal healing of crack [90,91]. In fact, the presence of water at the interface affects adhesive and cohesive bonds during both the healing phenomenon and the damage process [49]. Moisture damage, indeed, degrades the pavement mechanical properties through a complex phenomenon that involves thermodynamic, chemical, physical and mechanical processes [92]. Mannan *et al.* [93] evaluated the effects of moisture conditioning on bituminous binders via time sweep-based healing test. They found that the instantaneous healing and long-term healing rate were abated due to the decreased cohesion and the increased activation energy required for diffusion process, respectively. In agreement, the findings of Lv *et al.* [94] based on CT-scanned images confirmed the negative effects of water on self-healing phenomenon, especially true for the instantaneous healing. Further studies underlined the affinity between water and Lewis acid-base components of the surface energy, which promotes the long-term healing rate, although the presence of water resulted in reduced resistance to fracture [46].

By referring to the loading levels, researchers are in agreement with the belief that the healing capability decreases as deleterious microstructural changes increase [67,79,95–97]. In fact, when the material undergoes damage, the microcracks propagate and coalesce to macrocracks which hardly self-repair due to the likely insufficient flow to close open cracks [5]. Moreover, it is accepted that self-healing response is dependent on the mode of loading application, either strain-controlled or stress-controlled, and the loading types of laboratory testing which can be intermittent or interrupted. The frequency of loading application also involves diverse healing response, that diminishes as the loading rate increases [75,80,98].

The extrinsic factors discussed above are summarized in Table 2.2.

Table 2.2 – Summary of extrinsic factors contributing to self-healing of bituminous binders.

Extrinsic Factor	Propensity to Healing
Rest period duration	High value
Temperature	High value
Presence of moisture	Low value
Deleterious microstructural change	Low value
Loading frequency	Low value

2.4 Macroscale Characterization of Self-Healing

Within the context of characterization of the self-healing response of bituminous binders, researchers have developed several multi-scale approaches to be performed in the laboratory or in the field. This is motivated by the need of understanding this intrinsic physico-chemical phenomenon, not only at molecular-scale level, but also at the binder level and on the bituminous mixture in the field. However, despite the manifold studies, self-healing of bitumen-based materials still lacks a unified evaluation protocol. A general approach relies on evaluating the healing response of the material in the damaged and undamaged conditions, that is with and without a single or multiple rest periods. At the macroscale level, observation of the healing response is generally carried out on the macroscopic mechanical changes of the bituminous binder and the mixture. Several test types have been proposed in the literature, which can be grouped into three main families recognized as fatigue-based healing tests, fracture-based healing tests, and field-based healing tests.

2.4.1 Fatigue-based Healing Tests

Laboratory simulation of the traffic conditions on the pavement generally involves cyclic sinusoidal or pulse loading. Fatigue-based healing approach arises from revising fatigue loading testing through the inclusion of unloading phases to consider the healing phenomenon. As the name suggests, it basically refers to a type of test in which the material is fatigued until a specific level of damage before imposing the rest time. Fatigue damage can be induced via time sweep (TS) tests, in which repeated sinusoidal loading are applied in constant strain- or stress-controlled mode [99,100]. Similarly to tests of bituminous mixtures, TS test was designated to simulate fatigue damage, captured by observing the material mechanical changes occurring in time. Due to the time consumption involved in TS tests, linear amplitude sweep (LAS) test was proposed as a surrogate, for expeditious characterization of fatigue performances [101]. Such a test is conducted by continuously increasing

the shear strain amplitude, linearly ranging from 0.1 % to 30 % [102]. However, it must be highlighted that such high strain levels involve non-linear effects that are confounded with the pure damage process.

The application of loading can be conducted in two possible modes, referred to as interrupted or intermittent loading condition. With specific emphasis placed on bituminous binders, fatigue-related healing tests are mostly implemented in dynamic shear rheometers.

In the case of interrupted loading condition, two repeated loading phases are applied to the sample, separated by the insertion of a rest period. During the rest interval, the material is left idle under specific conditions of time and temperature, in order the healing-related phenomena to take place. An overview of some experimental studies which involved fatigue-based healing tests in interrupted conditions is given in Table 2.3.

Table 2.3 – Experimental studies on bitumen via interrupted loading-controlled fatigue-related healing tests.

Authors	Temperature	Frequency	Load	Damage	Rest
Santagata et al. [30]	$T_{iso\text{-}stiff}$	10 Hz	250 kPa	50% of $\lvert G^* \rvert_0$	time for DER peak
Wang et al. [59]	20 °C	-	0.1 – 30 %	25, 50, 75, 125 of S_f	1, 5, 15, 30 min
Santagata et al. [67]	20 °C	1.56 Hz	100, 140 kPa	50, 100% of DER peak	3 times the loading time
Tan et al. [80]	25 °C	10 Hz	400 kPa, 6 %	20, 40, 60 % of $\lvert G^* \rvert_0$	1, 6, 12, 24, 48 h
Lu [82]	15 °C	25 Hz	1.6 %	50% of $\lvert G^* \rvert_0$	4, 17 h
Stimilli et al. [81]	$T_{iso\text{-}stiff}$	10 Hz	2, 3, 5 %	35% of $\lvert G^* \rvert_0$	1 h
Zhang et al. [85]	10 °C	10 Hz	1 %	50% of $\lvert G^* \rvert_0$	20 min
Sun et al. [88]	-	-	-	70% of $\lvert G^* \rvert_0$	1, 5, 15, 30, 60, 90 min at 15 – 50 °C
Pang et al. [97]	20 °C	-	400 kPa	40, 60, 80 % of $\lvert G^* \rvert_0$	0.5, 1, 3 h
Bahia et al. [103]	20 °C	1.6 Hz	20 %	After 5000 cycles	0.5, 1, 3, 12 h
Qiu et al. [104]	25 °C	10 Hz	8 %	After 5000 cycles	1 h at 25 – 65 °C

$\lvert G^* \rvert_0$= initial norm of complex modulus; DER = dissipated energy ratio; $T_{iso\text{-}stiff}$ = temperature of iso-stiffness; S_f = damage parameter to failure.

This test configuration was applied by Santagata *et al.* [67] on a neat and two polymer-modified binders. Materials were loaded in stress-controlled mode at two levels equal to

100 kPa and 140 kPa, and at a fixed temperature and frequency of 20 °C and 10 rad/s, respectively. Results were interpreted by means of dissipated energy ratio concept and a healing ratio was introduced to catch the healing responses. Differently, the testing procedure adopted by Stimilli *et al.* [81] consisted of strain-controlled TS performed on two neat and two SBS-modified binders in their virgin and aged states. Iso-stiffness conditions were adopted with the purpose of eliminating the effect of initial stiffness on fatigue response, and fatigue laws were determined by testing the materials at three strain amplitude levels. Results underlined the beneficial effects of multiple rest periods instead of a single rest interval with longer duration. The authors also highlighted that healing insights can be better captured on the fatigue life instead of haling indices. Both, controlled strain and controlled stress modes were adopted to test four neat binders by Tan *et al.* [80]. Three different microstructural damage levels and five rest interval durations were investigated, at a fixed temperature of 25 °C. Interpretation of results was conducted by introducing two healing indicators, based on moduli ratio and cycles numbers ratio, which reasonably reflected the bituminous binder healing performances. A different framework was instead implemented by Wang *et al.* [59], based on linear amplitude sweep test conducted upon reaching predefined damage level before applying rest intervals of several durations, at a temperature of 20 °C. The healing response of three neat bituminous binders and an SBS-modified material was determined by introducing an index, based on the viscoelastic continuum damage theory. Comparison between constructed healing master curves indicated the best healing performance was exhibited by the binder with the highest penetration grade. Lu [82] investigated the binder healing response via strain-controlled fatigue-related healing tests, at a frequency of 25 Hz, and results underlined the application of a single rest interval leads to the restoration of complex modulus which does not directly result in extended fatigue life.

In fact, as introduced in Section 2.1.1, the nature of bitumen can involve other parasitic time-dependent phenomena to occur during the rest interval. These effects, not related to self-healing of structural damage, can lead to the recovery of properties which biases the final restoration response. Thus, discrimination of their effects from those ascribable to true self-healing performance is of primary importance. With respect to loading, applied stress or strain amplitudes generally exceed the linear viscoelastic domain, in order the fatigue damage to accrue over adequate duration of laboratory tests. Thus, non-linear effects need to be properly discriminated from the damage response. Moreover, although the presence of a single prolonged rest period allows detection of the development of self-healing process, it must be underlined that it does not properly reflect the intermittent nature of traffic occurring on real pavement.

In this regard, the intermittent loading conditions are applied to likely simulates the discontinues nature of traffic loading, by means of repetitive pulse-rest cycles. However, it is im-

plicit that different combinations of loading and rest durations yield diverse healing responses. Lu [82] observed that the healing effects of specimens, subjected to repetitive stress-controlled pulse-rest conditions, were significant only in those cases in which the rest period was longer than ten times the loading. The procedure adopted by Shen *et al.* [68] consisted of the insertion of rest periods ranging from 0 to 6 seconds every 10 load pulses applied at a frequency of 10 Hz and at two temperatures equal to 15 and 25 °C. They found that the fatigue life, resulting from the inclusion of a 6 s rest intervals, was extended of 7 and 17 times, for the neat and polymer-modified materials, respectively.
A different approach was implemented by Canestrari *et al.* [31] who modified the TS test by inserting intermittent multiple rest periods of equal duration. Loading phases were performed at a frequency of 10 Hz and a temperature of equal stiffness of materials. The loading was then interrupted upon reaching a predefined level of damage. In order to take into account the material healing response, the fatigue endurance limit was extended by considering the cumulative self-healing contribution, based on the number of endurable loading cycles, during each loading phase, not ascribable to fictious reversible phenomena. Few researches on bituminous binders are reported in literature, involving fatigue-based healing tests in intermittent conditions, listed in Table 2.4.

Table 2.4 – Experimental studies on bitumen via intermittent loading-controlled fatigue-related healing tests.

Authors	Temperature	Frequency	Load	Damage	Rest
Canestrari et al. [31]	$T_{iso\text{-}stiff}$	10 Hz	5 %	35% of G''_0	30 min (multiple)
Shen et al. [68]	15, 25 °C	10 Hz	60 – 230 kPa	1 s	2, 4, 6 s
Lu *et al.* [82]	15 °C	25 Hz	184, 210, 237 kPa	20 s	20, 100 s
Shen and Sutharsan [75]	15, 20, 25, 30 °C	10, 15, 20, 25 Hz	3 %	-	2, 4, 6 s
Bodin et al. [14]	15 °C	25 Hz	1.3 %	500 s	500 s

G''_0 = initial loss modulus.

2.4.2 Fracture-based Healing Tests

In the context of fracture-related healing tests, some attempts have been done to characterize the healing capabilities of bituminous binders subjected to fracture. In a general sense, fracture-healing tests consist of the application of rest times to the material, whose fractured faces are previously brought into contacts. Simulation of the bonding fracture within the

binder, in the configuration happening between two aggregates, was proposed by de La Roche *et al.* [105] with the repeated local fracture test. Such a test was conducted with two lenses of bituminous material, placed in contact between two hemispherical steel protuberances, and subjected to displacement-controlled tension loading. The healing response was studied by spacing the tension stages by rest intervals of different durations, after replacing the initial configuration of the system during which the sample was compressed to its initial geometry [95]. As expected, results suggested dependence of the healing capability on rest time and temperature and indicated a nearly complete healing of the crack triggered with the application of the first loading. Moreover, non-destructive test, involving acoustic waves, was used to detect the crack evolution. Results revealed the formation of bridge-like structures at the crack interfaces occurring when the material was left idle during the rest, which provided agreement with the interpretation based on the force-displacement curves. Maillard *et al.* [106] also combined the local fracture test with non-destructive techniques to investigate the crack size evolution. Appropriate calculation technology relied on viscoelasticity concepts and stiffness evolution in the presence of the crack to provide prediction of the force required in the fracture test at any conditions.

Other researchers simulate the fracture-healing process in the bituminous body by introducing two-pieces healing test [43]. Basically, two disks of bituminous binders were affixed to the measurement system, to the top and bottom parallel-plate of a dynamic shear rheometer. Intimate contact between the 3.5 mm thick pieces was achieved upon reaching the target thickness of 5 mm. Changes in the norm of complex modulus were then recorded by applying a small amplitude shear strain equal to 0.001 % at a fixed temperature and frequency. The crux of the test is that the wetting contribution can be simulated and eliminated though the intimate contact between the faces of the specimens. Thus, the intrinsic healing response can be gathered through observation of mechanical properties of the fractured sample undergoing healing, compared to those of an intact specimen [44,76]. Further investigations with the same testing approach allowed discrimination between the initial healing stage ascribable to the gap closure and the time-dependent healing phase [86]. Insights on the second phase were gathered by monitoring the modulus variation with two different configurations: fixed gap and fixed normal force. It was found that the modulus restoration recorded in the normal force-controlled mode, happened to a greater rate compared to the gap-controlled mode, which underlined the beneficial effect of compressive normal stress.

Although the experimental studies on this topic are not extensive, they have provided enough understandings on the closing process of the crack and on the intermolecular diffusion phenomena. However, some problems can arise due to the irregularities of the fractured interfaces. This leads to discontinuous contact caused by permanent deformations in-

evitably occurring due to the normal forces applied when the two fractured surfaces are brought in contact [12].

2.5 Highlights

Self-healing is a material built-in property, dependent on the inner characteristics of the pristine bitumen, altered by the presence of modifiers, and affected by several extrinsic factors. Due to the difficulty of controlling the chemicals of the binder, the most relevant factors are represented by the rest intervals among successive vehicular loading, the temperature dependence, and the material state undergoing deleterious microstructural changes. Moreover, the characterization methods are recognized to be dominant in the assessment of binder healing mechanism. In fact, although self-healing is a material property, its response is possibly altered by the testing configuration. Thus, difficulties arise when results of mechanical-phenomenological approaches are interpreted, due to the lack of appropriate models. From a macroscale perspective, mechanical tests are grouped into fatigue-healing test using intermittent or interrupted loading mode and fracture-healing test. Results of such approaches are coherent with the kinetics of self-healing process, believed to involve initial contact of crack faces by flow, then cohesion by wetting, and finally diffusion of intermolecular chains. However, it must be underlined that the material restoration observed during the test is a combination of self-healing and other parasitic effects which eventually lead to misrepresented evaluations.

3. MATERIALS AND TEST METHODS

Preamble

The experimental approaches to evaluate the macroscale self-healing response of bituminous binders are generally based on the use of dynamic shear rheometer. Different methods have been proposed in literature, based on fatigue loading tests. However, due to the physicochemical complexity of the phenomenon, conflicting results are generally obtained. This is also due to the dependence of self-healing on several factors, which govern the kinetics of the process. To gather deeper understandings on this topic, three DRS-based rheological tests were performed on neat and SBS-modified bituminous binders. Description of the testing apparatus is given at the beginning of this chapter, and the materials tested during the experimental plan are introduced afterwards. The core of the chapter is represented by the methodology section, which describes the different protocols selected to fulfil the first objective of this thesis. Further discussion is held to present the testing approach that have been followed in the assessment of time and temperature effects on the material self-healing response, as second objective of the thesis. The third objective places the focus on the modeling aspect of data gathered through the abovementioned approach. Detailed discussion and mathematical background of it will be properly given in Chapter 4.

3.1 Testing Equipment

The experimental measurements were collected by means of the rotational rheometer MCR301, from Anton Paar Physic Inc. The DSR is a stress-controlled device equipped with an air bearing-supported synchronous motor, providing torque values in the range 0.01 μNm – 200 mNm with a resolution of 0.1 nNm. A compressed air film supports the motor spindle in order to minimize any vibration, friction and possible heating. Control of the torque is given by the motor, through magnetic forces generated by permanent magnets of high energy, necessary due to the absence of physical contact. Moreover, control of the normal force is enabled by means of deformation of the air-bearing spindle [107]. Shear strains and shear rate are recorded by means of the optical incremental encoder, which

measures the angular rotation with a minimum value of 0.1 μrad and a resolution lower the 0.1 μrad. The measuring cell is equipped with an environmental chamber characterized by a Peltier element, which is needed to control the temperature in order to ensure a constant environment to the sample. A quick-fitting coupling is connected to the air bearing-supported synchronous motor and optical encoder. It allows a fast installation of a variety of measuring systems, whose choice is dictated by the characteristics of the material. Figure 3.1 displays the DRS equipment used in this thesis.

Figure 3.1 – Dynamic shear rheometer MCR 301 from Anton Paar Inc.

Shear stress and shear strain outputs are calculated based on the adopted geometry, as indicated in the following. The parallel-plates (PP) geometry is generally used for higher viscosity materials, in the presence of large particles and for Newtonian fluids. However, some disadvantages can arise due to non-homogeneous flow between the plates, which leads to variation of shear stress and shear strain with the plate radius. Moreover, other drawbacks are linked to inertia and secondary flow, shear heating and edge failure. Inertia and secondary flow are caused by high rate and elasticity, whereas at low shear rates, edge failure occurs by flow of the material from the middle to the surfaces. Shear heating is related, instead, to the increase in temperature due to the viscous dissipation, which results in reduction of viscosity and concomitant reduction of torque. However, it must be underlined that these problems can be minimized by operating at a smaller gap or by introducing appropriate mathematical corrections [108].

In the case of one plate stationary and the other plate rotating at Ω, under the following assumptions:

- Steady, laminar, isothermal flow;

- Negligible inertial forces;
- Absence of flip a the surfaces;
- Cylindrical edges;
- $v_\theta(r,\theta) > 0$ and $v_r = v_z = 0$

The velocity is equal to:

$$v_\theta(r_h, z) = \frac{r\Omega z}{h} \quad \text{(Eq. 16)}$$

Where r_h is the horizontal direction along the radius, z is the vertical direction and h is the gap size, as illustrated in Figure 3.3.

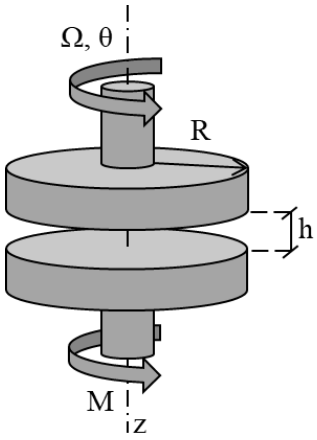

Figure 3.2 – Schematic representation of parallel-plates geometry.

The shear rate, $\dot{\gamma}$, is then equal to:

$$\dot{\gamma}(r) = \frac{r\Omega}{h} \quad \text{(Eq. 17)}$$

Similarly to the shear rate, shear strain is not homogeneous, and is dependent on the radius, going from zero at the sample center to the maximum value at the sample edge, as given in Eq. 18:

$$\gamma = \frac{r\theta_{UP}}{h} \quad \text{(Eq. 18)}$$

Where θ_{UP} is the angle of which the upper plate is twisted, called deflection angle.
As the case of the shear strain, also the shear stress is dependent on the radius and for Newtonian fluid, its variation with the radius is linear. The relationship between the shear stress and the torque is given in Eq. 19, in the integral form:

$$M = 2\pi \int_0^R r\tau_{12}(r) r dr \quad \text{(Eq. 19)}$$

By considering Eq. 17 at the generic value of r and at the edge, R_{PP}, and rearranging for r:

$$r = \frac{\dot{\gamma} h}{\Omega} = \frac{\dot{\gamma} R_{PP}}{\dot{\gamma}_R} \quad \text{(Eq. 20)}$$

By deriving Eq. 20 and substituting in Eq. 19:

$$dr = \frac{R_{PP}}{\dot{\gamma}_R} d\dot{\gamma} \quad \text{(Eq. 21)}$$

$$M = 2\pi \int_0^{\dot{\gamma}_R} \left(\frac{R_{PP}}{\dot{\gamma}_R}\right)^3 \dot{\gamma}^2 \tau_{12} d\dot{\gamma} \quad \text{(Eq. 22)}$$

After rearranging and differentiating by means of Leibnitz's rule:

$$\tau_{12}(R) = \frac{M}{2\pi {R_{PP}}^3}\left[3 + \frac{dlnM}{dln\dot{\gamma}_R}\right] \quad \text{(Eq. 23)}$$

For an unknown fluid, the shear stress is derived from Eq. 23 which takes into account the variation of lnM as a function of the variation of $ln\dot{\gamma}_R$, corresponding to the angular velocity. In the case of Newtonian fluid, the angular velocity is equal to 1, leading to Eq. 24, which is generally adopted by rheometer calculation. The parallel-plates are generally adopted for the measurements of viscoelastic material functions such as modulus and compliance, evaluated at the sample edge. Thus, the calculation of shear strain is the same as Eq. 18, evaluated ad the maximum radius of the plates R_{PP}, as define in Eq. 25.

$$\tau_{12}(R) = \frac{3M}{2\pi {R_{PP}}^3} \quad \text{(Eq. 24)}$$

$$\gamma = \frac{R_{PP}\theta_{UP}}{h} \quad \text{(Eq. 25)}$$

Moreover, loading and unloading operations of soft and viscous materials are easy to be perform.

3.2 Bituminous Materials

Bitumen is classified as viscoelastic polymer, naturally occurring as in the deposit of Pitch Lake or the tar sand of Athabasca, and generally manufactured as refined product from the distillation process of crude oils [25,109]. Commonly used in road construction field, bituminous materials are also adopted to produce waterproofing materials.

The bitumen chemical composition is very complex, and it comprises different types of chemicals. From an elementary perspective, it mostly consists of hydrocarbons up to 90

wt%, coexisting with heterocyclic groups in a lower quantity and heteroatoms such as oxygen, nitrogen, and sulphur [110,111]. However, the bitumen chemical composition and morphology strongly varies with the crude oil source and with the production processes [47,112], thus making it infeasible to link the structure of all the molecules to engineering properties. Rather, the bitumen chemical compounds are commonly distinguished based on their attributes, such as polarity [113–115]. Two broad chemical families can be recognized to form the bituminous matrix, referred to as asphaltenes and maltenes. The latter can be furtherly divided into three other groups, named saturates, aromatics, and resins. Saturates represent a low molecular weight non-polar group in the form of viscous colorless oil, characterized by branch and straight chains, and constituting 5 % to 15 % of the total bitumen. Aromatics, also known as naphthenic aromatics, are manifested as a dark brown viscous compound, forming 30 % to 45 % of the binder, and are characterized by non-polar carbon chains. Resins, also called polar aromatics, are polar dark brown solid, mostly consisting of carbon and hydrogen and, like aromatics, they form 30 % to 45 % of the binder. Asphaltenes are high molecular weight compound, possessing the highest polar nature. They compose the 5 % to 20 % of the bitumen in the form of black/brown amorphous solid, characterized by carbon and hydrogen, along with oxygen, nitrogen, and sulphur [54,110]. From the rheological perspective, asphaltenes govern the bitumen viscosity, imparting elasticity and stiffening effects (together with resins), whereas saturates and aromatics deals with the viscous softer part of bitumen [113,116,117]. When conventional bituminous binders are blended with modifiers, the microstructural picture changes. With specific emphasis placed on synthetic polymers, styrenic block copolymers, such as styrene-butadiene-styrene (SBS), are characterized by three-dimensional cross-linking of molecular chains which is responsible of its elasticity and strength [118]. The interaction between SBS and bitumen leads to swollen rubber-elastic networks, which are the result of absorption process of bitumen oil fractions and are dependent on both, bitumen and polymer nature, as well as their compatibility [73,118,119]. Although it is recognized the SBS modification confers outperformed characteristics to the base binders, in terms of long time behavior, temperature susceptibility and rheological properties [118,120–123], its effect on the self-healing-related capabilities is still debated.

For such a reason, in the case of the experimental investigation carried out in this thesis, four different materials have been considered, including two neat bitumens, and two polymer modified binders. Neat bituminous binders are named as N1 and N2, and belong to the 70/100 and 40/60 penetration grade, respectively; whereas the modified binders, labelled as S1 and S2, are classified as 25/55 and 45/80 penetration grade, respectively.

Preliminary fingerprint of the materials comprised the determination of glass transition temperature (T_G) and softening point temperature (T_S). Identification of T_G required tem-

perature ramp tests performed by means of DSR equipment. Tests were conducted at a frequency of 1 Hz and temperature ranging from 10 °C and -35 °C at a cooling rate of 1 °C/min. Identification of T_G relied on the determination of the peak in the curve of loss modulus [124,125]. T_S was determined by means of an automatic ring and ball system, as per EN 1427. Values of T_G and T_S are listed in Table 3.1 for the four bituminous binders considered in the present investigation.

Table 3.1 – Glass transition temperatures and softening points.

	N1	N2	S1	S2
T_G / °C	-17.8	-27.2	-19.1	-24.9
T_S / °C	45.8	53.6	62.1	52.3

3.2.1 Preliminary Operations

Each material was preliminarily prepared prior to testing by following the procedure described below. Firstly, the binder was annealed to remove any reversible phenomena related to molecular associations occurring over time during isothermal storage. Annealing process was conducted by avoiding heating the material at temperatures above 163 °C and by minimizing the heating time, in order to prevent any thermal hardening effect [126]. Once the material was sufficiently fluid to be homogenized and stirred to remove any air bubbles, it was poured in a beam silicon mold. Such bitumen beams were kept frozen until testing, with the purpose of impeding structure-change processes to occur during storage, due to the continuous reorganization of the molecules.

Before each test, pre-molded specimens were prepared by heating 0.250 g of bitumen, for 5 minutes at a temperature of 130 °C and 150 °C, for neat and polymer modified binders, respectively. The small amount of material was homogenized by stirring action, then left to cool at room temperature for 5 minutes. This process was also required to eliminate possible reversible physical hardening occurring at very low temperature. Afterwards the bitumen was put at -6 °C for other 3 minutes to allow material demolding. The disk was then sandwiched between the two plates, previously preheated at a temperature close to the material T_S to allow proper adhesion at the plate-bitumen interface. Excess of material was then trimmed off at a gap of 2.1 mm between the plates, which was eventually reduced to 2 mm, thus creating a lateral bulge in the sample [126]. All the rheological measurements were conducted by means of an 8-mm parallel-plates geometry with 2-mm gap between 4 °C and 40 °C. The procedure described above is summarized by the pictures of Figure 3.3 which represents the consecutive steps of the material preparation process.

In the case of glass transition tests from 10 °C to -35 °C, the parallel-plates geometry was characterized by 4-mm of diameter with an initial gap equal to 1.75 mm. Due to the cooling process, a progressive reduction of the gap between the plates was always induces by volume changes of the sample. This was done with the purpose of avoiding internal tensile stress possibly occurring due to volume changes.

1. Before oven 2. After oven 3. After freezing 4. Before trim 5. Lateral buldge

Figure 3.3 – Successive steps for sample preparation before testing.

3.2.2 Linear and Non-Linear Viscoelastic Characterization

Preliminary rheological fingerprint of the materials included temperature-frequency (T-f) sweep tests at multiple temperatures to investigate the linear viscoelastic properties. For this purpose, prior to testing, strain amplitudes needed to be properly selected within the linear viscoelastic domain, ranging between 0.05 % and 0.9 % according to the temperature/frequency combination. Temperatures were selected ranging between 4 °C and 34 °C, with 6 °C increment, with angular frequency varying in the range 1 – 100 rad/s.

The non-linear viscoelastic response of the selected binders has been explored by means of repeated strain sweep (RSS) test [127]. The temperature was constant all over the test and multiple testing temperatures were investigated ranging from 4 °C to 34 °C, with 6 °C increment. RSS test consisted of three groups, and each of the group was composed of three blocks. During each block, the strain amplitude was increased with a logarithm ramp from an initial value to a final value. The initial value, common in all the blocks of all the groups, was dictated by the instrumental resolution and set equal to 0.05 %. The final strain value changes from group to group. In the first group, such a value was set equal to 0.5 % in order not to overpass the linear viscoelastic threshold of the material. The linear-non-linear frontier was assumed as the shear strain amplitude corresponding to a 5 % reduction of the initial norm of complex modulus, based on what suggested by the Strategic Highway Research Program (SHRP) [128]. In the second and third group, the highest imposed strain was increased to explore the non-linear domain. The most appropriate values to avoid premature rupture of the sample were found to be equal to 5 % and 7 % for the second and third group, respectively. Exception was made for the test run at the temperature of 4 °C,

which comprised a smaller value of the maximum strain amplitude ranging between 1.8 % and 4 % depending on the materials, due to the high torque value close to instrumental limits. A schematic representation of the strain history is displayed in Figure 3.4 (a) in which for each group, the three blocks are represented. The output of such a test, in terms of norm of complex modulus normalized with respect to the LVE values versus strain, is displayed by way of example in Figure 3.4 (b). By referring to Figure 3.4 (b), it can be observed that the curves of group 1 overlap each other due to the fact that the maximum shear strain was selected to be in the LVE domain. Once the LVE region is overpassed, in group 2, a reduction in modulus is recorded because of the combined effects of non-linearity and damage. Due to the existence of the damage component, the curve of the second block of group 2 starts from a lower value of the normalized norm of complex modulus. Whenever the maximum shear strain of the first block of a specific group is raised for the first time, compared to the previous one, a reduction in modulus is exhibited as a consequence of damage.

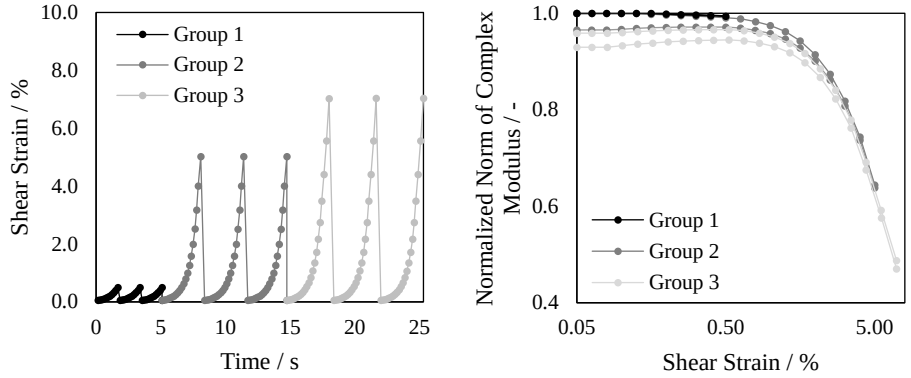

Figure 3.4 – Shear strain versus time (a) and normalized norm of complex modulus versus shear strain (b) from RSS test (binder N1 tested at 10 °C).

3.3 Testing Measurements: I Objective

The macroscale self-healing responses of materials were investigated by means of fatigue-based healing tests. Three protocols have been adopted, named by the acronyms TS-FRF_S, TS-FRF_M, and LAS-FRF_S (see §3.3.1, §3.3.2, §3.3.3). Each acronym is composed of two parts: the first part denotes the type of fatigue loading which can be based either on Time Sweep (TS) or Linear Amplitude Sweep (LAS) tests; the second part refers to the number of rest periods interrupting the fatigue loading, which can be single (S) or multiple (M). The

methods shared common testing conditions such as the loading frequency, simulating the speed of vehicle, which was fixed equal to 10 Hz, and the temperature imposed during the loading phases, hereinafter indicated as T_F. For the accomplishment of the first objective of the experimental program, T_F was fixed to 20 °C and kept constant all over the test. Such a choice of temperature relies upon the belief that diffusion mechanisms dictate the true self-healing restoration, thus the temperature needs to be properly selected to likely trigger the diffusion onset [68]. Thermal equilibrium of the specimen at the T_F was achieved by adopting a conditioning time equal to 30 minutes, for all the test types. During the conditioning phase, a low strain amplitude of 0.1 % was applied to ensure the achievement of steady state conditions through observation of changes in material mechanical properties.

Based on the selected temperatures, preliminary strain amplitude sweep tests have been performed in order to explore the material linear viscoelastic domain. Such a test consisted of a strain sweep in which the strain amplitude is logarithmically increased from 0.01 % to 10 %. A schematic representation of the test is reported in Figure 3.5. In the linear region, the norm of complex modulus is constant due to its independence on the shear strain level, occurring at values of strain amplitude bounded between a lower and an upper limit. While the lower limit depends on the rheometer resolution, the upper threshold dictates the frontier between the linear and non-linear region [129]. The linear viscoelastic region is arbitrarily considered as the region of strains in which the material exhibits values of the norm of complex modulus greater than 95 % of the plateau value [126]. Definition of the frontier of the linear viscoelastic region is of primary importance in the selection of the strain value to be imposed during the oscillatory loading in TS-based tests. In fact, the strain amplitude level needs to be conveniently high to induce significant microdamage within the specimen and to entail adequate duration of laboratory tests.

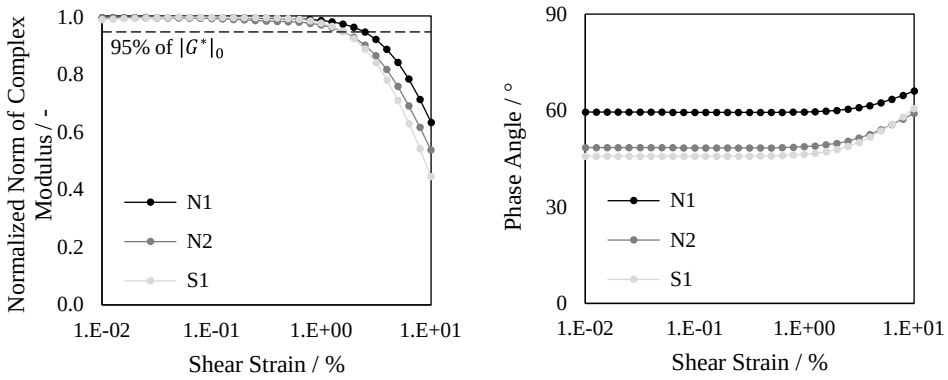

Figure 3.5 – Normalized norm of complex modulus (a) and phase angle (b) versus shear strain.

As displayed in Figure 3.5, it can be noticed that the binders showed roughly similar extensions of the linear viscoelastic domain, with limiting strain values comprised between 1.7 % and 2.5 %. Thus, the most appropriate value was found to be 3 % for the binders at the testing temperature of 20 °C.

3.3.1 TS-based FRF_S Method

The testing method named TS-based FRF_S is based on time sweep (TS) test and consists of two fatigue loading intervals separated by the insertion of a single prolonged rest period (FRF_S) [30]. During the first loading, the material is subjected to cyclic oscillatory loading at a fixed frequency and a constant strain amplitude. The choice of the strain-controlled loading relies upon the need of avoiding temperature effects possibly arising within the specimen due to dissipated energy changes [14]. The first loading was interrupted upon reaching a predefined value of damage, hereinafter termed as $\Delta|G^*|$, evaluated as a reduction of the initial norm of complex modulus ($|G^*|_0$), representative of the material in its undamaged state. Three different damage levels have been considered, equal to 10 %, 35 % and 50 % reduction of $|G^*|_0$, to gather information on the healing response in different material damaged states. Following the first loading, a single rest period of 2 hours was applied, during which changes in mechanical properties were monitored by imposing a low value of strain amplitude equal to 0.1 %. In addition, with the purpose of accounting for time-dependent effects not ascribable to self-healing, the abovementioned TS-FRF_S method was supplemented with test in which a single loading phase elapsed after the rest period (TS-RF_S). The schematic representation of both the test types is shown in Figure 3.6.

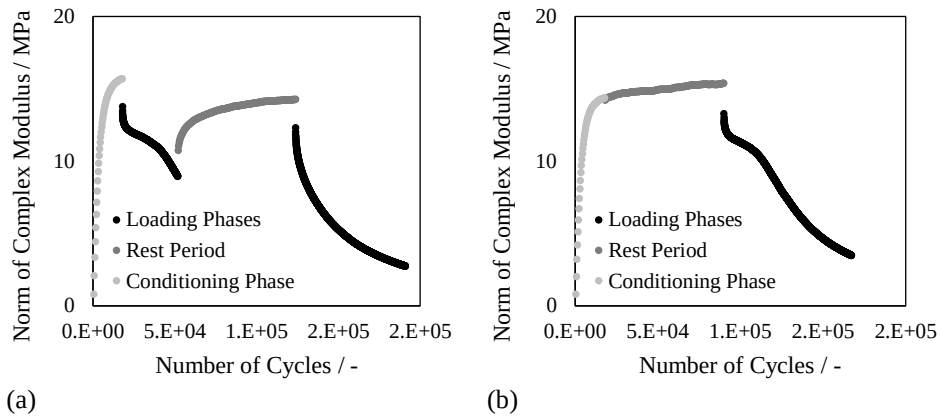

Figure 3.6 - Example of results obtained from TS-FRF_S (a) and TS-RF_S (b) tests (binder S1 tested at 20 °C with a rest period of 2 hours).

3.3.2 TS-based FRF_M Method

The testing approach named TS-based FRF_M is based on time sweep test, but differently from the previous method, it is characterized by multiple fatigue loading phases (FRF_M), which cease upon reaching 35% reduction in the initial loss modulus (G''_0) [31]. During the loading intervals, a constant strain amplitude is applied to the specimen at a fixed loading frequency. Multiple rest periods of duration equal to 30 minutes are inserted between successive loading intervals, and at least 14 load-rest cycles were performed. During the rest intervals, application of a low strain amplitude equal to 0.01 % allows monitoring the material loss modulus. Figure 3.7 reports typical results of the test. It can be observed that as the number of rest intervals increases during the test, the loading cycles endurable in the subsequent loading phase are less than the previous loading. This results in a faster reduction of the loss modulus as the load-rest cycles advance, until a steady state can be reached during which the reduction rate of loss modulus remains constant. This phenomenological observation is the base of the analytical operations (see §4.2.2) implemented to take into account the thixotropy-related effects of the material.

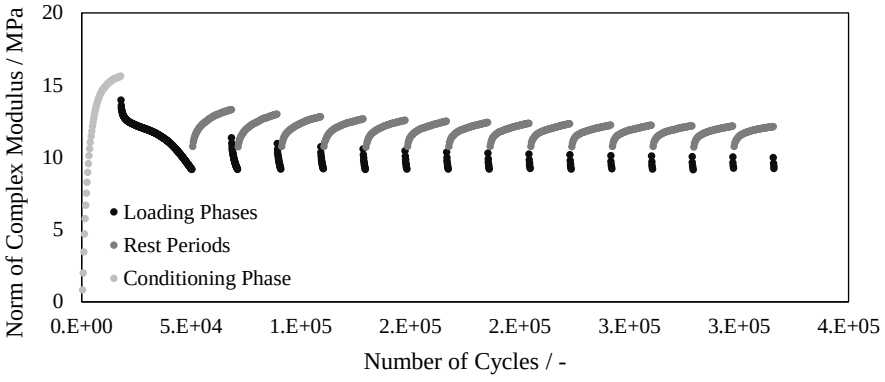

Figure 3.7 – Example of results obtained from TS-FRF_M test (binder S1 tested at 20 °C with rest periods of 30 minutes).

3.3.3 LAS-based FRF_S Method

The LAS-based FRF_S method is based on the linear amplitude sweep test [102]. LAS test consists of oscillatory sweep of strain amplitude values linearly increasing from 0.1 % to 30 % within the course of 5 minutes, at a fixed loading frequency. The test allows identification of the critical damage parameter (S_f) and the corresponding strain amplitude to failure.

LAS-based FRF_S test consists of an interrupted LAS test, in which the oscillatory loading is ceased upon reaching a predefined damage level. In the case of this experimental investigation, the damage level was selected as the strain value corresponding to 50 % of the strain amplitude to failure (γ_f). Subsequent application of a rest interval allows the material to stay idle, thus eventually leading to restoration of its properties. Four different durations of rest time have been imposed to materials, equal to 60, 300, 900, and 1800 seconds. Finally, the second loading interval is resumed from the strain amplitude imposed prior to the rest interval, increasing linearly as the case of continuous LAS test [130]. In addition, frequency sweep tests were required to explore the linear viscoelastic behavior of the undamaged bitumen, by ranging the frequency between 0.1 rad/s to 100 rad/s at the testing temperatures of 5 °C, 20 °C and 35 °C.

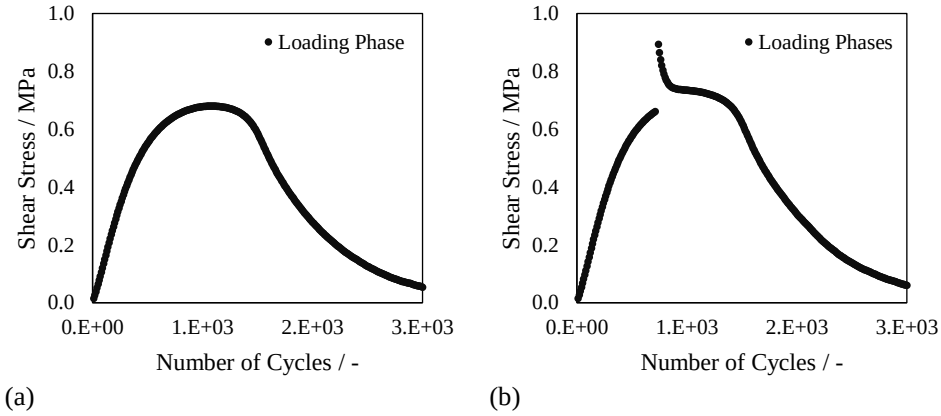

Figure 3.8 – Example of results obtained from LAS (a) and LAS-FRF_S (b) test (binder S1 tested at 20 °C with rest period of 30 minutes).

3.3.4 Remarks on Methods

The test methods adopted in the experimental investigation are classified as fatigue-based healing tests. By comparing the testing characteristics of the three methods, detailed in Table 3.2, some differences and similarities can be underlined:

- All the methods were performed with same values of fixed loading frequency and constant testing temperature;
- Two methods are based on time sweep test (TS-based), which requires the selection of a constant value of oscillatory strain amplitude;
- One method is based on linear amplitude sweep test (LAS-based), which imposes strain amplitudes continuously increasing in a linear way;

- For two methods, application of loading is conducted in interrupted mode, namely with a single rest period (FRF_S);
- One method adopts the loading mode as intermittent, with the insertion of multiple rest intervals (FRF_M);
- TS-FRF_S and TS-FRF_M methods attempt to discriminate time-dependent artefacts from the self-healing response;
- Among the methods, the damage level is evaluated on different variables, namely $|G^*|$ for TS-based FRF_S method, G'' for TS-based FRF_M method, and γ_f for LAS-based FRF_S method.

Table 3.2 – Summary of testing conditions adopted for the considered fatigue-based healing methods.

Method	Material	Temperature	Frequency	Load	Damage	Rest
TS-based FRF_S	N1, N2, S1	20 °C	10 Hz	3 %	0, 10, 35, 50 % of $\|G^*\|_0$	S: 2 h
TS-based FRF_M	N1, N2, S1	20 °C	10 Hz	3 %	35 % of G''	M: 30 min
LAS-based FRF_S	N1, N2, S1	20 °C	10 Hz	0.1 - 30 %	50 % of γ_f	S: 1, 5, 15, 30 min

$|G^*|_0$ = initial norm of complex modulus; G'' = loss modulus; γ_f = strain amplitude to failure; S = single rest; M = multiple rest

3.4 Testing Measurements: II and III Objective

Investigation of the macroscale effects of time and temperature on the self-healing process was conducted by adopting the method TS-based FRF_S. Such a test method was chosen due to the presence of a single rest period which allows observation of the restoration process of materials as a result of varying time and temperature. As detailed in the previous section (§3.3.1), the TS-based FRF_S consists of a prolonged rest interval interposed between two oscillatory loading phases. The first loading interval was interrupted at predefined level of fatigue damage, induced in the specimen based on the reduction of the initial norm of complex modulus. The second loading interval was prolonged until material failure. Thermal equilibrium of the material at the T_F was ensured by imposing 30 minutes of conditioning time at the beginning of the test. Mechanical changes occurring during the rest period interposed between the loading phases were monitored by imposing strain amplitude values within the linear viscoelastic domain. Duration (t_{RP}) and temperature (T_{RP}) values of rest interval, along with the damage level of the first loading phase were chosen such that extent

of the tests were reasonable for laboratory activities. With respect to T_{RP}, two different scenarios can be distinguished:

- First case scenario: T_{RP} equal to T_F;
- Second case scenario: T_{RP} different than T_F.

In the first case scenario, the temperature was kept constant all over the test, whereas three values of rest interval duration were imposed. T_F were gathered from the master curves of the norm of complex modulus in the linear viscoelastic domain, such that equi-stiffness condition of 34 MPa were ensured to all the specimens. Equi-stiffness level was adopted for the sake of avoiding problematic stiffness dependence of damage process. Moreover, such a stiffness value is comprised in the range 10-50 MPa which was proven to be appropriate for triggering the onset of cohesive fatigue microcracks rather than instability flow or adhesion loss. Shear strain amplitude imposed during the loading phases were estimated by means of preliminary strain amplitude sweep tests (see §3.3.1). Output of strain amplitude sweeps are displayed in Figure 3.9. It can be noticed that, when T_F was set to achieve equal stiffness conditions, all the materials showed similar extensions of the linear viscoelastic domain, with limiting strain values comprised between 1.3 % and 1.4 %. Therefore, the most suitable value, required to be in the vicinity of the linear viscoelastic threshold, was found to be equal to 2%.

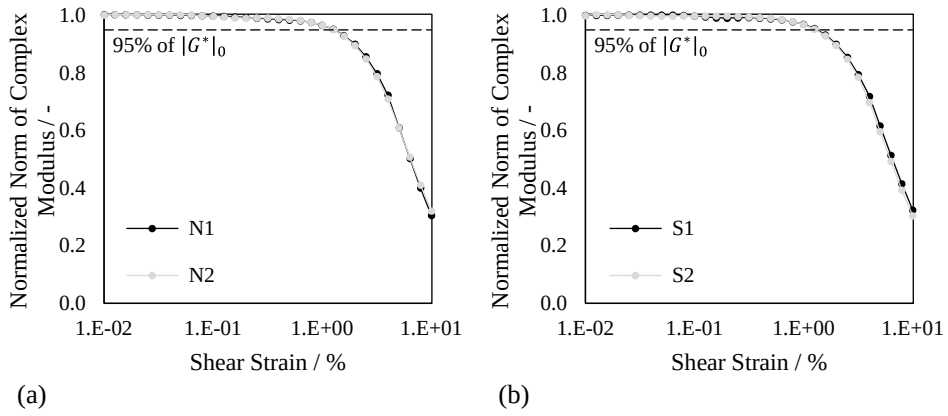

Figure 3.9 – Normalized norm of complex modulus versus shear strain for neat binders (a) and polymer-modified binders (b).

In the second case scenario, T_{RP} values were increased without exceeding the material softening point. This required the last 30 minutes of rest to be conducted at T_F in order to re-establish stable thermal conditions in the specimen before resuming the loading.

Discrimination of time-dependent artefacts not ascribable to self-healing was accomplished by supplementing the TS-based FRF_S testing procedure with tests characterized by a single

loading phase preceded by a prolonged rest period (TS-based RF_S). Since RF_S tests lacks the first loading phase, materials in this testing configuration are meant to have a null damage level (0 %). Summary of the adopted values of damage level, strain amplitude loading, T_F, T_{RP}, and t_{RP} are listed in Table 3.3.

Table 3.3 – Testing conditions imposed in TS-FRF_S and TS-FRF_M tests.

Material	Damage %	Load %	T_F °C	T_{RP} °C	t_{RP} h
N1 and N2	0, 35, 50 of $\|G^*\|_0$	2	10	10	2
			10	10	4
			10	10	6
			10	20	2
			10	30	2
S1	0, 35, 50 of $\|G^*\|_0$	2	14	14	2
			14	14	4
			14	14	6
			14	20	2
			14	30	2
			14	40	2
S2	0, 35, 50 of $\|G^*\|_0$	2	09	09	2
			09	09	4
			09	09	6
			09	20	2
			09	30	2
			09	40	2

A supplementary set of TS-based FRF_S and TS-based RF_S tests was performed by arbitrarily choosing T_{RP} and t_{RP} values, with the purpose of model validation (see §4.3). Testing conditions adopted in these supplementary tests are indicated in Table 3.4.

Table 3.4 – Supplementary testing conditions imposed in TS-based FRF_S and TS-based RF_S tests.

Material	Damage %	Load %	T_F °C	T_{RP} °C	t_{RP} h
N1	0, 35 of $\|G^*\|_0$	2	10	25	2
			10	15	3
N2	0, 35 of $\|G^*\|_0$	2	10	40	2
			10	25	3.5
S1	0, 35 of $\|G^*\|_0$	2	14	40	2
			14	25	3
S2	0, 35 of $\|G^*\|_0$	2	09	40	2
			09	25	3.5

In addition, one binder out of fours has been selected for extra TS-based FRF_S and TS-based RF_S tests, as listed in Table 3.5, for the accomplishment of objective III of the present thesis (see §4.4). For this objective, the reference response to fatigue cracking was also investigated by subjecting all the binders to sinusoidal loading upon failure (without rest periods), hereinafter named TS-based F tests, carried out at the equi-stiffness temperature.

Table 3.5 – Supplementary testing conditions imposed in TS-based FRF_S and TS-based RF_S tests.

Material	Damage %	Load %	T_F °C	T_{RP} °C	t_{RP} h
N1	0, 35, 50 of $\lvert G^* \rvert_0$	2	10	15	2
			10	17.5	2
			10	22.5	2
			10	25	2
			10	27.5	2

3.5 Highlights

Four bituminous binders of different sources have been selected for the experimental investigation. The set of materials included two neat binders and two polymer modified binders. Three of them were tested for the assessment of the macroscale self-healing capabilities by means of three testing protocols implemented in DSR. Specimens were fatigued until preselected levels of damage and left idle afterwards to allow healing-related mechanisms to take place. According to the loading application mode, two methods are conducted under interrupted loading condition, whereas the other testing protocol is performed under intermittent loading mode. By comparing the methods, some similarities and differences can be underscored, and comparison of corresponding results is meant to address the first objective of this thesis. Investigation on the macroscale effects of time and temperature have been addressed by furtherly developing the testing program on one of the three methods, performed on the four binders. Testing conditions included two material damage levels, and multiple values of duration and temperature of the rest interval. This set of experiments accomplished the second objective of the thesis. Analysis of corresponding results within the viscoelastic continuum damage framework (see §4.4) is meant to fulfil the third objective of this experimental study.

4. INTERPRETATION OF RESULTS

Preamble

The macroscale characterization of self-healing responses of bituminous binders is generally conducted by monitoring the mechanical properties when the material undergoes damage, and during rest periods. Based on the material mechanical behavior, specific analytical efforts are implemented on different DRS-based rheological tests. The attempt is generally to construct indices with the purpose of ranking the healing-related performances of materials. Detailed information on the analytical calculations followed by each protocol adopted in this experimental thesis is given in the first section, which is dedicated to the comparison of different fatigue-based healing methods. This is needed to accomplish the first objective of the thesis. The second section places the focus on the effects of time and temperature. In this regard, a new approach is described for the evaluation of time-temperature superposition effects on healing in which spurious thixotropic effects are removed. Further modeling is then devoted to the S-VECD framework, as third objective, by also including in the analysis the effects of non-linearity. Master curves of self-healing are finally constructed to describe the healing stage achieved by each material.

4.1 Linear and Non-Linear Viscoelastic Characterization

Raw data collected from T-f tests are displayed in the black diagrams of Figure 4.1, which represent the norm of complex modulus versus the phase angle. Such a representation allows exploration of data consistency without requiring any manipulation prior to representing the results. A continuous smooth curve denotes a thermo-rheological simple behavior as depicted for the materials in Figure 4.1.

When considering binders N1 and N2, it is interesting to observe that the difference in their penetration grade have non negligible differences in the overall shape of the Black curves, thus indicating that the two materials exhibited a different rheological response in the transition from the glassy to the viscous state. Polymer-modified binders S1 and S2 were found

to be associated to Black curves with a very similar shape, probably as a consequence of the presence of the same type of polymer in the blends.

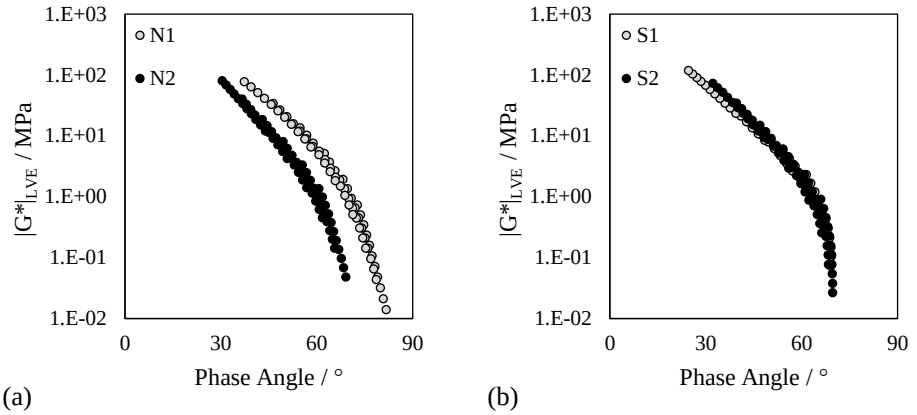

Figure 4.1 – Norm of the complex modulus versus phase angle for neat (a) and polymer-modified (b) binders.

Such raw data were processed by implementing the generalized Maxwell model through a Prony series discretization to analyze the linear viscoelastic response of the materials. The crux of this approach is represented by the possibility to easily interconvert functions from the frequency domain to the time domain. Moreover, the LVE modeling was required for the subsequent analysis within the NLVE region.

In this effort, raw data were firstly shifted to a reference temperature of 10 °C, by means of time-temperature superposition (hereinafter termed as t-TS) principle, which relied on William-Landel-Ferry (WLF) function of Eq. 28 [131]. This entailed the introduction of the reduced angular frequency (ω_R) obtained by multiplying the measured frequency by the shift factor (a_T) (more details are given in section §4.4.1). Master curves were then constructed by fitting the shifted data with Christensen-Anderson-Marasteanu (CAM) model presented in Eq. 26 and Eq. 27. Results are displayed in Figure 4.3 and corresponding parameters listed in Table 4.1.

$$|G^*|_{LVE}(\omega_R) = |G^*|_g \left[1 + \left(\frac{\omega_c}{\omega_R}\right)^{\frac{log2}{R_1}}\right]^{-\frac{mR_1}{log2}} \quad \text{(Eq. 26)}$$

$$\delta_{LVE}\,(\omega_R) = \frac{90 \cdot m}{\left[1 + \left(\frac{\omega_R}{\omega_c}\right)^{\frac{Log2}{R_1}}\right]} \quad \text{(Eq. 27)}$$

$$loga_T = \frac{-C_1(T - T_R)}{C_2 + T + T_R} \quad \text{(Eq. 28)}$$

Where:

- $|G^*|_{LVE}$ and δ_{LVE} are the LVE norm and phase angle of complex modulus;
- ω_R is the reduced frequency;
- $|G^*|_g$ is the glassy modulus;
- ω_c, R_1, and m are CAM model parameters;
- a_T is the time-temperature shift factor,
- T_R is the reference temperature;
- C_1 and C_2 are fitting coefficients.

Table 4.1 – Model parameters of the master curves.

	N1	N2	S1	S2
Log($\|G^*\|_g$)	8.90	9.03	8.60	8.74
Log(ω_c)	3.03	1.84	2.47	3.21
R_1	1.38	1.98	1.29	1.37
m	0.99	1.07	0.88	0.88
C_1	17.6	14.0	13.7	18.4
C_2	155.1	113.8	109.0	155.9

Determination of the Prony series required the definition of Prony coefficients (G_i) which were calculated by means of the collocation method. Eq. 29 provides the definition of the relaxation modulus as a function of time for a Prony series made up with k number of elements:

$$G(t) = \sum_{i=1}^{k} G_i \cdot e^{-t/\rho_i} \quad \text{(Eq. 29)}$$

Where i refers to the i-th element characterized by the stiffness G_i and the relaxation time ρ_i. From a physical perspective, such a representation pertaining to the generalized Maxwell model, assembles k number of Maxwell models in parallel, each composed with two elements of linear spring and linear viscous dashpot, connected in series.
The collocation method is defined in Eq. 30. It requires the adoption of a set of 32 Maxwell elements, by arbitrarily choosing relaxation times ρ_i and angular frequencies ω_k (fixed equal to ρ_i) such that 16 decades of frequency were covered.

$$\{G_i\} = [A]^{-1}\{G'\} \quad \text{(Eq. 30)}$$

$$A_{ik} = \frac{\rho_i^2 \omega_k^2}{1 + \rho_i^2 \omega_k^2} \quad \text{(Eq. 31)}$$

$$\{G'\} = |G^*|(\omega_k) \cdot cos\delta_k \quad \text{(Eq. 32)}$$

The array $\{G_i\}$ represents the unknown Prony coefficients and $[A]$ is the Kernel matrix defined in Eq. 31. $\{G'\}$ is the storage moduli array, calculated by means of Eq. 32, where $|G^*|$ and δ_k are the norm of complex modulus and the phase angle evaluated at the angular frequency ω_k by means of Eq. 26 and Eq. 27, respectively.

After calculating the values of the Prony coefficients, Eq. 29 can be used to evaluate the relaxation modulus in the time domain, whereas Eq. 33 and Eq. 34 can be used to calculate the norm of the linear viscoelastic modulus and the phase angle in the frequency domain.

$$|G^*|_{LVE} = \sqrt{\left(\sum_{i=1}^{m} \frac{\omega_R^2 \rho_i{}^2 G_i}{\omega_R^2 \rho_i^2 + 1}\right)^2 + \left(\sum_{i=1}^{m} \frac{\omega_R \rho_i G_i}{\omega_R^2 \rho_i^2 + 1}\right)^2} \qquad \text{(Eq. 33)}$$

$$\delta_{LVE} = \tan^{-1}\left(\frac{\sum_{i=1}^{m} \frac{\omega_R \rho_i G_i}{\omega_R^2 \rho_i^2 + 1}}{\sum_{i=1}^{m} \frac{\omega_R^2 \rho_i{}^2 G_i}{\omega_R^2 \rho_i^2 + 1}}\right) \qquad \text{(Eq. 34)}$$

Non-linear moduli, $|G^*|_{NLVE}$, were directly obtained by means of RSS tests. The process required the permanent component of damage to be separated from non-linearity. With this purpose the curve of the second block of group 3 (see §3.2.2) was vertically shifted in order to expand the viscoelastic representation beyond the linear region. This was performed by assuming that the component of permanent damage was reversible in the test timescale. This was supported by the fact that possible healing-related mechanisms are hindered due to the absence of rest period between successive blocks. Moreover, additional damage was observed to occur only in those cases in which higher limits of shear strain were explored. This is particularly true when considering the third block of either group 2 or group 3, which showed negligible additional damage compared to the previous block.

Obtained shifted curves of $|G^*|_{NLVE}(T, \omega, \gamma)$ normalized by $|G^*|_{LVE}(T, \omega)$ are presented in Figure 4.2 for binder N1 (a), N2 (b), S1 (c) and S2 (d). It can be observed that the curves initially assume values equal to 1 because the applied shear strains are low enough to be in the LVE domain. As the strain is raised over the upper threshold of the linear domain, the effect of non-linearity is highlighted by the modulus reduction. Moreover, it is worth noting that the curves corresponding to different testing temperatures do not cover the same range of strain amplitudes, because the highest imposed strain level was chosen in order to avoid the breakage of the specimen, depending on both material features and testing conditions.

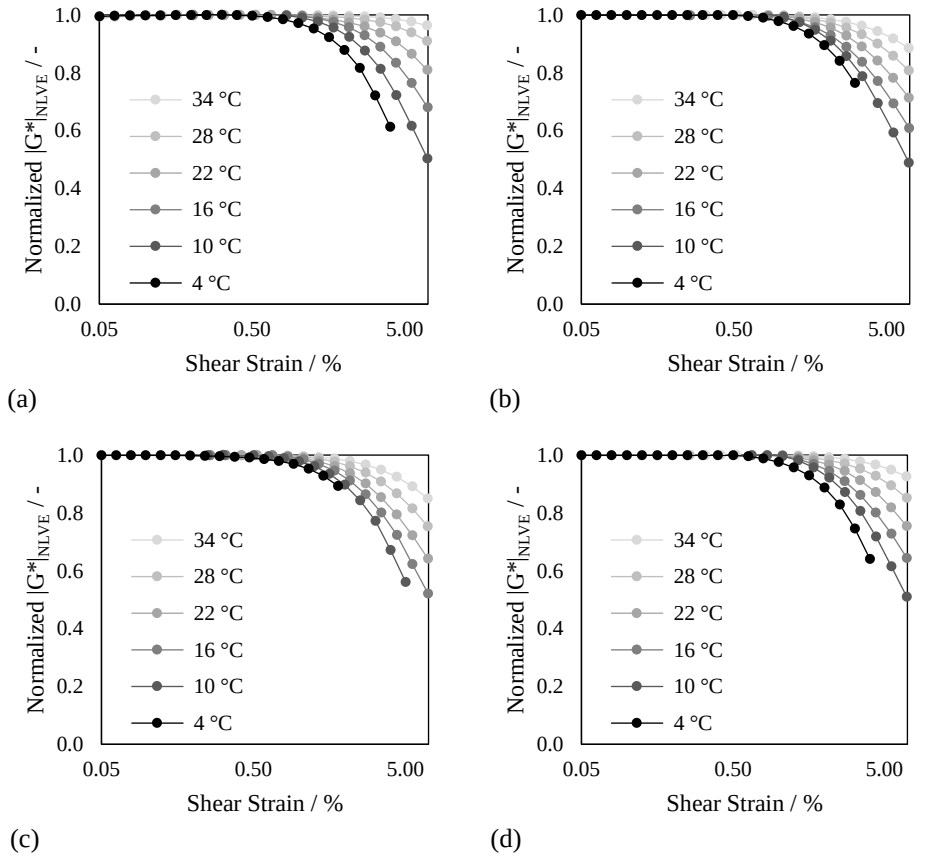

Figure 4.2 – $|G^*|_{NLVE}(T,\omega,\gamma)$ normalized by $|G^*|_{LVE}(T,\omega)$ versus amplitude shear strain.

Master curves of $|G^*|_{NLVE}(T,\omega,\gamma)$ were then constructed at reference strain levels, by shifting experimental data measured in RSS tests at different temperatures. Such a process was conducted by assuming that the time-temperature shift factors are not dependent on shear strains. LVE and NLVE master curves are presented in Figure 4.3 for binder N1 (a), N2 (b), S1 (c) and S2 (d) at preselected strains equal to 0.5 %, 3.5 % and 7.0 %.

Afterwards, the non-linear viscoelastic behavior was modelled by means of an optimization process performed between $|G^*|_{LVE}$ and $|G^*|_{NLVE}$ master curves, such that two non-linear shift factors (a_γ and h_G) were introduced to reduce the linear viscoelastic solution to the non-linear domain. The factor a_γ allows for horizontal shifting of the reduced frequency thus changing the logarithmic slope of the linear viscoelastic master curve. The factor h_G is a vertical shift acting on $|G^*|$. This is mathematically described in Equations 35 and 36:

$$\omega'_R = a_\gamma \omega_R = a_\gamma \omega a_T \quad \text{(Eq. 35)}$$

$$|G^*|_{NLVE}(\omega_R) = \frac{1}{h_G}|G^*|_{LVE}(\omega'_R) \qquad \text{(Eq. 36)}$$

Where ω'_R is the strain-dependent reduced angular frequency and $|G^*|_{LVE}(\omega'_R)$ is evaluated by Eq. 33 in which ω_R is substituted by ω'_R. Non-linear shifts are displayed in Figure 4.4.

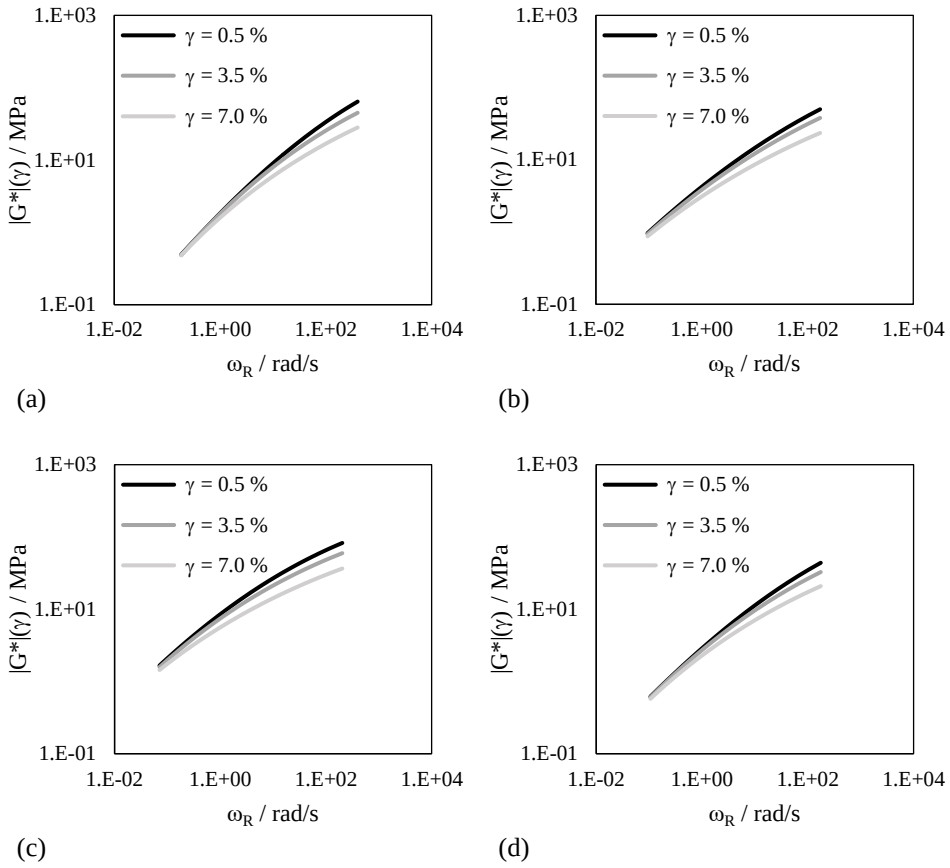

Figure 4.3 – Norm of complex modulus versus reduced frequency at strain value of 0.5 %, 3.5 % and 7.0 % for binder N1 (a), N2 (b), S1 (c) and S2 (d).

By referring to the obtained results, the non-linear shift factors are presented as a function of the shear strain, in Figure 4.4 (a) in the case of a_γ and (b) in the case of h_G. Inspection of such a figure can give a synthetic description of the non-linear behavior of the materials. For strain amplitudes approaching zero, both the factors tend to the value 1, which means that the non-linear solution is reduced to the linear viscoelastic response. By considering the shift a_γ, the lowest deviation from the linear domain was showed by bitumen S1, followed by binders S2, N1 and N2. In the case of the shift h_G, binders N1 and N2 showed

and overturned behavior, thus indicating a higher impact of non-linearity on the vertical position of the non-linear master curves of binders N1 with respect to binder N2.

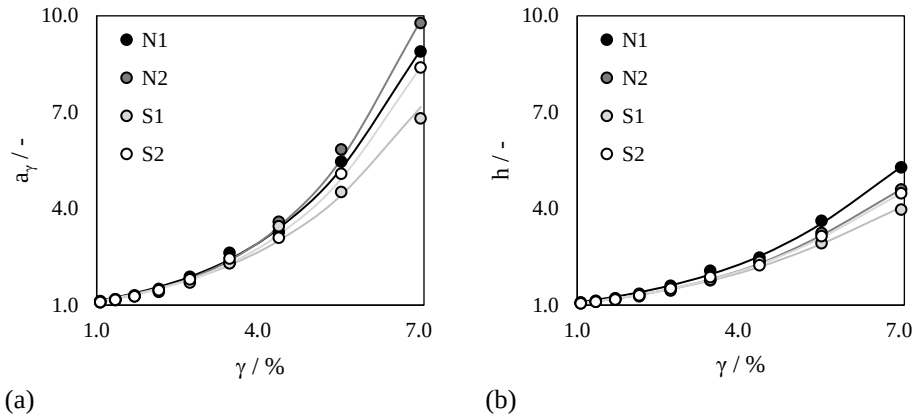

Figure 4.4 – Non-linear shift factors, a_γ versus γ (a) and h_G versus γ (b).

4.2 I Objective: Comparison of Self-Healing Protocols

The first objective of this thesis is the application of three testing protocols by means of a DSR to investigate the self-healing capabilities of selected binders. The obtained data were processed to calculate self-healing indices, based on analytical approaches specific to each method. Corresponding calculation and results are reported in the following sections.

4.2.1 TS-based FRF_S Method

TS-based FRF_S method aims to explore the self-healing capability of binders by implementing a dissipated energy approach on the mechanical changes observed due to insertion of the rest period [132]. The use of the energy approach allows to combine the material stiffness and the elasticity into a single parameter. The dissipated energy per unit volume (w_i), at a given cycle i, can be calculated as expressed in Eq. 37:

$$w_i = \pi \cdot \tau_i \cdot \gamma_i \cdot sin\delta_i \quad \text{(Eq. 37)}$$

Where:

- τ_i = shear stress amplitude at cycle i;
- γ_i = shear strain amplitude at cycle i;

- δ_i = phase angle at cycle i.

A typical output from TS-based FRF_S (a) and RF_S (b) tests is given in Figure 4.5, where the dissipated energy is plotted as a function of the number of loading cycles. It worth noting that the order of magnitude of the energy dissipated during the loading phases is much higher, due to higher imposed shear strain amplitude (3 %) and corresponding shear stress amplitude, compared to the energy restoration occurred during the rest phase (with imposed shear strain of 0.1 %). In order to distinguish such different values in Figure 4.5, values of dissipated energy during loading are plotted on the left y-axis, whereas values of restored energy during rest period (and that occurring during the thermal stabilization phase) are showed on the right y-axis.

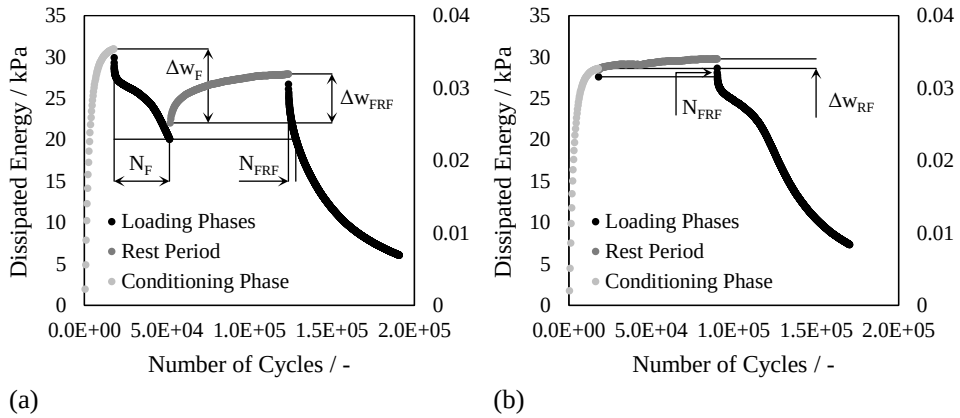

Figure 4.5 – Typical outputs obtained from TS-based FRF_S (a) and RF_S (b) (Example of binder S1).

Moreover, with the purpose of gathering mechanical information on the isothermal micro-structural reorganization occurring in RF_S test, few loading cycles were applied immediately before the rest period, to reproduce similar testing conditions to those occurring in the initial part of the first loading interval of FRF_S tests.

Information on the material self-healing capability are given by introducing an energy-based self-healing index, HI_w, and a number of loading cycles-based self-healing index, HI_N, defined as:

$$HI_w = \frac{\Delta w_{FRF} - \Delta w_{RF}}{\Delta w_F} \cdot 100 \qquad \text{(Eq. 38)}$$

$$HI_N = \frac{N_{FRF} - N_{RF}}{N_F} \cdot 100 \qquad \text{(Eq. 39)}$$

Where:

- Δw_F = dissipated energy due to the first loading phase of FRF_S test

- Δw_{FRF} = dissipated energy restored due to the rest phase of FRF_S test;
- Δw_{RF} = dissipated energy recovered in RF_S test;
- N_F = number of loading cycles applied to reach the preselected reduction of the norm of the complex modulus in the first loading phase of FRF_S test;
- N_{FRF} = number of loading cycles applied to reach the preselected reduction of the norm of the complex modulus in the second loading phase of FRF_S test;
- N_{RF} = number of loading cycles recovered RF_S test.

Obtained results in terms of HI_w and HI_N values for bituminous binders N1, N2, and S1 are listed in Table 4.2 and displayed in Figure 4.6. It can be observed that both the indices decreased as the percentage of damage increases, as expected. Moreover, HI_w was always found lower that HI_N, thus suggesting the latter is more prone to reflect the degree of healing achieved withing the material. By referring to the ranking of materials, this is dependent both by the considered index and the damage level. However, it is worth noting that for the two indices, the worth healing performance was shown by binder N2, whereas binder N1 overall exhibited the greatest self-healing potential for higher value of imposed damage.

Table 4.2 – Values of indices HI_w and HI_N for the binders at the considered damage levels.

Index %	Damage %	N1	N2	S1
HI_w	15	69.1	41.9	73.3
	35	52.2	38.1	51.4
	50	48.0	25.3	48.4
HI_N	15	28.7	13.4	70.3
	35	17.6	7.5	12.3
	50	16.8	7.1	10.9

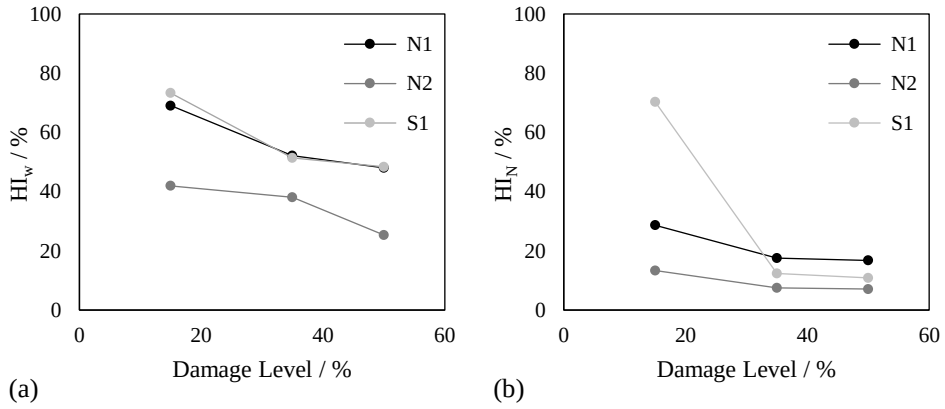

Figure 4.6 – HI_w (a) and HI_N (b) for the considered binders in the three damage levels.

With the purpose of evaluating the kinetics of the healing process during the unloading phase, the difference (Δw) between the energy dissipated at the generic rest time and that measured at the beginning of the rest period was calculated. However, due to fluctuations occurring in the experimental data, the increment in dissipated energy during the rest interval was fitted to the Eq. 40:

$$\Delta w(t) = \Delta w_{(t=\infty)} \cdot \left(1 - \frac{1}{e^{\varphi t}}\right)^{\chi} \qquad \text{(Eq. 40)}$$

Where:

- $\Delta w_{(t=\infty)}$ = asymptotic value of dissipated energy attained at infinite time;
- φ and χ = regression coefficients.

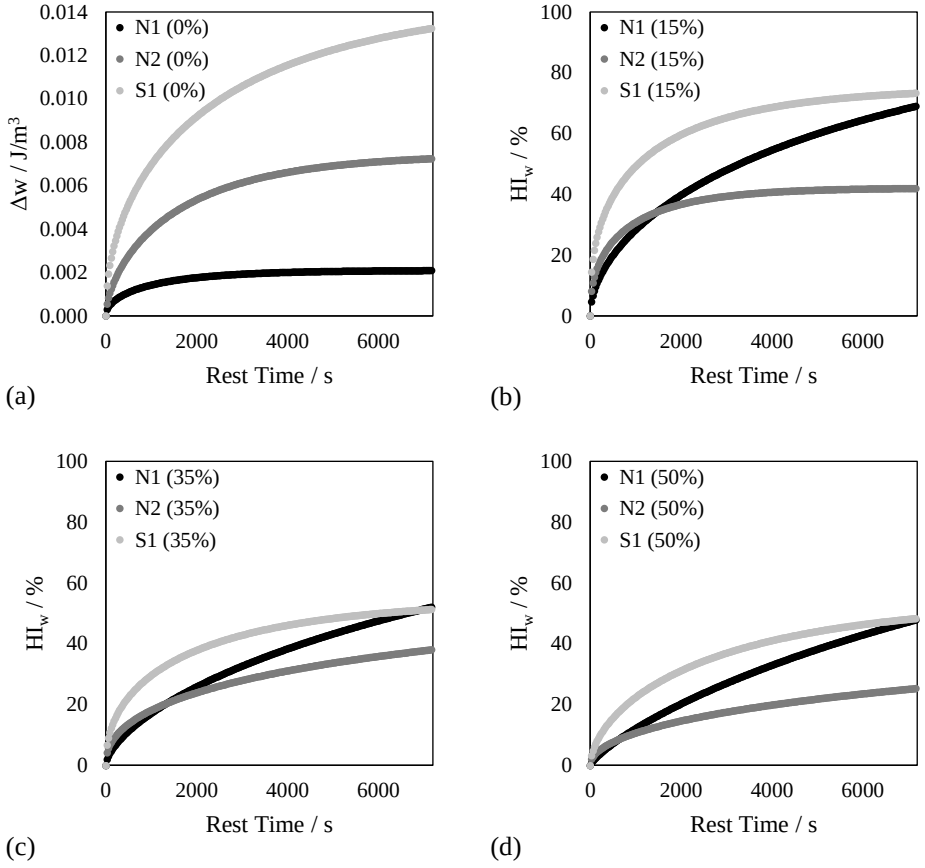

Figure 4.7 - Δw versus rest time from FR_S tests (a), and HI_w versus rest time from FRF_S and FR_S tests for damage level equal to 15 % (b), 35 % (c), and 50 % (d) of $|G^*|_0$.

Evolution of HI_w values over the rest period, obtained for the considered binders are presented in Figure 4.7 for each damage level, equal to the reduction of 15 % (b), 35 % (c), and 50% (d) of the initial norm of complex modulus ($|G^*|_0$). In the case of RF_S tests (damage level of 0 %), results are given in terms of dissipated energy Δw over the rest period time (a), because such tests do not provide information on self-healing. By referring to Figure 4.7 (a), it is worth noting that the highest increment was exhibited by the polymer modified binder, followed by bitumen N2 and N1. By considering the evolution of the index HI_w, although binder S1 outperformed the neat binders in the measured rest time, it can be noticed that rate of increase of HI_w in the case of binder N1 is higher, thus suggesting that a greater HI_w value can be attained at longer rest time.

4.2.2 TS-based FRF_M Method

TS-based FRF_M testing approach focuses the analysis on the loss modulus (G'') [31], expressed in Eq. 41 at a given cycle i, which is equivalent to the dissipated energy (Eq. 37).

$$G''_i = |G^*|_i \cdot sin\delta_i \quad \text{(Eq. 41)}$$

Where $|G^*|_i$ and δ_i are the norm of complex modulus and the phase angle at the generic cycle i. Observation of the typical experimental output showed in Figure 4.8, suggests that after the first loading interval, characterized by an initial value N_F of loading cycle, the application of the first rest interval allows the material to endure ΔN_1 loading cycles. As the load-rest cycles increase, the endurable number of loading cycles ΔN_i, after each successive rest period, tends to decrease, upon ultimately reaching a constant value. Thus, the amount ΔN_i, after a given rest interval i, consists of two contributions ascribable to self-healing (ΔN_{H_i}), and to parasitic phenomena (ΔN_T), such as steric hardening or thixotropy. Both the contributions allow the material to resist under loading. However, the reduction in successive values of ΔN_i is assumed to be related to the progressive exhaustion of material healing capability. Contrariwise, the material still benefits from thixotropic effects, which occur by involving constant recovery even though the material is damaged. This is illustrated in Figure 4.8, and presented in the analytical form of Eq. 42, where n is the number of rest intervals.

$$N_{Total} = N_F + \sum_{i=1}^{n} \Delta N_i = N_F + \sum_{i=1}^{n} \left(\Delta N_{H_i} + \Delta N_T\right) \quad \text{(Eq. 42)}$$

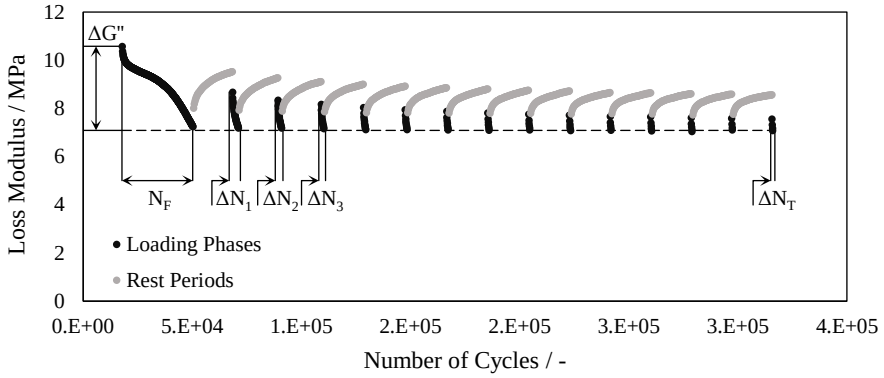

Figure 4.8 – G'' versus number of cycles of FRF_M test (Example of binder S1).

Insights on the evolution of the healing potential can be gathered by plotting the summation of $(\Delta N_{H_i} + \Delta N_T)$ as a function of rest intervals. A typical output is that presented in Figure 4.9. The area under the curve represents the total number of loading cycles, restored by the material value. The healing contribution can be modelled by means of the exponential law at each rest interval, given in Eq. 43, and its summation is a convergent geometric series:

$$\sum_{i=1}^{n}\left(\Delta N_{H_i} + \Delta N_T\right) = \sum_{i=1}^{n}\left(k_1 e^{-\alpha_1 i} + n \cdot \Delta N_T\right) = k_1 \frac{1 - e^{-\alpha_1 n}}{e^{\alpha_1} - 1} + N_T \qquad \text{(Eq. 43)}$$

Where:

- k_1 and α_1 = fitting coefficients;
- n = number of rest intervals.

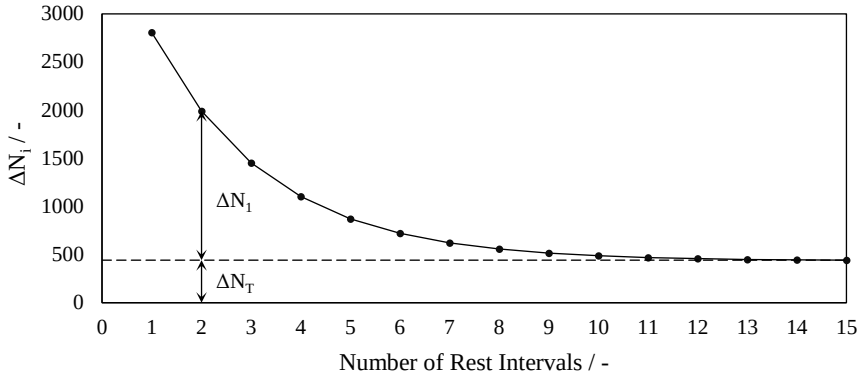

Figure 4.9 – Endurable number of loading cycles ΔN_i, versus the number of rest intervals (Example of binder S1).

When $n \to \infty$, the maximum theoretical number of cycles ascribable to self-healing (N_H), for the predefined damage level, can be evaluated by means of Eq. 44:

$$N_H = \frac{k_1}{e^{\alpha_1} - 1} \quad \text{(Eq. 44)}$$

Direct comparison between bituminous binders can be finally conducted by means of the self-healing index (HI_N), calculated in Eq. 45 as the ratio between the cumulated value N_H, and the number of loading cycle endurable by the pristine material in the first loading phase (N_F). Moreover, the recovery index (RI_N) is introduced to gather information on thixotropic contribution, by substituting the numerator of Eq. 45 with the cumulated number of loading cycles recovered due to thixotropy (N_T), as expressed in Eq. 46. Corresponding results are listed in Table 4.3 and illustrated in Figure 4.6 in terms of HI_N (a) and RI_N (b).

$$HI_N = \frac{N_H}{N_F} \cdot 100 \quad \text{(Eq. 45)}$$

$$RI_N = \frac{\Delta N_T}{N_F} \cdot 100 \quad \text{(Eq. 46)}$$

Table 4.3 – Values of indices HI_N and RI_N for the considered binders.

Index %	N1	N2	S1
HI_N	10.9	4.7	20.9
RI_N	4.0	1.0	1.3

By observing the obtained results, the proposed indices allowed to distinguish the self-healing performances of the material, whose ranking is characterized by binder S1, followed by bitumen N2 and N1. Instead, binders N1 showed the highest thixotropic attitude.

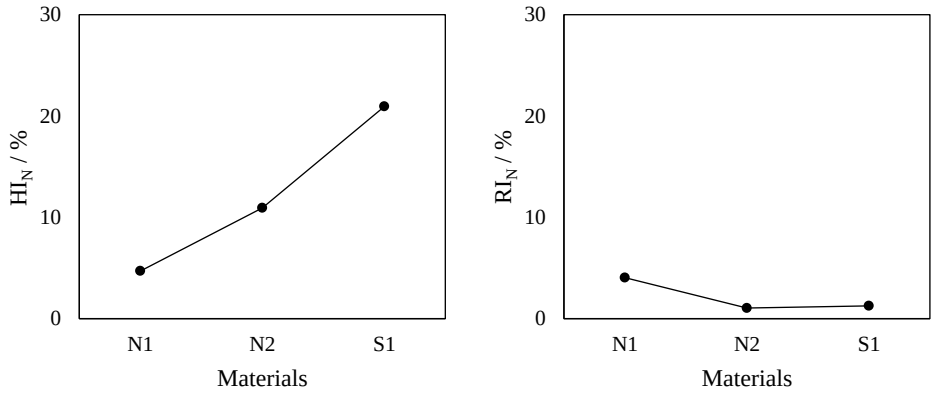

Figure 4.10 – Values of HI_N (a) and RI_N (b) for the considered binders.

4.2.3 LAS-based FRF_S Method

LAS-based FRF_S method aims to quantify the self-healing potential of bitumen by implementing the simplified viscoelastic continuum damage (S-VECD) framework [130]. A clear picture of the model framework is properly given in the next section (see §4.4). However, it is necessary to mention that the crux of the model is represented by the damage characteristic curve (DCC). The DCC defines the relationship between the material integrity and the damage parameter, thus providing insights on the resistance of materials when they undergo fatigue damaging. The material integrity and the damage intensity are represented by the pseudo secant modulus (C), and the internal state variable (S), respectively. A typical output in terms of norm of complex modulus as a function of loading cycles, gathered from LAS test is presented in Figure 4.11 (a), and corresponding representative DCC is given in Figure 4.11 (b). LAS test is required in order to know the material resistance to damage and to identify the occurrence of fatigue failure in DCC. This is necessary prior to inserting an interruption in LAS loading, which leads to LAS-based FRF_S test.

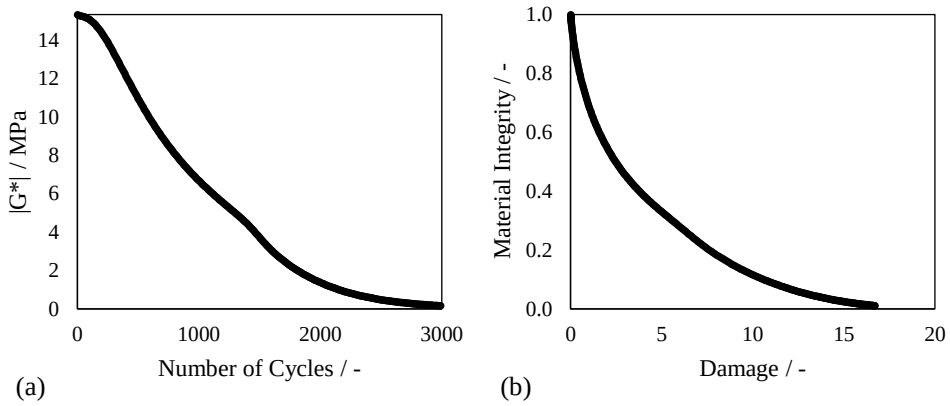

Figure 4.11 – $|G^*|$ versus number of cycles (a) from LAS test, and corresponding DCC (b) (Example of binder S1).

Identification of fatigue failure involves the use of a mechanistic-based parameter [133], called pseudo strain energy (W^R). The total pseudo strain energy (W_t^R) comprises two contributions, namely the stored (W_s^R), and the released (W_r^R) pseudo strain energy, defined in Eq. 47-49. The increasing progression of the W_s^R expresses the material ability to store energy as the damage process is growing. Contrariwise, as the W_s^R decreases, the material is no longer capable of retaining energy, which leads to the identification of a univocal peak in W_s^R curve, representing the cohesive fatigue failure. This is illustrated in Figure 4.12. where the failure strain (γ_f) is marked in both, stress-strain (a) and W_s^R-strain (b) curves.

$$W_t^R = W_s^R + W_r^R = \frac{1}{2}\tau_{p(LVE)} \cdot \gamma_p^R = \frac{1}{2}\left(\gamma_p^R\right)^2 \quad \text{(Eq. 47)}$$

$$W_s^R = \frac{1}{2}\gamma_p^R \cdot \tau_p = \frac{1}{2}C\left(\gamma_p^R\right)^2 \quad \text{(Eq. 48)}$$

$$W_r^R = \frac{1}{2}\gamma_p^R \cdot \tau_p = \frac{1}{2}(1-C) \cdot \left(\gamma_p^R\right)^2 \quad \text{(Eq. 49)}$$

Where:

- γ_p^R = peak value of pseudo strain amplitude (Eq. 73);
- $\tau_{p(LVE)}$ = peak shear stress in the undamaged material;
- τ_p = peak shear stress in the material undergoing damage;
- C = pseudo secant modulus.

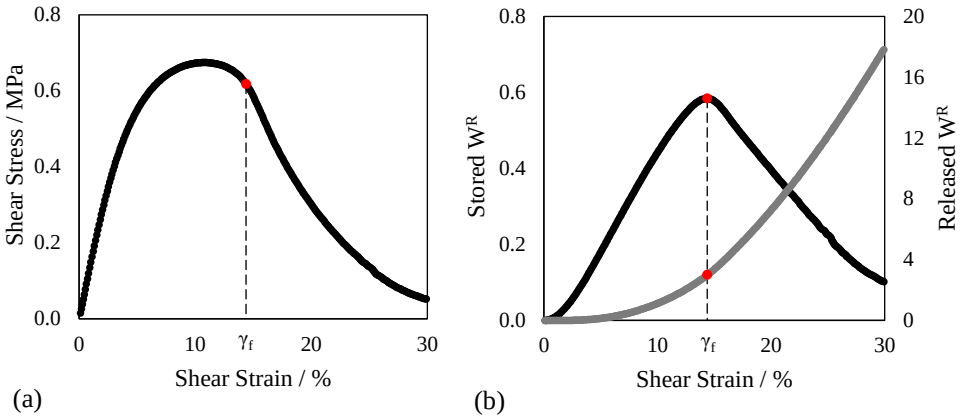

Figure 4.12 – Failure point in τ-γ curve (a) from LAS test, and in W_s^R- γ and W_r^R- γ curves (b) (Example of binder S1).

Once the failure shear strain was obtained from LAS test, LAS-based FRF_S tests were interrupted upon reaching the 50 % of γ_f. The analysis of raw data involved the calculation of material integrity and damage parameter. Afterwards, information on the material self-healing capability was given by introducing the S-based restoration index defined in Eq. 50.

$$RI_S = \frac{S_F - S_{FRF}}{S_F} \cdot 100 \quad \text{(Eq. 50)}$$

Where:

- S_F = cumulated damage measured immediately before rest;
- S_{FRF} = cumulated damage measured immediately after rest.

The value of S_{FRF} is dependent on the values of material integrity before (C_F) and after the rest period (C_{FRF}). In fact, the change in material integrity due to the rest period ($C_F - C_{FRF}$) needs to be considered in absolute value when referring to the Eq. 51 because C_{FRF} can be greater than C_F if some restoration occurs. In addition, the duration of rest period (t_{RP}) is removed from the difference ($t_F - t_{FRF}$), thus accounting only for the loading time. These tricks are necessary to compute the amount of damage restored due to the rest period, which needs to be subtracted from S_F, as expressed in Eq. 51. Illustration of the abovementioned information is given in Figure 4.13.

$$S_{FRF} = S_F - \sum_{i=1}^{N} \left[\frac{DMR}{2}(\gamma^R)^2(|C_F - C_{FRF}|)\right]^{\frac{\alpha}{\alpha+1}} [(t_{FRF} - t_F) - t_{RP}]^{\frac{1}{\alpha+1}} \qquad \text{(Eq. 51)}$$

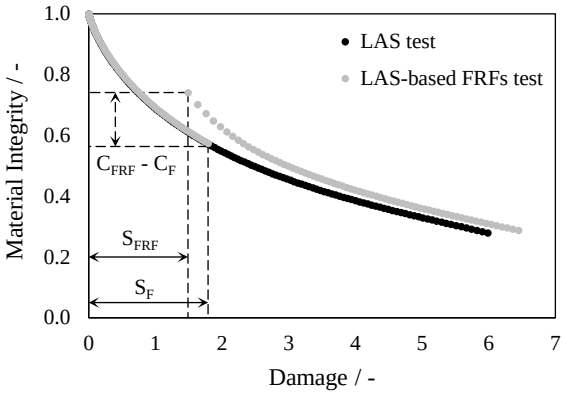

Figure 4.13 – Illustration of DCCs from LAS test and LAS-based FRF_S test (Example of binder S1).

Corresponding results of RI_S for the binders at the investigated durations of rest period (1, 5, 15, 30 min) are listed in Table 4.4 and displayed in Figure 4.14. It can be observed that the proposed index increases as the imposed rest time is longer, as expected, due to the time-dependence of self-healing phenomena. However, it is worth highlighting that such an index reflects the material restoration in which self-healing is confounded with other biasing effects. In terms of relative ranking, binder N1 was followed by binder N2 and S1.

Table 4.4 – Values of indices RI_S for the considered binders.

Index %	Rest Time min	N1	N2	S1
RI_S	1	16.1	12.0	13.8
	5	17.5	15.4	15.5
	15	18.0	16.3	15.8
	30	21.0	18.0	16.7

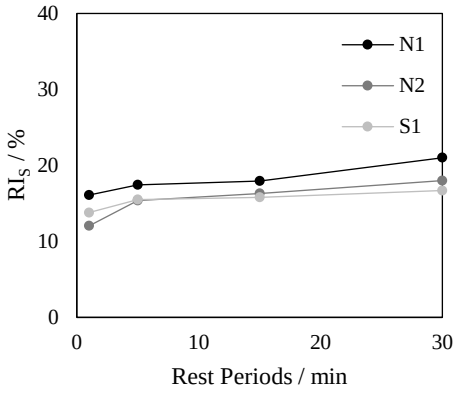

Figure 4.14 – Values of RI_S versus the rest period for the considered binders.

4.2.4 Comparison

The ranking between the investigated materials (N1, N2, S1) is provided in Figure 4.15, for the three adopted experimental testing protocols (TS-based FRF_S, TS-based FRF_M, LAS-based FRF_S). The values of indices obtained with the TS-based FRF_S method were calculated by Eq. 39, in the case of 35 % drop of $|G^*|_0$, as imposed damage level, and a rest period of 2 hours; in the case of TS-based FRF_M method, indices were evaluated through Eq. 45, by imposing 35 % reduction of G''_0 and multiple rest periods of 30 minutes; LAS-based FRF_S method involved the use of Eq. 50, in the case of damage level equal to 50 % abatement of γ_f and a rest period of 30 minutes.

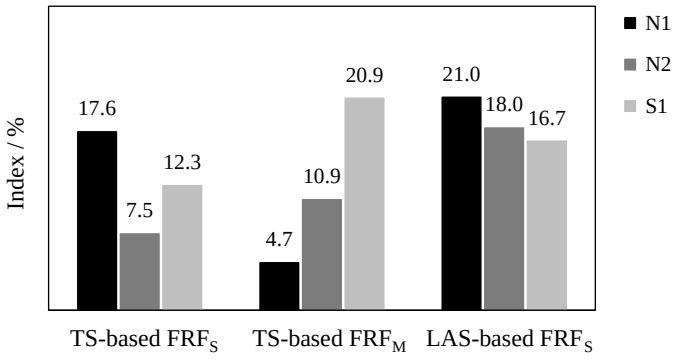

Figure 4.15 – Values of healing indices gathered from TS-based FRF_S, TS-based FRF_M, LAS-based FRF_S tests.

First observation arises by focusing on the ranking order of materials, which was found to come down to the adopted testing method. In fact, although the oscillatory shear loading was imposed at the same testing frequency and temperature, unexpectedly, a unique ranking cannot be established. In particular, binder N1 exhibited greater self-healing performances than binder N2 and S1, by adopting the approaches of TS-based FRF_S and LAS-based FRF_S. Contrariwise, the TS-based FRF_M method indicated binder S1 as best performer, which was found instead to lead to the worst healing capability in the case of LAS-based FRF_S.

Differences found in the rankings of materials stands out the urgent need of having a unique standardized protocol for the self-healing assessment. In fact, the role played by the adoption of different testing conditions and diverse analytical manipulations was found to be extremely relevant and non-negligible. Based on the results, such a universal protocol should account for a wide range of testing hallmarks, likely being the most simulative of in-field conditions, in terms of environment and vehicular loading characteristics. In this way, the healing response of materials could be univocally established in representative scenarios, which could allow a more appropriate material selection during the design procedures of road pavements [98].

Further considerations of the testing protocols can be drawn up based on the practical testing advantages/drawbacks and based also on the computational efforts required to post process the data. The methods TS-based FRF_S and FRF_M are found to take a long time to be performed, compared to the LAS-based FRF_S approach. Despite this, the first two testing protocols provide suitable tools to discriminate biasing effects, confounded with self-healing during the restoration process. Moreover, TS-based FRF_S approach also comprises the analysis of self-healing occurring during the rest phase. Furthermore, the multiple rest intervals introduced by TS-based FRF_M method represent the most simulative condition of in-field vehicular passages.

By referring to the loading input imposed to the sample, TS-based FRF_S and FRF_M methods require to apply a constant value of shear strain amplitude, chosen in the vicinity of the linear viscoelastic threshold, thus limiting the occurrence of non-linear effects. Contrariwise, LAS-based FRF_S protocol involves high strain history within the specimen, imparting strong non-linearities which are untrivial to untangle from damage. Nevertheless, from an analytical perspective, differently from TS-based FRF_S and FRF_M approaches, such a method comprises the use of viscoelastic constitutive modeling. Despite it requires some assumptions, such a modeling framework allows for isolation of damage from linear viscoelasticity and for inclusion of time-temperature dependence principles.

Based on these considerations, further investigations have been carried out by means of TS-based FRF_S approach, in order to exploit the advantages coming from the presence of a sin-

gle rest period. In fact, this allows to investigate different testing scenarios, as detailed in section 4.3, in terms of rest time and rest temperature. The advantages introduced by the viscoelastic constitutive theory have been also exploited by implementing it to account for self-healing, and to remove non-linear and thixotropic biasing effects, as properly discussed in section 4.4.

4.3 II Objective: Impact of Rest Temperature and Time

The second objective of this thesis aims to provide understanding on the effect of rest time and rest temperature on the self-healing properties of selected binders. Based on the results obtained in the accomplishment of the first objective, deeper investigation was required to evaluate how different tensing conditions could affect the self-healing process, and consequently the results in terms of ranking among materials. With this purpose, the TS-based FRF_S test was selected as the single rest period can allow implementation of a wide spectrum of testing conditions, in terms of duration (t_{RP}) and temperature (T_{RP}) of rest period. The choice of TS-based test, in place of LAS-based test, relied on the sake of avoiding strong non-linearities to be confounded with the material damaging process. In addition, TS test of bituminous binders, characterized by 2 mm height and 4 mm radius, has been demonstrated to correlate well with bituminous mixture, in capturing the material fatigue resistance [100]. In such a testing scenario, fatigue damage was verified to occur through microfractures that manifest at the sample periphery and propagate inward, thus exhibiting a “factory roof” morphology characterized by radial peaks and valleys [134]. This is pictured, by way of example, in Figure 4.16, which showed the specimen at the end of the test, after detaching the upper plate from the lower plate. In one case, a yellow paint was applied before the detachment, to better differentiate the fractured zone from the intact area.

Figure 4.16 – Representation of fractured sample with and without paint application

The cracked rough surface is recognized to be caused by edge fracture due to torsional loading, rather than flow instability occurring when normal forces are generated [135].

4.3.1 Quantification of Self-Healing

Assessment of the effects of different testing scenarios on the material self-healing property was conducted by introducing two distinct self-healing indicators. Definition of indices was based on the characteristic parameters outlined in Figure 4.17, which shows typical outputs obtained from TS-based FRF_S and RF_S tests, in terms of norm of complex modulus versus number of loading cycles. The characteristic parameters are defined as follows:

- $|G^*|_{C,f-FRF}$ is the norm of the complex modulus recorded at the end of the thermal conditioning phase of FRF_S test;
- $|G^*|_{R,i-FRF}$ and $|G^*|_{R,i-RF}$ are the norms of complex modulus at the beginning of rest period of FRF_S and RF_S tests, respectively;
- $|G^*|_{R,f-FRF}$ and $|G^*|_{R,f-RF}$ are the norms of the complex modulus recorded at the end of the rest period in FRF_S and RF_S tests, respectively;
- N_F, N_{FRF}, N_{RF} are the numbers of loading cycles applied to reach the predefined reduction of the norm of the complex modulus in the first and second loading phase of FRF_S tests, and in the single loading phase of RF_S tests, respectively;

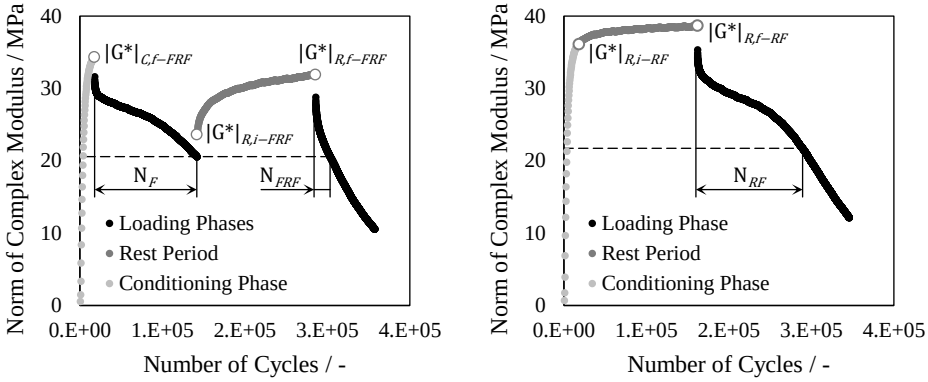

Figure 4.17 – Typical outputs obtained from TS-based FRF_S (a) and RF_S (b) (Example of binder S1).

Based on the abovementioned parameters, the two self-healing indices, I_G and I_N, are defined in Eq. 52 and Eq. 53, respectively [136]:

$$I_G = \frac{\Delta|G^*|_{R-FRF} - \Delta|G^*|_{R-RF}}{\Delta|G^*|_{F-FRF}} \cdot 100 \quad \text{(Eq. 52)}$$

$$I_N = \frac{N_{FRF}}{N_{RF}} \cdot 100 \quad \text{(Eq. 53)}$$

Where:

- $\Delta|G^*|_{R-FRF}$ is the difference between $|G^*|_{R,f-FRF}$ and $|G^*|_{R,i-FRF}$, in FRF tests;
- $\Delta|G^*|_{R-RF}$ is the difference between $|G^*|_{R,f-RF}$ and $|G^*|_{R,i-RF}$, in RF tests;
- $\Delta|G^*|_{F-FRF}$ is the difference between $|G^*|_{C,f-FRF}$ and $|G^*|_{R,i-FRF}$, in FRF tests.

The index I_G accounts for the gain of stiffness observed during the rest interval, divided by the modulus loss imposed during the first fatigue loading of FRF tests. As previously introduced (see §4.2.1), the contribution of stiffness restored after the loading removal is not totally attributed to self-healing, because time-dependent parasitic phenomena (which includes thixotropy/steric hardening) can be superimposed to the observed restoration. The coexistence of these phenomena is supported by experimental evidence provided in Figure 4.18, which shows the comparison between the increasing trend in the norm of the complex modulus, $\Delta|G^*|_R$, observed in a damaged specimen during the rest period (from FRF_S test), and that recorded for the same material in its undamaged state (from RF_S test). Fitting curves of $\Delta|G^*|_R$ values are introduced to smooth possible fluctuations occurring during experimental data acquisition, by means of Eq. 54.

$$\Delta|G^*|_R(t) = \Delta|G^*|_{R_{(t=\infty)}} \cdot \left(1 - \frac{1}{e^{\varphi_1 t}}\right)^{\varphi_2} \quad \text{(Eq. 54)}$$

Where:

- $\Delta|G^*|_{R_{(t=\infty)}}$ = asymptotic value of $\Delta|G^*|_R$ theoretically attained at infinite time;
- φ_1 and φ_2 = non-linear regression coefficients.

Moreover, it is worth noting that the difference $\Delta|G^*|_R$ can be calculated all over the rest period, thus allowing the assessment of the progression of the stiffness gain, I_G, as a function of the rest time, as illustrated in the example of Figure 4.19.

However, I_G does not provide information on the actual material resistance, as indicated by the fact that it is evaluated in the low strain conditions, which allows to monitor the growing pattern of the material stiffness without, most importantly, hindering healing-related mechanisms to take place. Therefore, the index I_N is introduced based on the loading cycles endurable by the binder, thus providing information on the gain in fatigue endurance achieved after the rest period. Differently from the index I_G, the value of index I_N can be calculated only at the specific rest period duration considered in testing.

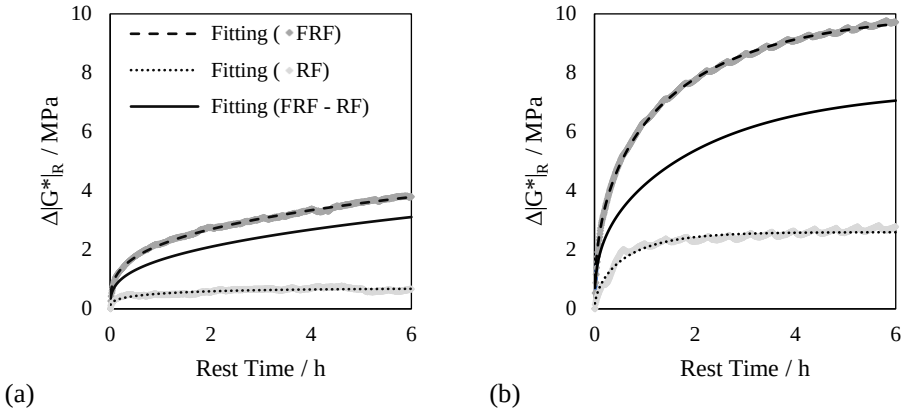

Figure 4.18 – Example of $\Delta|G^*|_R$ versus rest time gathered from TS-based FRF_S and RF_S tests for binders N1 (a) and S1 (b).

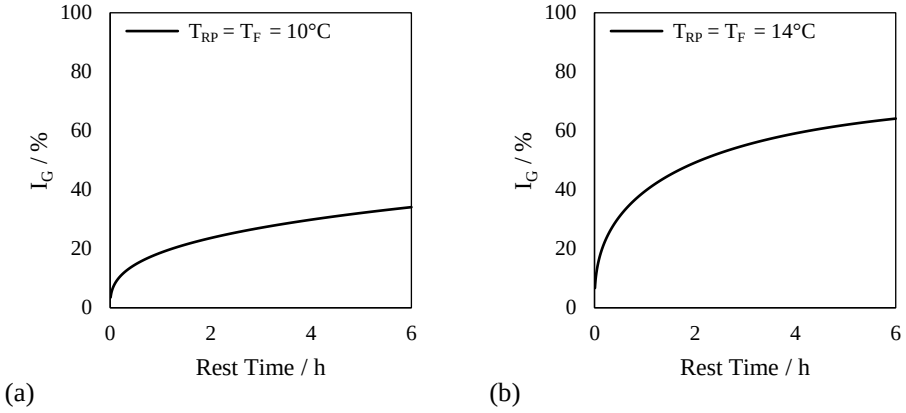

Figure 4.19 – I_G versus rest time calculated at $T_{RP} = T_F$ for binders N1 (a) and S1 (b).

The relationship between the two indices is reported in the I_G-I_N diagram of Figure 4.20. Every single data point displayed in the diagrams refers to each specific testing condition, previously listed in Table 3.3 and 3.4. As evident from the diagrams, in all the cases (i.e. for each binder at all the testing conditions), results reveal that stiffness gain (I_G) is invariably greater than fatigue endurance gain (I_N), as indicated by the fact that all data points are below the identity line (I_N=I_G). The dissimilarity between values of I_G and I_N can be explained by referring to the molecular diffusion theory developed to describe the self-healing mechanism (see §2.2.1) [34].

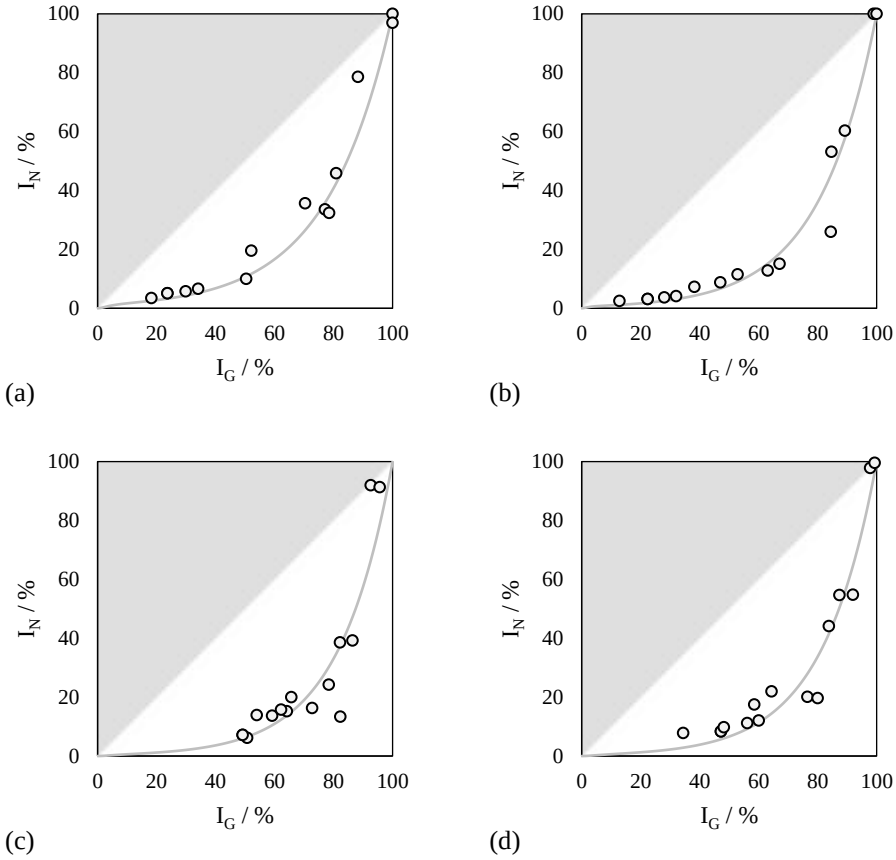

Figure 4.20 – I_N versus I_G for the materials N1 (a), N2 (b), S1 (c) and S2 (d).

In particular, this observation points to the likelihood that when imposing low strain conditions during the rest period, stiffness gain can be initiated by material flow and interfacial cohesion between microcrack faces driven by wetting, which can eventually lead to partial interdiffusion [42]. However, it is reasonable to suppose that if the self-healing process is not properly developed, application of higher strain conditions can lead to low values of strength gain, due to the weak interactions occurred at the microcrack interfaces and the inability of ruptured chains to resist further damage [18]. It can be fairly postulated that only in those cases in which advantageous conditions coexist, i.e. enough resting time and sufficiently high temperature, significant interfacial bonding strength can be achieved, encouraged by diffusion phenomena and eventual entanglement across microcracks, as established in the literature [34,69,137].

Moreover, it is worth noting that, for all the materials, data points seem to lie on the same path, regardless of the influencing conditions imposed during test. This suggests that a

unique relationship between I_G and I_N may exist for each binder. This implies that a specific healing stage can be reached by means of different combinations of testing conditions. Trend of corresponding pairs of points (I_G, I_N) has been fitted with the following equation:

$$I_N(I_G) = \frac{\alpha_2(e^{\alpha_3 I_G} - 1)^2}{e^{\alpha_4 I_G}} \cdot 100 \qquad \text{(Eq. 55)}$$

Where α_2, α_3, α_4 are regression coefficients.

Although both the proposed indicators contribute to outline the self-healing capabilities of the investigated materials, the index I_N was found to be more conservative. In fact, the fatigue endurance gain seems to be more sensitive to the degree of molecular interdiffusion and entanglement, which represent the conclusive phases of the healing phenomenon [18,96,137]. Based on this rationale, the index I_N was considered in the subsequent analysis with the purpose of quantifying the self-healing potential of considered binders.

4.3.2 Rest Temperature-related Effects

Assessment of the effect of rest temperature was conducted by referring to a specific set of data, which comprised tests identified by the following hallmarks (see §3.4):

- Different values of T_{RP} and t_{RP};
- Equal stiffness conditions among all the materials, involving different T_F values;
- Equal loading amplitude of shear strain equal to 2 %;
- Damage level corresponding to 35 % and 50 % reduction of $|G^*|_0$.

Direct comparison of the healing capabilities of bituminous binders was represented in a T_{RP}-I_N diagram, displayed in Figure 4.21 and Figure 4.22, in the case of $\Delta|G^*|$ equal to 35 % and 50 %, respectively, at the reference t_{RP} of 2 hours [138]. Upper boundary corresponding to complete healing (100 % of I_N) was assumed to occur at the material softening point temperature (T_S) [87]. Contrariwise, no healing (0 % of I_N) was supposed to be achieved in the region of glass transition temperature (T_G) where the self-healing aptitude ceases due to the impossibility of material flow and molecular interdiffusion to occur at microcrack interfaces [84]. Experimental data points were fitted to the generalized logistic function reported in Eq. 56, and regression parameter are listed in Table 4.5.

$$I_N(T_{RP}) = \frac{100}{[1 + \delta \cdot e^{-\eta(T_{RP} - \vartheta)}]^{\delta^{-1}}} \qquad \text{(Eq. 56)}$$

Where:

- δ = shape factor;

- η = slope of the $I_N(T_{RP})$ curve;
- ϑ = inflection point.

Table 4.5 – Regression coefficients of healing functions obtained at the reference t_{RP} value of 2 hours.

Binders	N1		N2		S1		S2	
$\Delta\lvert G^*\rvert$ / %	35	50	35	50	35	50	35	50
δ / -	12.44	2.18	6.85	6.98	9.21	4.14	21.99	8.36
η / °C^{-1}	2.35	0.50	0.93	1.01	0.88	0.46	2.11	0.83
ϑ / °C	24.7	23.2	32.1	32.4	37.4	35.3	34.9	33.5

By observing the results of Figure 4.21 and Figure 4.22, the values of indices were found to increase with increasing T_{RP}, as expected, consistently with prior findings [64,66,112]. Most importantly, the performances of the investigated materials are clearly distinguished, which allows to define a ranking order of their healing response. However, this ranking order cannot be univocally established because it depends upon rest period temperature. In particular, binder N1 showed superior self-healing potential for T_{RP} values higher than 15 °C, achieving the full restoration of the pristine matrix at temperatures significantly lower than those of the other materials. This is also suggested by η and ϑ regression coefficients, which indicate that the healing curve of binder N1 was characterized by the highest slope value and the lowest temperature corresponding to maximum growth. In the region of temperatures comprised between 25 °C and 35 °C, where bitumen N1 is fully healed, binders N2 and S2 exhibited similar responses as indicated by the $I_N(T_{RP})$ curves which run close to each other. Instead, the material S1, whose healing curve is further to the right of the graph, was found to require higher temperatures during rest period to attain reasonably important restoration. As the values of T_{RP} are gradually decreased below 20 °C, the discrepancy among the curves progressively vanishes towards the glass transition region. This indicates that healing responses of materials tend to wane due to the reduction of viscous flow and molecular mobility caused by the lower temperatures. By comparing the healing responses in the case of the two investigated damage levels, the materials exhibited negligible differences, possibly due to the proximity of the two damage levels. However, values of indices were found to be lower when subjecting the material to the highest microstructural change, as expected. This is also evident by considering the slope of the $I_N(T_{RP})$ curves which decreased passing from $\Delta\lvert G^*\rvert$ equal to 35 % to 50 %, which indicates a lower kinetics of the self-healing process. The only exception was found in the case of binder N2 that exhibited roughly similar values.

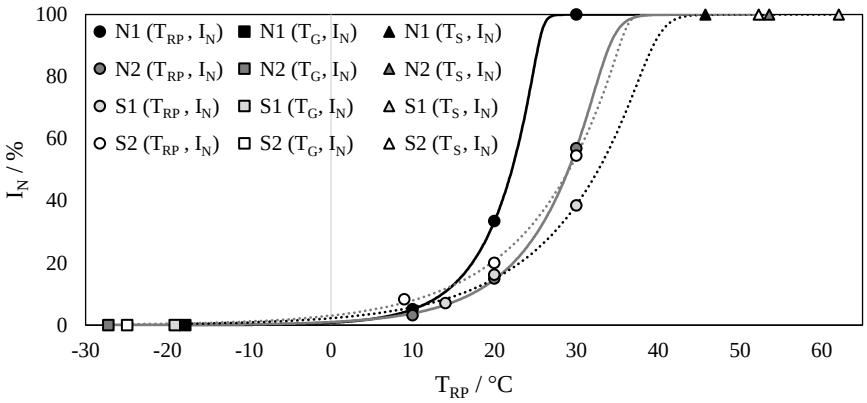

Figure 4.21 – Healing functions obtained at the reference t_{RP} value equal to 2 hours for $\Delta|G^*|$ equal to 35 %.

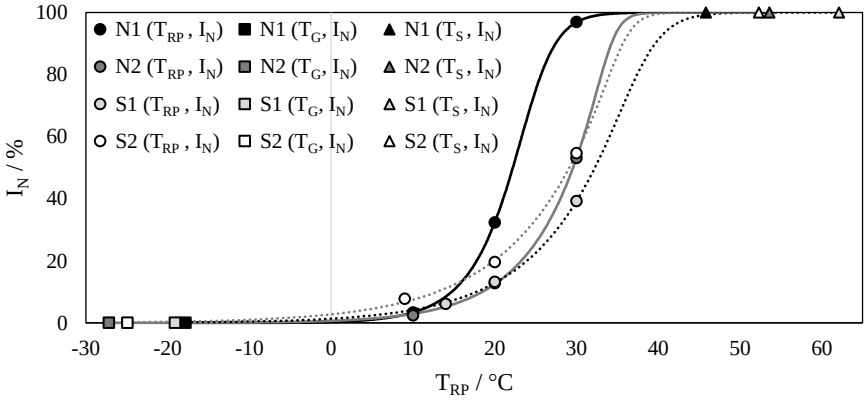

Figure 4.22 – Healing functions obtained at the reference t_{RP} value equal to 2 hours for $\Delta|G^*|$ equal to 50 %.

4.3.3 Full Healing Flow Properties

The temperatures of rest period at which full healing conditions were achieved by the different binders were calculated by means of Eq. 56. These temperatures, indicated as T_{FH}, are listed in Table 4.6.

Table 4.6 – Full healing temperatures (T_{FH}).

Binders	N1		N2		S1		S2	
$\Delta\|G^*\|$ / %	35	50	35	50	35	50	35	50
T_{FH} / °C	28.0	38.4	40.3	40.0	46.1	51.7	38.5	42.7

It is worth noting that T_{FH} was always found to be significantly lower than the softening point temperature, thus indicating that the previously discussed empirically based assumption (I_N equal to 100 % at T_S) is quite conservative.

In order to correlate full healing conditions with the rheological behavior of the different binders, further analyses were focused on the flow properties. Such properties were evaluated by considering the norm of the complex viscosity $|\eta^*|$ retrieved from frequency sweep tests and calculated as the ratio between the norm of the complex modulus $|G^*|$ and the angular frequency ω. At each specific test temperature, obtained data were fitted to Eq. 57:

$$|\eta^*| = m \cdot \omega^{n-1} \quad \text{(Eq. 57)}$$

where m and n are regression coefficients which refer to the test temperature under consideration. The parameter n, known as the flow behavior index, can vary between 0 and 1. When n is equal to 1, $|\eta^*|$ is independent of ω and the behavior corresponds to that of a Newtonian fluid [58].

Calculated values of the flow behavior index, n, were plotted as a function of temperature as shown in Figure 4.23 in the case of $\Delta|G^*|$ equal to 35 % (a) and 50 % (b). It can be observed that neat binders N1 and N2, reached a value of n close to 1 at the highest T-f test temperature (76 °C), whereas modified binders S1 and S2 displayed values of n lower than 0.9 in the entire range of investigated temperatures. Moreover, it is worth noting that the n values of binder N1 were at all temperatures greater than those of the other materials. This outcome is consistent with the findings synthesized in Figure 4.21 and 4.22 since it is reasonable to assume that binder N1 exhibited the highest self-healing potential as a result of its enhanced flow behavior that promotes the quick closure of microcracks.

When considering the shape of the curves displayed in Figure 4.23, it can be noticed that the modified binders, S1 and S2, were characterized by the presence of a steady-like region in the temperature range comprised between 34 °C and 52 °C, where the flow behavior does not change with temperature as a consequence of the existence of an inner elastic polymer network. On the contrary, neat binders showed trends of the n coefficient that were found to be monotonically increasing with temperature.

For each binder, the flow behavior index was assessed at a temperature equal to T_{FH}, highlighted with the dashed lines in Figure 4.23. It was found that full healing conditions correspond to n values lower than 1 that do not reveal a fully Newtonian behavior. In particular, all binders reached a full-healing state at n values comprised between 0.77 and 0.87 in both the cases of $\Delta|G^*|$ equal to 35 % and 50%.

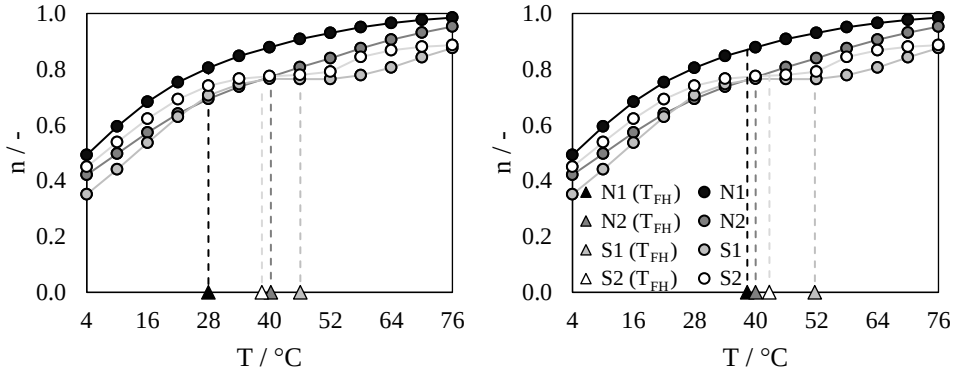

Figure 4.23 – Flow behavior index at different temperatures and T_{FH} values in the case of $\Delta|G^*|$ equal to 35 % (a) and 50 % (b).

4.3.4 Time-Temperature Self-Healing Charts

With the purpose of including within the analysis the results obtained from tests performed at different t_{RP}, the healing function presented in Eq. 56 was modified to incorporate the rest time. Such an analysis was conducted only in the case of $\Delta|G^*|$ equal to 35 % at which data corresponding to the condition of $T_{RP}=T_F$ and increasing t_{RP} were collected.

Based on the assumption that t-TS principle holds for bitumen-based materials in the case of self-healing process [78], the $I_N(T_{RP})$ curves obtained at the reference t_{RP} of 2 hours have been shifted to account for longer t_{RP}. This was practically conducted by keeping constant the coefficients δ and η, whereas the parameter ϑ was changed by means of a regression process. In other terms, the influence of rest time was assumed to impact only on the temperature at which the inflection point, ϑ, occurred, thus neglecting any effect on the shape of the curve, dictated by the slope, η, and the shape factor, δ. Results of such an optimization process are presented in Figure 4.24, which shows the parameter ϑ as a function of t_{RP}. In particular, it can be noticed that the reduction of ϑ values with increasing t_{RP} clearly distinguished the attitude of neat binders (N1 and N2) from that of the SBS-modified binders (S1 and S2). The latter showed a higher slope of t_{RP}-ϑ regression lines compared to the first ones. Explanation to such a higher sensitivity to rest time variation exhibited by the modified binders can rely on the disentanglement and rearrangement of long polymer chains, more likely to occur to a greater extent, thus promoting molecular motion and diffusion processes. After determining the relationship between ϑ and t_{RP}, derivation of material healing function can be conducted by arbitrarily imposing any duration of rest interval.

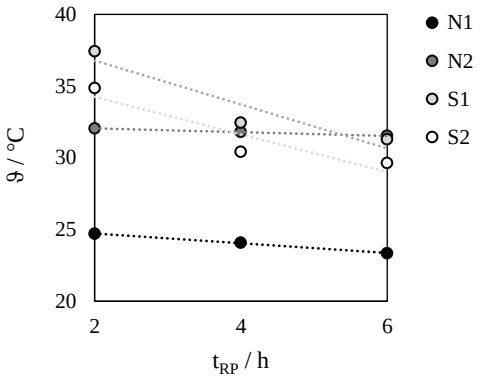

Figure 4.24 – Temperature of inflection point occurrence as a function of investigated values of t_{RP}.

In the case of data experimentally gathered in the current thesis, the healing functions $I_N(T_{RP})$ were derived at t_{RP} equal to 6 hours, displayed in Figure 4.25. By comparing Figure 4.25 and 4.21, it is observed that increasing the t_{RP} from 2 to 6 hours is equivalent to horizontally shift the curves obtained at the reference t_{RP} of 2 hours. As an obvious consequence, the ranking order among the binders at various rest period temperatures can vary, thus underlining the importance of the effects of rest time and temperature that need to be appropriately combined for a reliable evaluation of material self-healing performance. Thus, a single healing index is not capable of conveying a reliable ranking between materials, since it is found to be valid only for the specific testing condition adopted to determine that index. It follows that self-healing functions, relying on the incorporation of both time and temperature of rest period, can entail adequately reasonable results.

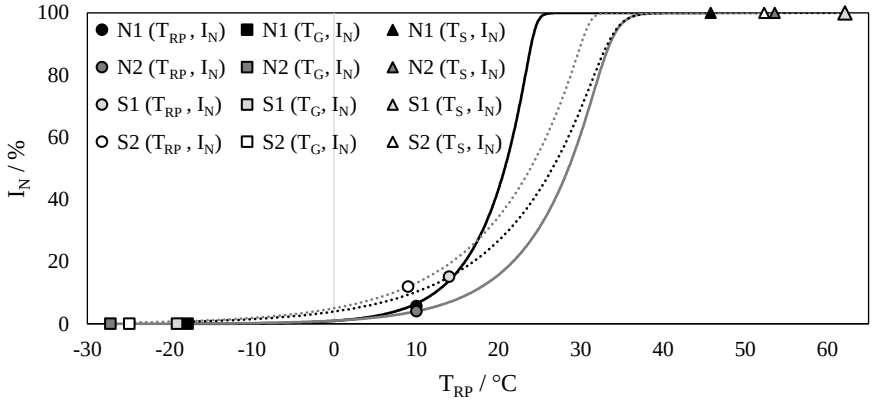

Figure 4.25 – Healing functions obtained by shifting at t_{RP} value equal to 6 hours.

Based on the analysis presented above, the parameter ϑ was assumed to linearly vary as a function of t_{RP}. Thus, Eq. 56, explicating the I_N dependence on the rest period temperature, was modified to incorporate the effect of rest period duration, by substituting a linear relationship, characterized by an intercept κ and a slope λ, in place of ϑ, as indicated in Eq. 58:

$$I_N(T_{RP}, t_{RP}) = \frac{100}{[1 + \delta \cdot e^{-\eta(T_{RP}-(\lambda \cdot t_{RP}+\kappa))}]^{\delta^{-1}}} \quad \text{(Eq. 58)}$$

Where κ and λ values are listed in Table 4.7.

Table 4.7 – Regression coefficients of linear functions ϑ (t_{RP}).

Binders	N1	N2	S1	S2
λ / °C/h	-0.34	-0.13	-1.53	-1.31
κ / °C	25.4	32.3	39.8	36.9

Implementation of Eq. 58 leads to the derivation of isochronal self-healing curves for different rest interval durations, which are presented in Figure 4.18 in the form of self-healing charts. Such self-healing charts are meant to provide a straightforward and simple prediction tool for the healing performances of bituminous binders at any combination of rest time and temperature. Moreover, further inferences are related to the fact that a specific value of I_N can be obtained at higher T_{RP} and shorter t_{RP}, or rather at lower T_{RP} and longer t_{RP}. This substantiates the concept of t_{RP}-T_{RP} equivalency principle, which allows superimposition of the effects of rest time and rest temperature. By visually comparing the charts, it can be noted that the healing curves of unmodified binders, N1 (a) and N2 (b), are closer to each other, while those of the modified materials, S1 (c) and S2 (d), are well outdistanced. This is the effect of different dependencies on rest time (greater for modified binders), as discussed above, clearly reflected in the self-healing charts.

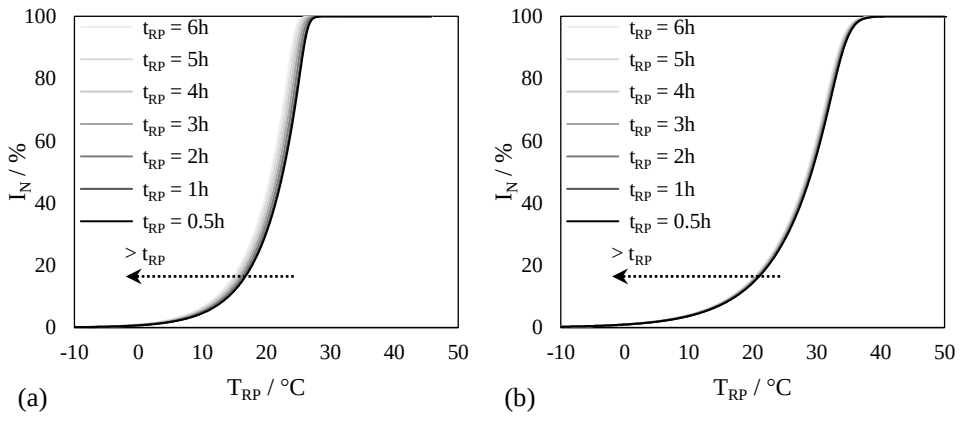

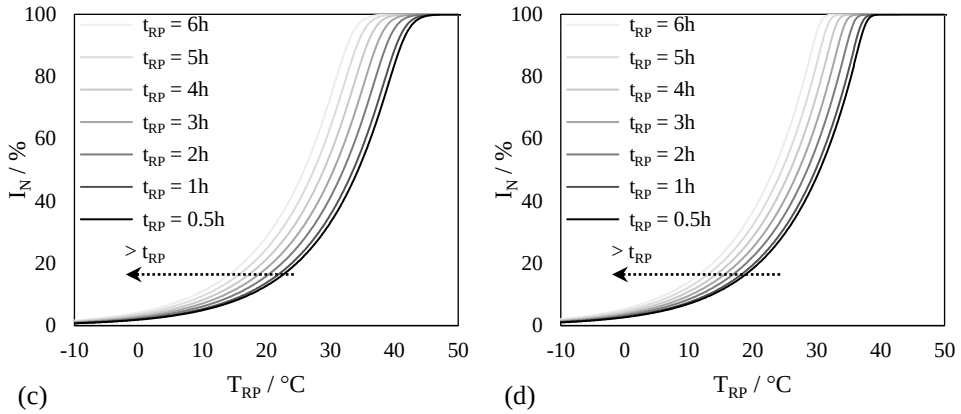

Figure 4.26 – Self-healing charts for binders N1 (a), N2 (b), S1 (c) and S2 (d).

Preliminary validation of the mathematical function proposed in Eq. 58 was conducted by introducing the values of I_N, determined from the supplementary set of tests listed in Table 3.4. The agreement between experimental results of I_N and those predicted by means of the healing function is presented in Figure 4.27. Results provide overall positive verification on the predictive capability of model, for all the considered binders, with relative differences that were found to be always lower than 7 %. In particular, it worth noting that, when imposing temperatures above the highest value considered so far, in the case of binders N2, S1, and S2, an almost complete restoration of fatigue endurance was exhibited, thus substantiating the reliability of the healing function also outside of the investigated region of rest period temperature.

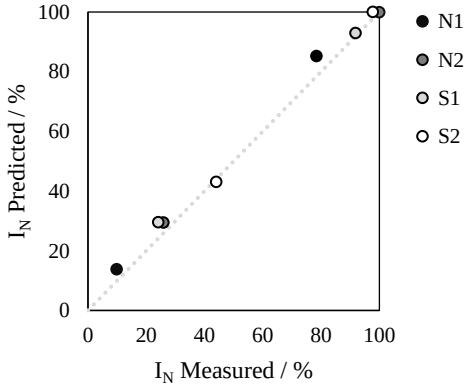

Figure 4.27 – Comparison between values of measured and predicted I_N.

It follows that for the construction of such self-healing charts is sufficient to perform a pre-selected set of 4 tests, specifically related to the desired damage level. Such a set needs to include two values of T_{RP}, higher than T_F, and a single value of t_{RP}. Two tests are required to satisfy the condition $T_{RP}=T_F$ for two different t_{RP} values. Finally, a corresponding set of 4 tests with the same testing conditions needs to be performed in no-damage condition (RF_S).

4.3.5 Total Fatigue Life

The self-healing plots presented in section 4.3.3 and 4.3.4 allow the healing capability of different binders to be assessed and ranked over a wide range of rest period temperatures. However, such an analysis does not explicitly reveal the overall fatigue performance of binders in terms of the number of cycles that can be endured to failure when rest periods are interposed between loading phases. The definition of fatigue failure of asphalt binders in the present study included the traditional stiffness-based approach identified as 50 % loss in $|G^*|$. As indicated in Eq. 59, the total fatigue life (N_f) can be computed as the summation of two contributions: the fatigue life assessed during the pure loading without rest periods (N_F) and the additional fatigue endurance capability stemming from self-healing (N_H).

$$N_f = N_F + N_H \qquad \text{(Eq. 59)}$$

N_H values for each binder were derived from the corresponding I_N parameter to exclude thixotropic effects. Thus, calculations were carried out by referring to Eq. 60, derived from Eq. 56. Values of N_F, N_H and N_f are plotted in Figure 4.28 as a function of T_{RP} values.

$$N_H(T_{RP}) = \frac{N_F}{[1+\delta\cdot e^{-\eta(T_{RP}-\vartheta)}]^{\delta^{-1}}} \qquad \text{(Eq. 60)}$$

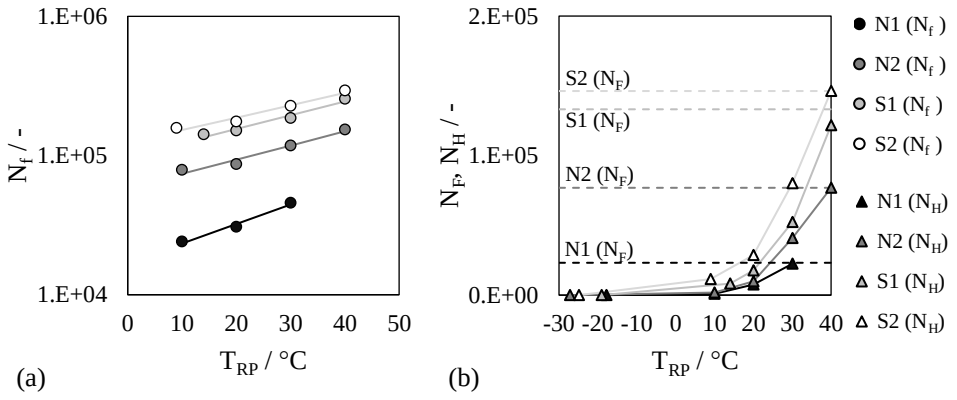

Figure 4.28 – N_f (a) and N_H, N_F (b) versus rest period temperatures.

While N_F is independent of the rest temperature by definition, the values of N_H and N_f were found to increase significantly for increasing values of T_{RP}.
It can be noticed that a univocal ranking can be established among the considered materials. Binder S2 clearly showed the best fatigue performance, followed by binders S1 and N2, with the lowest N_F, N_H and N_f values being displayed by binder N1. It was also observed that the slopes of the $N_f(T_{RP})$ curves for materials N2, S1 and S2, were similar, while binder N1 exhibited the highest slope value. This is consistent with the findings synthesized in Figure 4.21 and Figure 4.22, according to which binder N1 was characterized by the highest temperature sensitivity of its self-healing properties. It is interesting to point out that the abovementioned ranking was found to be different from the one based on the I_N index. This is due to the fact that I_N reflects the inner healing potential in relative terms, whereas N_f takes into account the effect of self-healing on the overall fatigue resistance [139].

4.4 III Objective: S-VECD Modeling Approach

The viscoelastic continuum damage (VECD) model is one of the most supported models in the bitumen community, used to describe the fatigue damage accumulation in bituminous materials [140–143]. Such a model is based on the continuum damage framework, which possesses the advantage of characterizing the material behavior from macroscale observations. Thus, the degradation of material integrity is meant to comprise any effect of microstructural changes distributed within the material undergoing damage. The VECD model was built on rigorous theoretical backgrounds represented by Schapery's work potential theory [144,145] which allows quantification of damage in bituminous mixtures. The relationship between the material integrity and the damage represents the crux of the VECD model, known as damage characteristic curve (DCC).
Schapery's theory was initially developed to describe the mechanical behavior of elastic bodies with growing damage [146]. Extension of such a theory to viscoelastic media was accomplished afterwards by introducing the elastic-viscoelastic correspondence principle, which allowed to discriminate the effect of viscoelasticity from damage [45,147]. Furthermore, incorporation of temperature effects in VECD model was conducted by proving the validity of t-TS principle, under microcracking states [148]. Due to the cumbersome computational aspects of the VECD modeling, a simplified form, named S-VECD, was derived to characterize uniaxial cyclic direct tension tests on bituminous mixtures, which was proven to reasonably produce accurate results by maintaining theoretical rigors [149,150].

In the context of bituminous binder fatigue testing implemented in DSR, the VECD model was firstly applied to describe the behavior of materials subjected to monotonic loading at constant strain rate [151]. However, due to the high stress level withstood by polymer-modified binders at high strains, the model application resulted adequate only for neat bitumen, which showed strain rate-independent DCCs [152]. Further drawbacks are related to the normal stresses arising when monotonic loading is imposed to the material, which affects the damage growth [99]. Recently, the binder yield energy test (BYE) and the DSR-based elastic recovery (DSR-ER) test were proposed to allow expeditious ranking of binder fatigue resistance [153,154]. Both the tests apply monotonic constant shear rate loading to measure the yield property and the elastic recovery of materials, respectively. Although promising results have been obtained in comparison with cyclic tests, BYE test was found to be inadequate for heavily modified binders, whereas DSR-ER test was not able to differentiate the elastic recovery of neat binders [154].
The VECD modeling approach was also extended to damage-inducing tests involving cyclic loading, such as TS and LAS tests. The model application on both types of tests provided adequate results, although mismatch was found between the damage characteristic curves generated from the two testing approaches. This is presumably due to the higher strain amplitudes involved in LAS test, which imply non-linearity effects to be superimposed to damage effects, thus impacting more on the material integrity reduction and endurable damage [99]. As in the case of bituminous mixtures, in order to ease the computational process, a simplified form of VECD procedure has been implemented for DSR-based tests, which consists of ignoring the full time histories of stress and strain, in favor of their peak values [99,133,155]. Furthermore, t-TS principle was proven to hold for LAS and TS tests, generating DCCs independent on temperature [99,156,157].

4.4.1 Theoretical Background

Linear viscoelasticity

Viscoelastic materials, as the name implies, refer to materials which show an intermediate behavior between an ideal elastic body and a viscous fluid. Such materials exhibit rate dependence, as indicated in Figure 4.29 by the creep (c) and relaxation (d) phenomena, occurring under constant stress (a) and constant strain input (b), respectively [11]. In the equations of Figure 4.29, τ and γ represent the shear stress and shear strain, respectively, $J(t)$ and $G(t)$ are functions of a linear viscoelastic material, known as creep compliance and relaxation modulus, respectively.

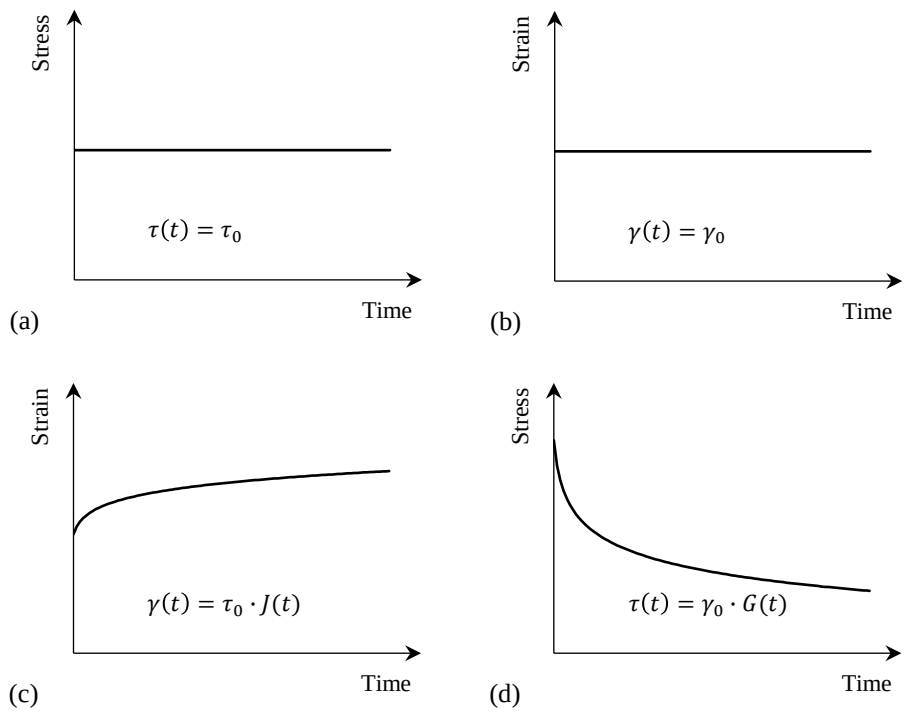

Figure 4.29 – Phenomenon of creep (c) under constant stress (a), and relaxation (d) under constant strain (b).

The rate dependence of viscoelastic materials corresponds to time dependence since their response is function of the current input and of the entire input history. If the input level is small enough, viscoelastic materials generally exhibit linear behavior, which becomes non-linear at high input levels. Viscoelastic systems are defined linear (LVE) if and only if they obey to homogeneity and superposition principles, as mathematically expressed in Eq. 61 (where c is a constant) and Eq. 62, respectively.

$$R\{cI\} = cR\{I\} \quad \text{(Eq. 61)}$$

$$R\{I_1 + I_2\} = R\{I_1\} + R\{I_2\} \quad \text{(Eq. 62)}$$

Homogeneity principle refers to the proportionality between the input (I) and the response (R) at any given time. Superposition principle states that the response of the combination of two arbitrary inputs (I_1, I_2) is equal to superimposing the response of each of the inputs, considered separately.

Due to the time-dependence of such materials, LVE response needs to be expressed as a function of time, in addition to all the input variables. From a mathematical perspective, LVE response is described by means of a convolution integral. In order to facilitate the mathematical manipulation, the input value can be conveniently defined by using the Heav-

iside Step Function, $H(t-\xi)$, where t is the time of interest and ξ is the time of loading. $H(t-\xi)$ is defined as a discontinuous function equal to 1 for $t > \xi$, and to 0 for $t < \xi$. By considering the case of constant input ΔI applied at $t = \xi$:

$$I = \Delta I \cdot H(t-\xi) \quad \text{(Eq. 63)}$$

$$R\{\Delta I \cdot H(t-\xi)\} = \Delta I \cdot R\{H(t-\xi)\} = \Delta I \cdot R_H \quad \text{(Eq. 64)}$$

Where R_H is the unit response function. In the case of creep and relaxation phenomena, the unit response functions are the creep compliance and the relaxation modulus, respectively. Application of Heaviside function by generalizing the superposition principle is given as follows.

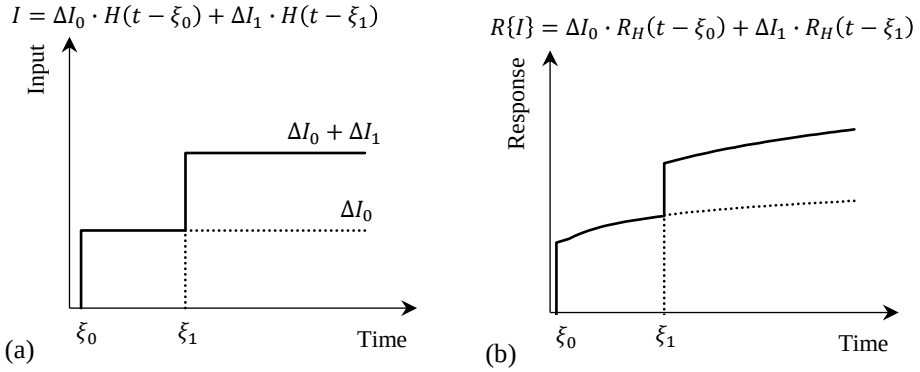

Figure 4.30 – Two-inputs history (a) and corresponding response (b).

In the case of (N+1) steps:

$$R = \sum_{i=0}^{N} \Delta I_i \cdot R_H(t-\xi_i) = \sum_{i=0}^{N} \frac{\Delta I_i}{\Delta \xi_i} \cdot R_H(t-\xi_i)\Delta\xi_i \quad \text{(Eq. 65)}$$

As the inputs become smaller, $N \to \infty$ and the loading increments of time $\Delta\xi_i \to 0$:

$$R = \lim_{\Delta\xi_i \to 0} \sum_{i=0}^{\infty} \frac{\Delta I_i}{\Delta \xi_i} \cdot R_H(t-\xi_i)\Delta\xi_i \quad \text{(Eq. 66)}$$

Which leads to the integral form of Eq. 67 in the case of continuous input, referred to as convolution or hereditary integral:

$$R = \int_0^t R_H(t-\xi)\frac{dI}{d\xi}d\xi \quad \text{(Eq. 67)}$$

By referring to the creep and relaxation phenomena, the convolution integrals depict the linear viscoelastic stress-strain relationships [158]. Eq. 68 describes the strain response de-

pendent on the prescribed stress history, $d\tau/d\xi$, whereas Eq. 69 expresses the stress response dependent on the prescribed strain history, $d\gamma/d\xi$.

$$\gamma(t) = \int_0^t J(t-\xi)\frac{d\tau}{d\xi}d\xi \quad \text{(Eq. 68)}$$

$$\tau(t) = \int_0^t G(t-\xi)\frac{d\gamma}{d\xi}d\xi \quad \text{(Eq. 69)}$$

Elastic-Viscoelastic Correspondence Principle

The elastic-viscoelastic correspondence principle was proposed by Schapery [45] for linear and non-linear material to account for viscoelasticity. This principle allows determination of viscoelastic solutions from the corresponding elastic case, by introducing pseudo variables in place of physical quantities [158]. Definition of torsional pseudo strains is given in Eq. 70, by means of the shear stress expression of Eq. 69.

$$\gamma^R(t) = \frac{1}{G_R}\int_0^t G(t-\xi)\frac{d\gamma}{d\xi}d\xi \quad \text{(Eq. 70)}$$

Where:

- γ^R = the pseudo strain;
- γ = time-dependent shear strain;
- ξ = integration variable representing time;
- $G(t)$ = relaxation modulus;
- G_R = constant reference modulus.

By substituting the integral form, the pseudo strain can be rewritten in the form of stress-strain elastic-like solution, as expressed in Eq. 71. This means that the shear stress response is linearly proportional to the pseudo shear strain response, through a reference modulus, G_R, arbitrarily assumed equal to 1, hereinafter, which dictates the slope of the stress-pseudo strain relationship.

$$\gamma^R(t) = \frac{\tau(t)}{G_R} \quad \text{(Eq. 71)}$$

Introduction of pseudo strains allows discrimination of material viscoelasticity from damage. In fact, the damage occurring within the specimen is reflected through changes of the slope in the stress-pseudo strain domain, indicating the deviation from linear viscoelasticity. This results in the material stiffness deterioration, which is represented by the pseudo secant stiffness [140], defined in Eq. 72, termed as C.

$$C = \frac{\tau_p}{\gamma_p^R} \quad \text{(Eq. 72)}$$

Shear stress and pseudo strain of Eq. 72 are indicated with the subscript p because they refer to the peak values. In fact, the full time history of stress and strain is generally ignored in favor of the peak values, due to the cumbersome effort involved in the computational process [99,149]. This leads to the simplified form of VECD (S-VECD). Thus, peak pseudo strains are calculated by introducing Eq. 73 rather than Eq. 70, because it was found to be suitable in the case of DSR-based cyclic loading with zero mean displacement [133].

$$\gamma_p^R = \gamma_p \cdot |G^*|_{LVE} \quad \text{(Eq. 73)}$$

Where $|G^*|_{LVE}$ is the material norm of complex modulus in the LVE domain for preselected values of frequency and temperature.

The final form of pseudo stiffness is given in Eq. 74, in which it is introduced a factor accounting for the specimen-to-specimen variability, denoted as dynamic modulus ratio (DMR). The DMR factor is evaluated by the ratio of the fingerprint modulus, indication of the stiffness of the tested specimen, and the LVE modulus, representing the overall material stiffness (Eq. 75).

$$C = \frac{\tau_p}{\gamma_p^R \cdot DMR} \quad \text{(Eq. 74)}$$

$$DMR = \frac{|G^*|_{fingerprint}}{|G^*|_{LVE}} \quad \text{(Eq. 75)}$$

The proportionality between pseudo strain and shear stress response allows the pseudo stiffness to be ranging from 1 to 0. The case of C = 1 corresponds to the material linear viscoelastic behavior, whereas as the specimen undergoes damage, the behavior deviates from linear viscoelasticity and C value decreases toward 0. However, part of the reduction of C can be attributed to non-linear effects which need to be properly discriminated as explained in the following (see §4.4.4). The pseudo stiffness is recognized to represent the integrity of the material.

Work Potential Theory

The work potential theory [45,144,159] is based on continuum damage mechanics which allows to account for microdamage effects by focusing on the overall constitutive behavior of material [143]. Schapery's theory was firstly built for elastic bodies by applying the thermodynamics of irreversible principle and afterwards adapted to viscoelastic materials by introducing the elastic-viscoelastic correspondence principle. The fundamentals of the Schapery's theory, extended for viscoelastic media, are [143]:

- The pseudo strain energy density function;
- The relationship between stress and strain ($\tau = \partial W/\partial\gamma$);
- The rate-dependent damage evolution law.

The rate-dependent damage, dS/dt, is defined in Eq. 76, in which the right hand side represents the available thermodynamic force for damage growth [160]:

$$\frac{dS}{dt} = \left(-\frac{\partial W^R}{\partial S}\right)^{\alpha} \quad \text{(Eq. 76)}$$

Where:

- S = internal state variable, indicating damage;
- α = damage evolution rate;
- W^R = pseudo strain energy density function.

The pseudo strain energy density function represents the work performed on the system by the external load and can be defined by the following expression [140,160]:

$$W^R = W^R(\gamma^R, S) = \frac{1}{2}\gamma^R \cdot \tau = \frac{1}{2}C(S)(\gamma^R)^2 \quad \text{(Eq. 77)}$$

The solution to the damage evolution law was given into the discrete form of Eq. 78, by substituting Eq. 77 into Eq. 76 and by applying the chain rule [140,142,158,161]:

$$S = \sum_{i=1}^{N}\left[\frac{DMR}{2}(\gamma^R)^2(C_{i-1} - C_i)\right]^{\frac{\alpha}{\alpha+1}}(t_i - t_{i-1})^{\frac{1}{\alpha+1}} \quad \text{(Eq. 78)}$$

The damage change in the time interval $(t_i - t_{i-1})$ is considered to occur with constant rate change and is dependent upon the changes of the material integrity $(C_{i-1} - C_i)$, and pseudo strains. The damage evolution rate, α, is an undamaged material constant, hereinafter assumed equal to $(1 + 1/m)$ [99], where m is a coefficient gathered by linear viscoelastic characterization as the steady-state slope of the norm of complex modulus master curve.

Time-Temperature Superposition

The t-TS principle states that the behavior of viscoelastic material can be stretched or shrunk in time, due to the effects of temperature above or below the reference temperature, respectively [11]. This equivalency allows to combine the effects of time and temperature in a single parameter, referred to as reduced time (t_R). In the general case of transient temperature with time, t_R is expressed in the integral form of Eq. 79 [162]:

$$t_R(t) = \int_0^t \frac{d\xi}{a_T[T(\xi)]} \quad \text{(Eq. 79)}$$

Where a_T is the time-temperature shift factor at a given temperature, t is the actual time of measurement and ξ is a time variable of integration. There exist several mathematical functions to define the shift factors, among which the empirical expression proposed by Williams *et al.* [163], reported in Eq. 28, is one of the most commonly used. In the simplest case, temperature value is constant, and Eq. 79 is reduced to the Eq. 80:

$$t_R = \frac{t}{a_T} \quad \text{(Eq. 80)}$$

Incorporation of t-TS into the S-VECD modeling approach can be accomplished by substituting the measured time in Eq. 78 with the reduced time. The final formulation of damage can be rewritten as in Eq. 81, which corresponds to shifting the DCC to the reference temperature, thus capturing the effect of temperature.

$$S = \sum_{i=1}^{N} \left[\frac{DMR}{2}(\gamma^R)^2(C_{i-1} - C_i)\right]^{\frac{\alpha}{\alpha+1}} \left(t_{R_i} - t_{R_{i-1}}\right)^{\frac{1}{\alpha+1}} \quad \text{(Eq. 81)}$$

4.4.2 S-VECD Modeling with Self-Healing

Application of continuum damage concepts to fatigue behavior modeling in the presence of self-healing has been attempted by few researchers in the literature [78,96,130,164,165]. However, the placeholder was established by Lee and Kim [140] who derived a uniaxial viscoelastic constitutive model accounting for damage growth and incorporating micro-damage healing of bituminous mixture. With this purpose, they introduced a healing function (H) to depict the changes in pseudo stiffness observed after imposing the rest period. This is schematically illustrated in Figure 4.31 in the case of a single rest period. It can be observed that the pseudo stiffness increases right after the rest (from A to A′) and progressively diminishes as the material is undergoing damage. The beneficial effect of rest period, in the healed material, is caught in region I (from A′ to B′) and gradually vanishes until reaching region II, where the stiffness decreasing rate is characterized by the same slope (from B′ to D′) of that exhibited by the virgin material (from B to D). However, the curve B′D′ is vertically shifted upwards by the amount BB′.

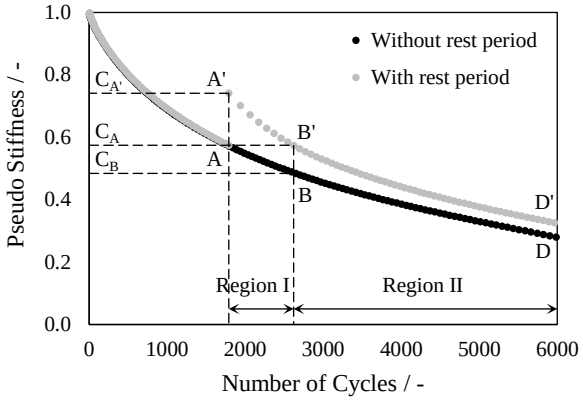

Figure 4.31 – Pseudo stiffness versus number of cycles in the case of material loaded with and without rest period.

This results in the mathematical form presented in Eq. 82 and Eq. 83:

$$\sigma = C_1(S_1)\varepsilon^R \quad \text{(Eq. 82)}$$

$$\sigma = [C_1(S_1) + H]\varepsilon^R \quad \text{(Eq. 83)}$$

Where σ and ε^R represent the stress and pseudo strain, respectively (in the case of uniaxial loading), and $C_1(S_1)$ is the material integrity before the rest period. The healing function, H, introduces two additional terms of pseudo stiffness and damage parameter, $C_2(S_2)$ and $C_3(S_3)$, respectively. The former accounts for material integrity restoration occurring during rest period, whereas the latter is physically related to the pseudo stiffness of the re-damaged material. By referring to i-th rest intervals, the healing function H is generalized in the form of Eq. 84, while the damage evolution S_2 and S_3 are given in Eq. 85 and Eq. 86, respectively.

$$H = \left[C_{A,i} + C_2\left(S_{2,i}\right)\right]C_3\left(S_{3,i}\right) - C_1(S_1) - \sum_{j=1}^{i-1}\left(C_{B',j} - C_{B,j}\right) \quad \text{(Eq. 84)}$$

$$S_2 = \int_o^{t_{RP}} \left[\frac{1}{2}(\varepsilon^R)^2 \frac{\partial C_2}{\partial S_2}\right]^{\alpha_2} dt \quad \text{(Eq. 85)}$$

$$S_3 = \left[-\frac{C_{A'}}{2}(\varepsilon^R)^2 \frac{\partial C_3}{\partial S_3}\right]^{\alpha_3} \quad \text{(Eq. 86)}$$

However, due to shortcomings in the rigor of the abovementioned model, a simplified version was proposed with the attempt of including a single term for material integrity and damage, in place of multiple parameters and damage functions. The basic concept of the simplified model is to assume that a single damage function governs the phenomenon. Dur-

ing the damage process accumulation, the material integrity decreases along $C(S)$ curve; during the healing process, the material is repaired backwards along the same curve. Thus, any reloading and rest period imposed to the material can impact only by moving back and forward along the same path [166]. This is illustrated in Figure 4.32. During the first loading, the material undergoes damage upon reaching the point A, where a rest period is imposed. This allows the material to heal the material integrity and damage back to point B. Then, reloading of material leads to damage growth until point C, where another rest interval is applied, thus resulting in gain of properties until point D, and so on.

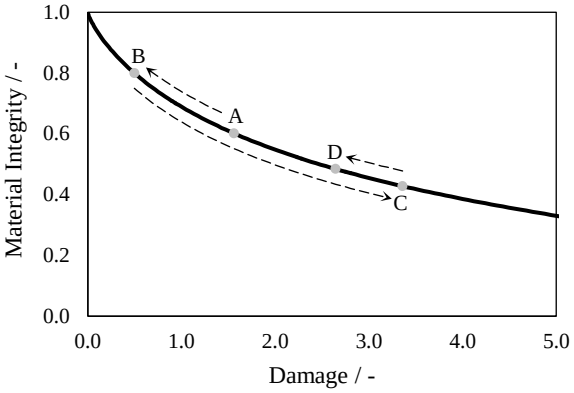

Figure 4.32 – Schematic diagram of material integrity versus damage for the simplified model.

Calculation of pseudo stiffness can be conducted by means of the formulation of Eq. 87, whereas the damage reduction due to healing, S_H, requires an optimization process such that the resulting pseudo stiffness is found to be of same value of that recorded at the end of the loading.

$$S_{i+1} = S_H + \left[-\frac{1}{2}(\varepsilon^R)^2 \frac{\partial C}{\partial S}\right]^{\alpha} \qquad \text{(Eq. 87)}$$

4.4.3 Preliminary Experimental Observations

Based on the simplified theory expressed above, in the case of bituminous binders, the first assumption is to considerer a unique governing $C(S)$ function for both the fatigue loading phases, before and after the rest period. However, this simplicity needs to cope with the experimental observation that the healed material behaves differently from the intact material, as witnessed in the case of mixture. In particular, it must be reminded that re-damaged specimens, after resting, are obviously more sensitive to loading than the first-damaged ma-

terial. It has been also observed that, as expected, the loading sensitivity exhibited by the healed binder was strongly dictated by the temperature imposed during rest. This is believed to reflect different stages of the self-healing mechanism within the bituminous matrix, as macroscopically displayed in Figure 4.33 and Figure 4.34, in terms of norm of complex modulus normalized by $|G^*|_0$, versus time. The figures show, by way of example, the responses of bitumen N1 (Figure 4.33) and modified binder S1 (Figure 4.34), derived by TS-based F and FRF_S tests by omitting the data recorded during the thermal conditioning phase and rest interval. For FRF_S tests, the response is showed in the case of 50 % reduction of $|G^*|_0$, for two different T_{RP} values, equal to T_F (a) and 30 °C (b), respectively. As highlighted by Lee and Kim [140] in the case of mixture, the response of the healed sample can be parted in two distinguished regions:

- Region I denotes the behavior of the partially-to-fully healed material, highlighting the beneficial effect of rest period due to microdamage healing and additional biasing effects;
- Region II identifies the damage growth in the partially-to-fully healed material, which corresponds to that of the virgin material, as indicated by the fact that the decreasing rate of the curve (A'B') of Region II is equivalent to that of the virgin matrix (AB).

In particular, the material behavior to fatigue loading after the rest period is marked by a deviation from that observed before resting. This is made explicit by the fact that stiffness gain is rapidly consumed by loading progression instead of following the same decreasing rate. Such a response is generally exhibited in both the materials, regardless of the presence of SBS polymer. In fact, in the diagrams of Figure 4.33 (a) and 4.34 (a) where the temperature is constant all over the test, it can be noted that the increase in modulus, recorded after the rest period, quickly vanishes after few reloading cycles until reaching same stiffness recorded before the rest. The incremental number of reloading cycles necessary to achieve a modulus equal to that at the end of the first loading (points A and A') impacts on the extension of fatigue life. This is significantly evident when T_{RP} is risen, as e.g. in the case of Figure 4.33 (b), where region I is found to be comparable to the first loading phase. Thus, the presence of the rest period allows reestablishment of the intact bituminous matrix to an extent that can be quantified in terms of modulus and endurance to loading cycle.
It is speculated that the rapid rate of decrease is imputed to the weak interactions occurred at the interfaces of microcracks, which can be easily disrupted unless high bonding strengths are developed and promoted by thermochemical factors. This result was previously highlighted in terms of healing indices (see §4.3), and visually denoted here by observation of examples of data gathered from tests.

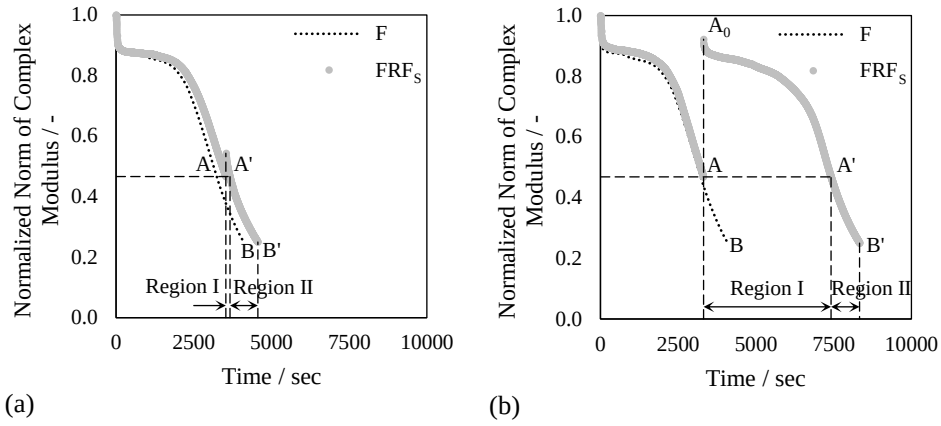

Figure 4.33 – Example of norm of complex modulus, normalized by $|G^*|_0$, versus time gathered from TS-based F tests (at T_F = 10 °C) and TS-based FRF_S tests, at $T_{RP} = T_F$ (a) and T_{RP} = 30 °C (b), for binder N1.

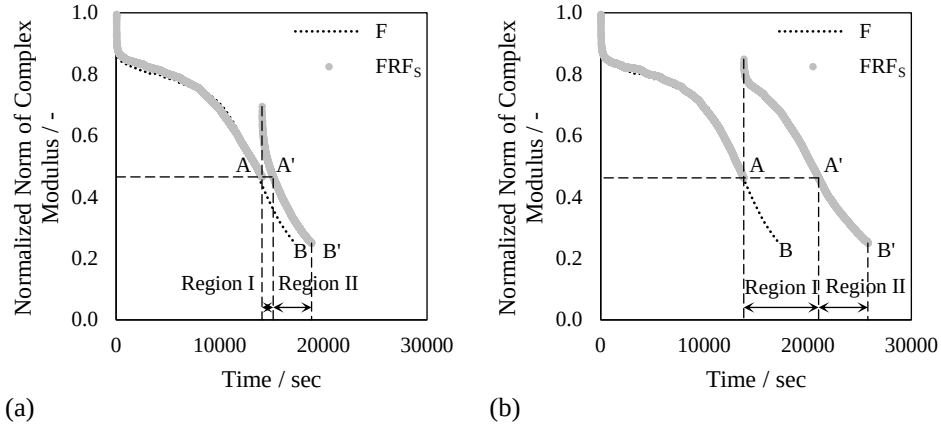

Figure 4.34 – Example of norm of complex modulus, normalized by $|G^*|_0$, versus time gathered from TS-based F tests (at T_F = 14 °C) and TS-based FRF_S tests, at $T_{RP} = T_F$ (a) and T_{RP} = 30 °C (b), for binder S1.

Notable condition occurs whereby the curve in region I (A_0A) is found to be more extended than the curve corresponding to the first loading. It is postulated that such an occurrence can be imputed to thixotropic effects which allows microstructural reorganization during rest periods leading to a stiffer network of the bituminous matrix.

Further observations arise by focusing on the solely second loading interval of TS-based FRF_S tests, for different T_{RP} values. As highlighted by Di Benedetto and co-workers [13] in the case of bituminous mixtures, the degradation process of bituminous binders can be described by three disparate stages:

- Phase I: the first stage, also recognized as adaptation phase, consist of a rapid drop in stiffness, which can be partially imputed to fatigue damage and partially exerted by undesired effects such as local heating, thixotropy and non-linearity;
- Phase II: the second stage, also referred to as quasi-steady phase, is characterized by a constant decreasing rate of stiffness with loading progression, mostly dictated by the material resistance to microcracks formation, in which parasitic factors still bias the response;
- Phase III: the third stage, also called failure phase, is related to propagation and coalescence of microcracks to macrocracks, characterized by a change in slope of the degradation curve, which eventually determines the material global failure.

Evidence of this is schematically presented in Figure 4.35, in which the three different phases can be clearly identified.

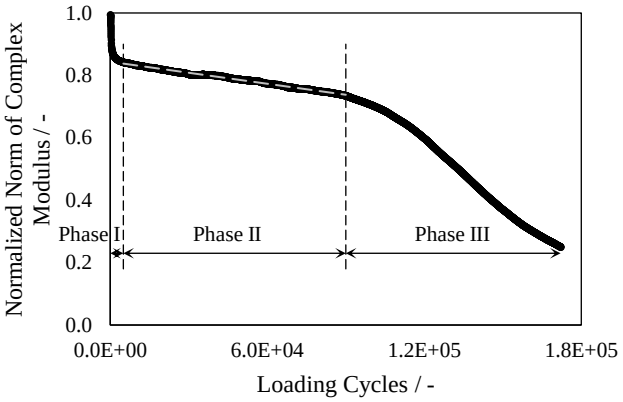

Figure 4.35 – Schematical representation of stiffness versus loading cycles derived from TS-based F test (Example of binder S1).

When focusing on the evolution of the norm of complex modulus derived from TS-based FRF_S tests, it is evident the diverse impacts of the rest period. Figure 4.36 displayed, by way of example, the behavior of materials in the second loading interval, after being damaged to 35 % abetment of $|G^*|_0$ and left to heal at different T_{RP}. By visually comparing the behaviors, it is worth observing that at the beginning of the loading application, phase I is generally exhibited, regardless of the imposed T_{RP}. Such an observation is presumably due to the fact that phase I is mostly driven by undesired biasing effects, independent on the damaged-healed microstructural state achieved due to healing. Instead, it can be assumed that the contribution of fatigue damage is minimal [132]. This is also supported by the experimental observation that, whenever the first fatigue loading is halted, a quasi-immediate stiffness increment is generally witnessed, caused by the progressive decrease of local heat-

ing and thixotropic effects [7]. The role of fatigue resistance is predominant in phase II, which plays an important role in retarding the occurrence of macrocracks of phase III. This is thought to reflect and discriminate the contribution of self-heling. In fact, it can be reasonably assumed that if the self-healing process is not completely developed in a specific cracked zone, phase I is followed by a rapid deterioration due to inability of the partially healed material to resist further degradation. As the self-healing mechanism is developed to a higher degree, phase II is found to be restored to a greater extent.

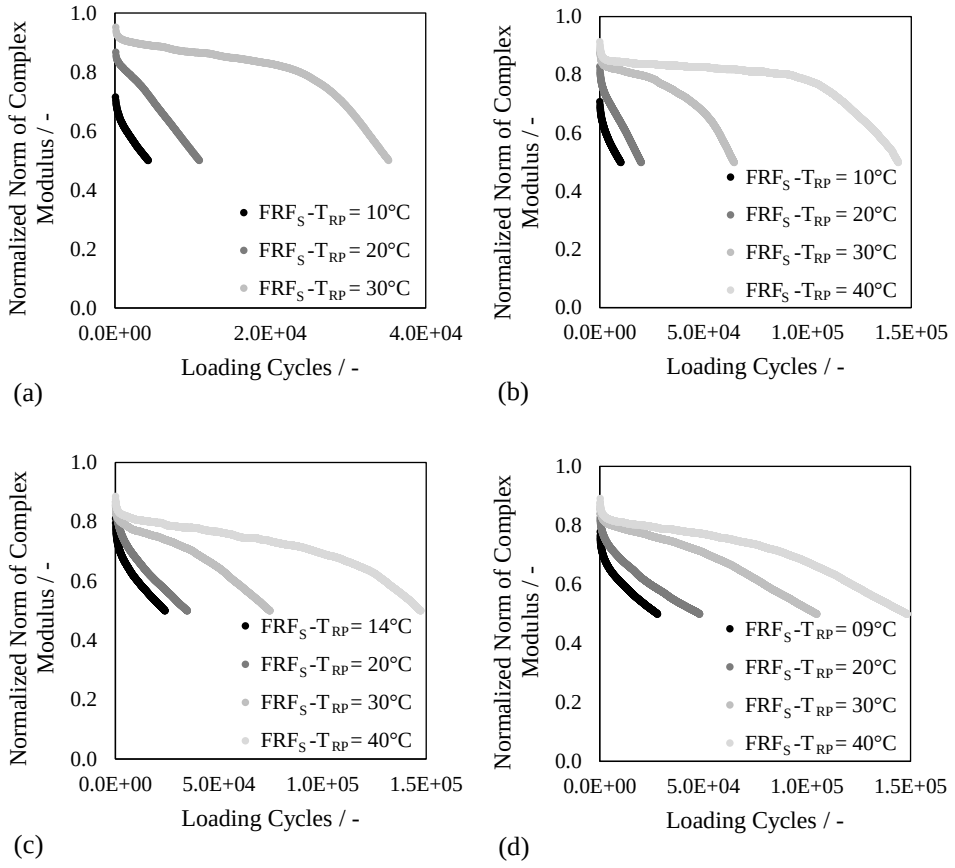

Figure 4.36 – $|G^*|/|G^*|_0$ versus loading cycles corresponding to the loading interval after rests at different T_{RP}, derived from TS-based FRF_S tests, in the case of 35 % drop of $|G^*|_0$, for binders N1 (a), N2 (b), S1 (c), S2 (d).

When focus is placed on the behavior of neat binders, it can be noted that the increase of T_{RP} value is found to have a progressively significant impact on both, stiffness and fatigue endurance gain. A different behavior, instead, can be depicted in the case of the polymer modified binder. In fact, it is interesting to note that roughly similar stiffness restoration is

achieved regardless of the T_{RP} value, although this is partially imputed to recovery. Rather, the endurance to loading cycles is significantly dependent on T_{RP}.
Whether it means that the fatigue endurance represents the state of cracks' closure, once the material is retested at high strain level, if cracks have not healed, they open very easily. Instead, it is postulated that whether low strains are applied, cracks stay close, thus resulting in higher stiffness gain. This reinforces the fact that stiffness is not a good state variable for healing because it does not exactly reflect the corresponding resistance to fatigue loading (as also outlined in section 4.3.1 in the case of index I_G and I_N).

4.4.4 General Methodology and Results

Based on the abovementioned observations, this section introduces the methodology implemented to quantify healing by means of the S-VECD concepts. The complete analytical steps are presented with respect to binder N1, for which additional tests have been performed with the purpose of corroborating the reliability of the results (as showed in Table 3.5). The S-VECD formulations (Eq. 74 and Eq. 81) have been implemented to calculate the DCC of the two loading phases of TS-based FRF_S tests. It is reminded that the DCC represents the unique function $C(S)$ existing between the material integrity C, and the damage S. Such a damage, according to the work potential framework, is the result of the incremental deterioration process. Healing, instead, allows for the progressive reversal of damage, driven by thermodynamic-chemical forces. This results in a net reduction of S by a quantity hereinafter termed as S_H, schematically represented in Figure 4.37. However, the value of S_H cannot be analytically computed, because it would require the relationships between S_H and the healing-related driving forces to be known [164]. Besides, it must be underlined that, from the theoretical perspective, damage could not be reversed because the damage evolution law is founded on irreversible processes.
Contrariwise, the value of pseudo stiffness after the rest period, C_{aR}, is immediately calculated by means of Eq. 74, which requires the solely viscoelastic properties and the shear stress response. This directly quantifies the microdamage healing in terms of material integrity (herein termed as C_H). However, it is underlined that the values of C_{aR} can be overestimated due to possible material recovery attributed to biasing effects, which merits further considerations, as discussed thereinafter.
Once the value of C_H is defined, it could be straightforwardly used to calculate S_H if the progression of damage within the partially healed specimen was the same of that occurring within the undamaged sample. However, as previously observed (see §4.4.3), damaging of previously damaged material behaves differently than damaging of non-damaged material.

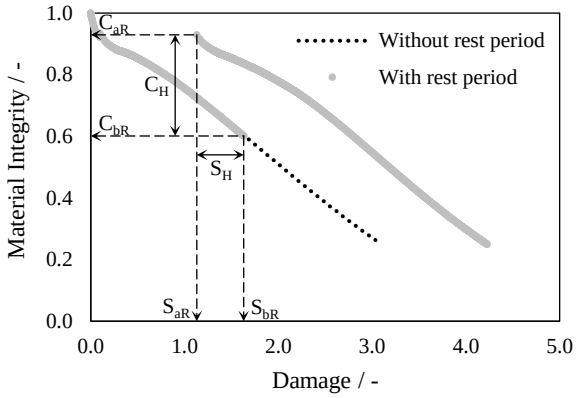

Figure 4.37 – Schematic representation of material integrity versus damage before and after the rest period.

It is inferred that this observation is reflected in the $C(S)$ function. Thus, in order to evaluate S_H, a reverse approach was adopted by starting with the assumption which underlines that the DCC governs, whether it is continuous loading or healing. This means that any rest period would lead to the restoration of C, directly corresponding to changes of S. However, when the material is reloaded, after a rest interval at some temperature and some time, the damage progression does not follow exactly the previous path, because the C values would change differently than the reversal of S values. Thus, C value changing is not an exact indication of how much the S value has changed.

Preliminary Application of S-VECD Model

It follows that the S-VECD analysis is preliminarily conducted by assuming that no damage is reversed after the rest period (S_{bR}=S_{aR} which implies S_H=0). Thus, the DCCs corresponding to the first and second loading phases (hereinafter indicated as DCC_I and DCC_{II}, respectively) are derived in Figure 4.38, by implementing Eq. 74 and Eq. 81 on data from TS-based FRF_S tests in the case of binder N1 corresponding to $\Delta|G^*|$ of 35 %, characterized by same testing conditions except for the values of T_{RP}. By looking at Figure 4.38, it can be noticed that all the DCC_I collapse on the same curve, corresponding to the DCC of TS-based F test that represents the reference fatigue behavior. The DCC_I eventually reach the imposed damage level (represented by the dashed line), after which the binder is left idle for t_{RP} equal to 2 hours at T_{RP}.

The progression of $C(S)$ of DCC_{II} curves, once the material is reloaded, are instead marked by an initial deviation from the DCC_I. It follows that the S value, for some time, may be governed by a different $C(S)$ relationship, until the deviation eventually vanishes once the

material returns to the material state achieved at the end of DCC_I. At this point, all the DCC_{II} are found to follow back along the same $C(S)$, as indicated by the fact that they become all parallel to the reference DCC.

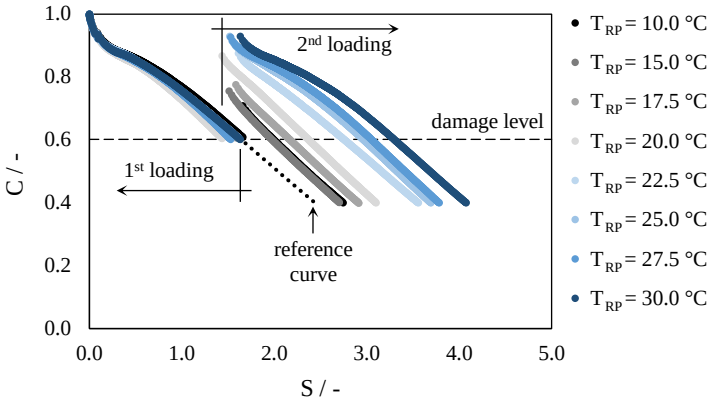

Figure 4.38 – DCCs gathered from TS-based FRF_S tests, evaluated at different values of T_{RP} (binder N1 damaged with $\Delta|G^*|$ of 35 % at T_F = 10 °C)

Non-Linear and Thixotropic Biasing Effects

By referring to both the first and second loading phases of TS-based FRF_S tests, it must be underlined that the imposed strain level equal to 2 % exceeds the linear viscoelastic frontier (see §3.4). Thus, it is postulated that part of the modulus reductions is attributed to deleterious microstructural damage, while another part is imputed to non-linearity. Therefore, non-linearity was implemented within the S-VECD framework by introducing the non-linear shift factors presented in section §4.1. The horizontal shift a_γ is applied to the reduced time, with the purpose of changing the extension of the damage, whereas the vertical shift h_G changes the value of C. This is mathematically described in Eq. 88 and Eq. 89, where t'_R represents the strain-dependent reduced time, and $\gamma^R_{p,NLVE}$ is the pseudo non-linear strain calculated by means of Eq. 90 [127].

$$t'_R = \frac{t_R}{a_\gamma} = \frac{t}{a_T \cdot a_\gamma} \qquad \text{(Eq. 88)}$$

$$C = \frac{\tau_p}{\gamma^R_{p,NLVE} \cdot DMR} \qquad \text{(Eq. 89)}$$

$$\gamma^R_{p,NLVE} = \gamma_p \cdot |G^*|_{NLVE}(\omega_R) = \gamma_p \cdot \frac{1}{h_G}|G^*|_{LVE}(\omega'_R) \qquad \text{(Eq. 90)}$$

After including non-linearity in the analysis, results of DCC_I and DCC_{II}, showed in Figure 4.39, were characterized by a vertical shift toward higher values of C and greater extent of S. This is consistent with the expectations since non-linearity is generally superimposed to damage, thus leading to underestimate the final material response.

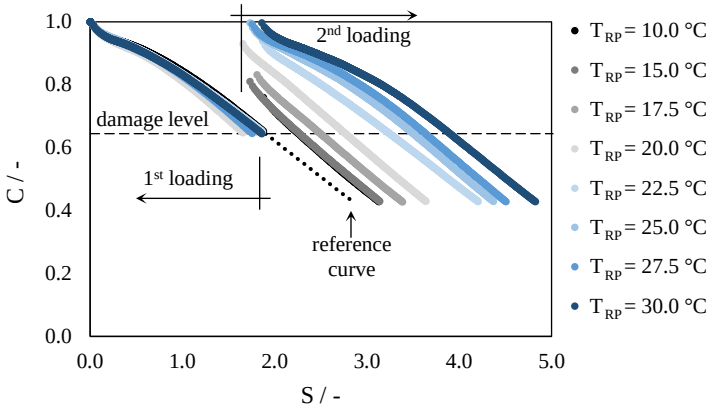

Figure 4.39 – DCCs gathered from TS-based FRF_S tests after including non-linearity (binder N1 damaged with $\Delta|G^*|$ of 35 % at T_F = 10 °C)

Whether non-linearity can cause underestimation of the results, thixotropy is referred to undesired effects superimposed to self-healing thus leading to overestimate the real self-healing capability. In fact, the increment in stiffness exhibited at the end of rest period due to hardening processes can be overlapped to that due to material self-healing. By referring to the S-VECD approach, this can result in an overestimation of the material integrity C, which may also reflect different changes in the state variable S, because C is directly distributed in the S calculation. For such a reason, results derived from the rest period of TS-based RF_S tests were analyzed to introduce a factor a_t evaluated in Eq. 91, as the ratio between the norm of complex modulus recorded at the end of the rest period and that measured at the beginning of the rest (see Figure 4.17). a_t is introduced to reflect the time and temperature-dependent increment in stiffness due to rest and it is ≥ 1 by definition.

$$a_t = \frac{|G^*|_{R,f-RF}}{|G^*|_{C,f-RF}} \qquad \text{(Eq. 91)}$$

$$C = \frac{\tau_p}{\gamma^R_{p,NLVE} \cdot DMR \cdot a_t} \qquad \text{(Eq. 92)}$$

Results obtained after introducing the factor a_t are presented by way of example in Figure 4.40 for binder N1 and Figure 4.41 for binder S1. The graphs show the comparison between the reference DCC obtained from TS-based F test and the DCC gathered from TS-based

RF_S test, before (a) and after (b) the application of the factor a_t. By referring to Figure 4.40 (a) and Figure 4.41 (a), it can be noted that when the specimen is subjected to a rest period prior to the application of a single loading phase, the initial point of the DCC is higher than 1, thus the whole DCC is shifted toward higher value as a result of possible thixotropy-related effects. When the factor a_t is introduced, the DCC of the TS-based RF_S test collapses on top of the reference DCC, as shown in Figure 4.40 (b) and Figure 4.41 (b).

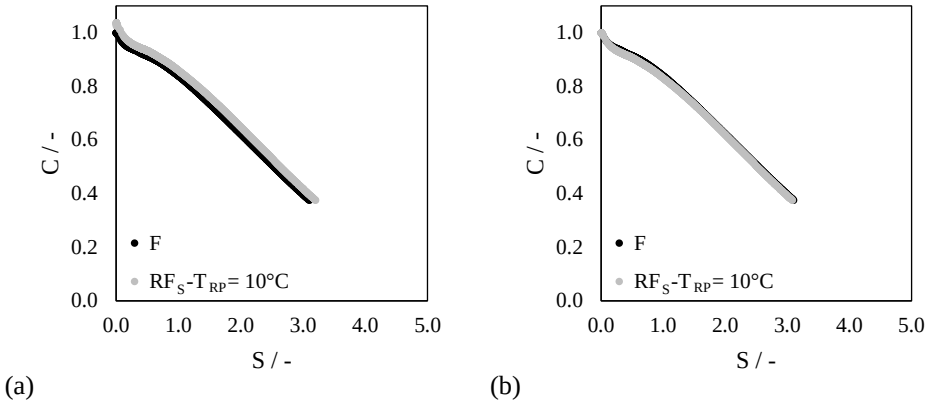

Figure 4.40 – Damage characteristic curves of binder N1, obtained from TS-based F and RF_S (T_{RP} = 10 °C) tests before (a) and after (b) the application of the factor a_t.

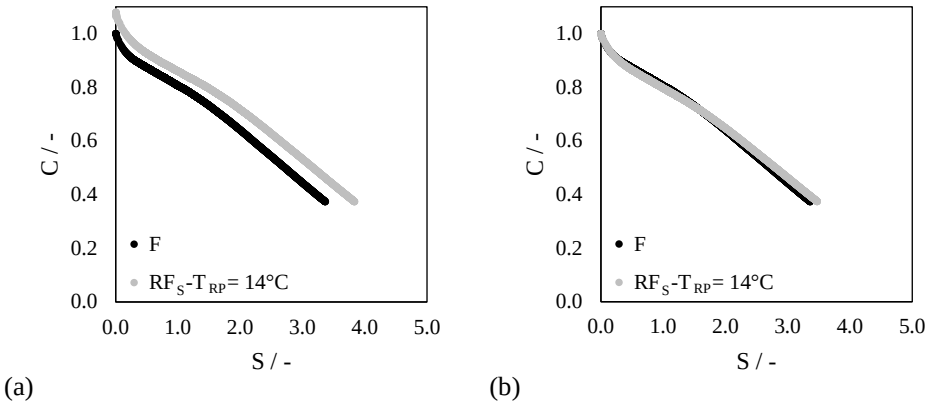

Figure 4.41 – Damage characteristic curves of binder S1, obtained from TS-based F and RF_S (T_{RP} = 14 °C) tests before (a) and after (b) the application of the factor a_t.

Figure 4.42 shows the results of C values calculated with Eq. 92 as a function of S variable after the T_{RP} conditions evaluated in TS-based RF_S test. It can be noticed that the damage characteristic curves are the same, irrespective of temperature history imposed during the rest period. The maximum deviations from the reference DCC were found for binder N2

(b), for C values lower than around 0.6, due to the higher variability of results in terms of extension of fatigue loading phase.

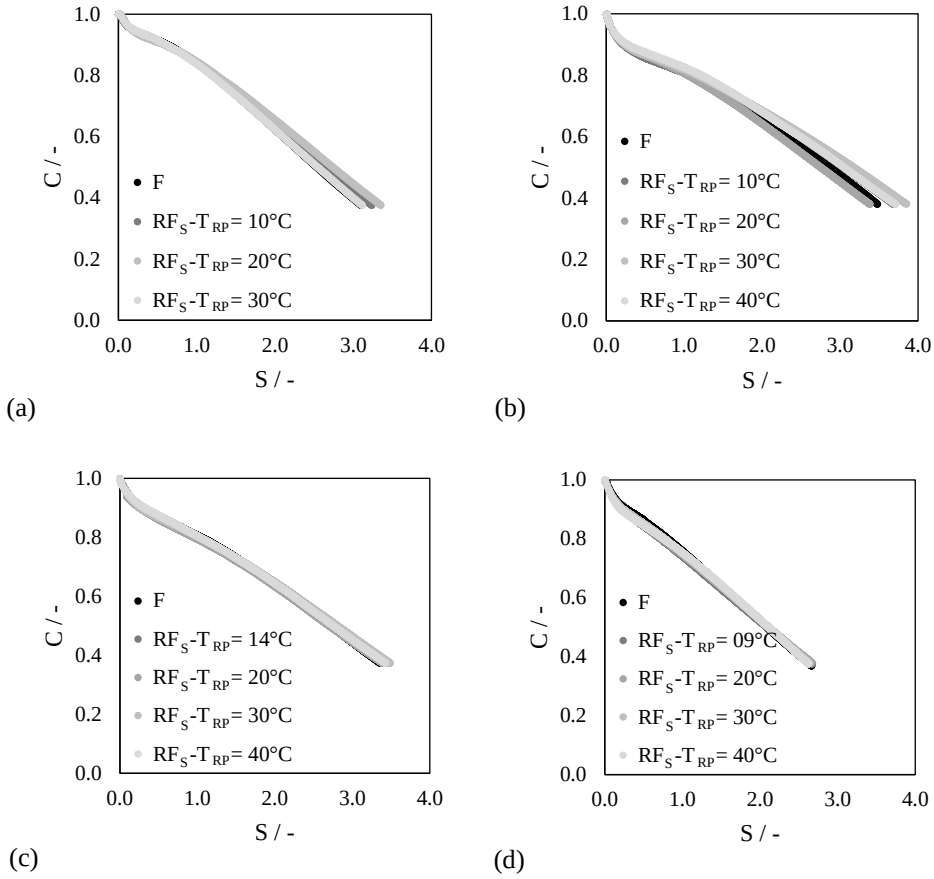

Figure 4.42 – Damage characteristic curves of binder N1 (a), N2 (b), S1 (c) and S2 (d), obtained from TS-based F and RF_S tests in several T_{RP} conditions after introducing the factor a_t.

Material Integrity and Microdamage Self-Healing

As observed in Figure 4.33 and Figure 4.34, by referring to the $|G^*|$ versus number of cycles, and in Figure 4.39 in terms of C versus S, during the reloading phase the modulus decreases in a way that is strictly dependent on the degree of molecular interdiffusion and entanglement of the healing process [138]. Such a reduction is prolonged upon reaching the same damage level achieved by the specimen before the rest. Eventually, the damage progressively increases in a way that is similar to the continuous cyclic fatigue test (F test). In this regard, as deeply discussed in the previous sections, it is important to remind that the number of loading cycles needed in the second loading phase to achieve same stiffness as

before the rest period (i.e. same damage level) directly affect the fatigue life extension (see §4.3.5). In this regard, self-healing effect on the fatigue life is grasped intuitively. However, in the context of the S-VECD model, the material endurance to damage is governed by the $C(S)$ curve, which requires the evaluation of the healed microdamage, S_H. Therefore, $S_H(T_{RP})$ resulting after the application of each rest period at the specific T_{RP}, has been back calculated by iteratively assuming a net reduction S_H, until the path of curve in region II collapsed on the $C(S)$ curve, obtained from F test (without any rest interval). The obtained values of S_H as a function of T_{RP} at a prefixed t_{RP} value are displayed in Figure 4.43, in the case of $\Delta|G^*|$ equal to 35 % (a) and 50 % (b).

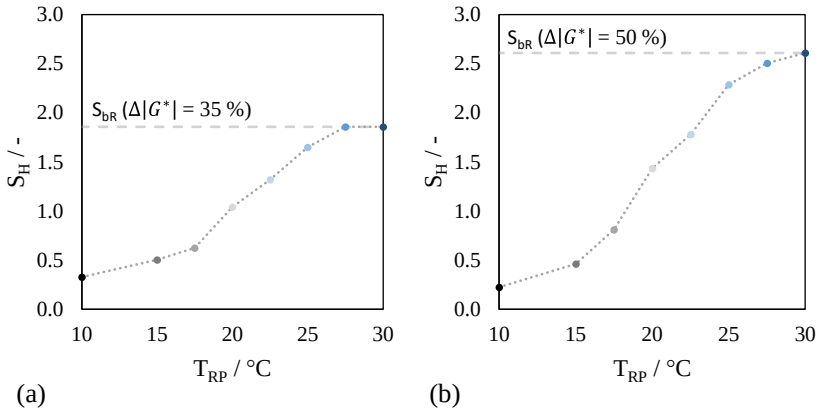

Figure 4.43 – Progression of S_H versus T_{RP}, corresponding to $\Delta|G^*|$ equal to 35 % (a) and 50 % (b).

From these results, the healing response of the binder is clearly highlighted. This allows to track the progression of the state variable S over the temperature of rest (T_{RP}), thus conveying hints about the material internal state. Instead, C refers to how this looks like in terms of material integrity at low strain. This is specifically true when considering the rest period, during which the shear strain is low enough to be in the linear viscoelastic domain. Thus, similar considerations drawn for the progression of S_H can be deduced in the case of C_H. However, differently from S_H which can be calculated at the end of the specific rest period, thus being a single value at the specific t_{RP}-T_{RP} combination, the progression of C_H can be evaluated over the entire rest period. This is mathematically obtained by means of Eq. 93:

$$C_H(\Delta t_{RP}) = \frac{|G^*|(\Delta t_{RP-i})_{FRF}}{DMR_{FRF}} \cdot \frac{DMR_{RF}}{|G^*|(\Delta t_{RP-i})_{RF}} \qquad \text{(Eq. 93)}$$

Where DMR_{FRF} and DMR_{RF} are both factors accounting for the specimen-to-specimen variability in FRF_S and RF_S tests. $|G^*|(\Delta t_{RP-i})_{FRF}$ and $|G^*|(\Delta t_{RP-i})_{RF}$ are the norms of complex modulus at each time step $\Delta t_{RP,i}$ of rest period in TS-based FRF_S and RF_S tests, re-

spectively. It is postulated that part of the $|G^*|(\Delta t_{RP-i})_{FRF}$ value can be attributed to self-healing, while another part is the consequence of the combined effect of transient temperature and thixotropy. Instead, $|G^*|(\Delta t_{RP-i})_{RF}$ values account only for thermal and thixotropic changes, as implied by the absence of a damage state prior to rest. Therefore, it is inferred that the C_H values reflect, by definition, the self-healing process happening in the low strain domain. Results of the C progression as a function of t_{RP} are derived at different T_{RP} values and displayed in Figure 4.44, in the case of $\Delta|G^*|$ equal to 35 % (a) and 50 % (b).

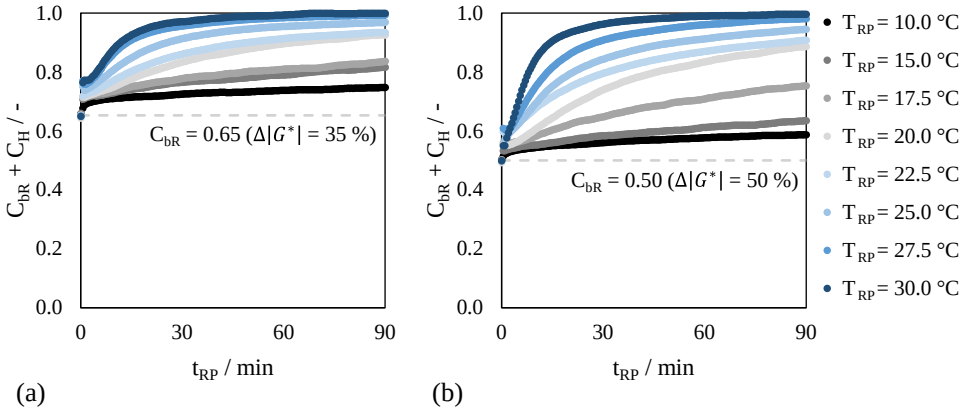

Figure 4.44 – Progression of C_H versus t_{RP}, corresponding to $\Delta|G^*|$ equal to 35 % (a) and 50 % (b).

From Figure 4.44, the material responses over time at different temperatures of rest are clearly distinguished. As expected, t_{RP} and T_{RP} play key roles in the material integrity restoration, leading to higher degree of healing mechanisms with the increase of both the factors. Based on the obtained outcomes, the healing model would require a fitting functional form to describe the trend in C_H and S_H, depending on the influencing factors such as t_{RP}, T_{RP} and $\Delta|G^*|$. In doing this, the t-TS principle, broadly proven to be viable to linear viscoelastic and damage responses, was applied to healing. In this regard, its applicability to healing was recently demonstrated to hold for bituminous binders and mixture, in the case of constant temperature all over the test [130,167]. Besides, it has been assumed to be viable in the previous section of this thesis (see §4.3.4). However, it has never been proven its applicability when the temperature of rest is varied. Therefore, in order to stretch the time scale of rest, values of C_H and S_H were reduced to a reference temperature assumed to be equal to 10 °C by means of t-TS shifting, relying upon WLF function (see §4.1). The reduced rest period, t_{RP_R}, was introduced by discretizing Eq. 79 into Eq. 94:

$$t_{RP_R} = \sum_{i=0}^{m} \frac{\Delta t_i}{a_T[T_{RP}(\Delta t_i)]} \qquad \text{(Eq. 94)}$$

Where m is the number of data points, Δt_i is the acquisition time (imposed to be equal to 30 seconds) during the rest period and a_T is the temperature shift factor evaluated at the temperature $T_{RP}(\Delta t_i)$. The values of $T_{RP}(\Delta t_i)$, assumed to be constant within the preselected acquisition time, were back calculated by rearranging Eq. 26 into Eq. 95 in order to obtain $\omega_R(|G^*|)$. Once the value of $\omega_R(|G^*|)$ is known, the shift factors a_T can be immediately calculated as the ratio of $\omega_R(|G^*|)$ and the testing angular frequency, ω. This allowed determination of the $T_{RP}(\Delta t_i)$ values by rearranging Eq. 28 into Eq. 96:

$$\omega_R(|G^*|) = \omega_0 \left[\left(\frac{|G^*|}{|G^*|_g} \right)^{\frac{log2}{mR}} - 1 \right]^{-\frac{R}{log2}} \quad \text{(Eq. 95)}$$

$$T_{RP}(\Delta t_i) = \frac{C_1 \cdot T_R + loga_T \cdot T_R - C_2 \cdot loga_T}{C_2 + loga_T} \quad \text{(Eq. 96)}$$

Reliability of $T_{RP}(\Delta t_i)$ values was verified by measuring the effective temperature of the specimen by means of a thermocouple placed in its core, during trial tests conducted with same T_{RP} history of that of TS-based FRF_S tests. This allowed to catch the transient temperature within the specimen, caused by changing the testing temperature from T_F to the target T_{RP}. Values of measured temperature was in overall good agreement with the back calculated temperature, as shown by way of example in Figure 4.45, which displays the temperature variation over the rest period from a T_F value equal to 10 °C to a T_{RP} value of 20 °C (a) and 30 °C (b).

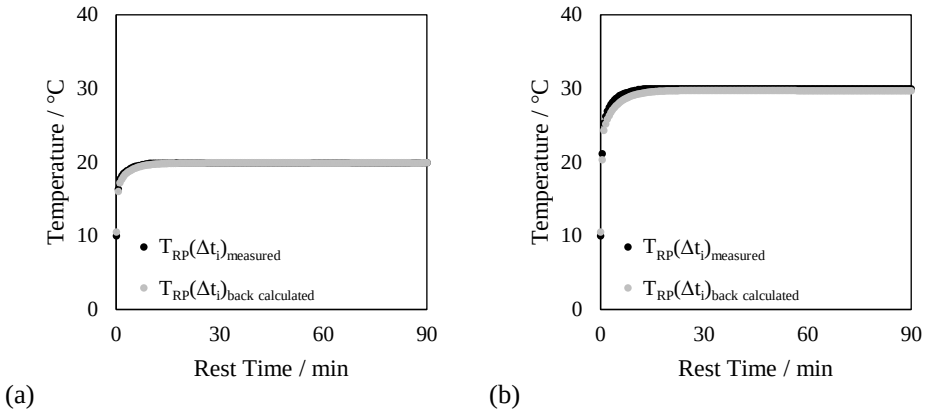

Figure 4.45 – Comparison between measured and back calculated temperatures during the transition from T_F value equal to 10 °C to T_{RP} value of 20 °C (a) and 30 °C (b).

The shifting process of data allowed the construction of self-healing master curves at the reference T_{RP} of 10 °C, which represent the healing capabilities of bituminous binders. This

is displayed in the form of C_H-t_{RP_R} and S_H-t_{RP_R} diagrams of Figure 4.46 in the case of $\Delta|G^*|$ equal to 35 % (a) and 50 % (b). For each binder, data points were fitted to the generalized logistic function presented in Eq. 97 and Eq. 98, for the material integrity and damage parameter, respectively. Upper boundary corresponds to complete healing (100 % of C_H and S_H) and lower limit depicts no healing (0 % of C_H and S_H).

$$C_H\left(t_{RP_R}\right)[\%] = \frac{100}{(1 - C_{bR})} \cdot \left(\frac{1}{\left[1 + \delta_C \cdot e^{-\eta_C\left(log t_{RP_R} - \vartheta_C\right)}\right]^{\delta_C{}^{-1}}} - C_{bR} \right) \quad \text{(Eq. 97)}$$

$$S_H\left(t_{RP_R}\right)[\%] = 100 \cdot \frac{1}{\left[1 + \delta_S \cdot e^{-\eta_S\left(log t_{RP_R} - \vartheta_S\right)}\right]^{\delta_S{}^{-1}}} \quad \text{(Eq. 98)}$$

Where:

- δ_C and δ_S = shape factors of $C_H\left(t_{RP_R}\right)$ and $S_H\left(t_{RP_R}\right)$ curves, respectively;
- η_C and η_S = slopes of the $C_H\left(t_{RP_R}\right)$ and $S_H\left(t_{RP_R}\right)$ curves, respectively;
- ϑ_C and ϑ_S = inflection points of the $C_H\left(t_{RP_R}\right)$ and $S_H\left(t_{RP_R}\right)$ curves, respectively.

Corresponding regression coefficients are listed in Table 4.8 and Table 4.9, in the case of C_H and S_H, respectively. By referring to Figure 4.46, it can be noted that the percentage of healing increases in the reduced time domain, i.e. increment in temperature. In the case of both the healing parameters, C_H and S_H, results show the validity of t-TS principle even in the case of healing, when the temperature is increased during the rest. This implies that a specific healing stage can be reached either at higher temperatures and shorter times, or at lower temperatures and longer times.

By considering Figure 4.47 in the case of $\Delta|G^*|$ equal to 35 % (a) and 50 % (b), results in terms of C_H were always found greater than S_H. This is indicated by the fact that all data points are below the identity line (S_H=C_H), similarly to the considerations made in section 4.3. Although their relative differences are lower than those exhibited in the case of indices I_G and I_N (see §4.3.1), it is worth highlighting that the parameter S_H was found more conservative than C_H. Even when the S-VECD analysis is implemented, accounting also for non-linearity and thixotropy, C_H which represents the material integrity was found to be more prone to reflect partial healing stages, thus leading to an overestimation of the real healing performance of binders. Instead, S_H is found to be more sensitive to the degree of molecular interdiffusion and entanglement, which represent the conclusive phases of the healing phenomenon.

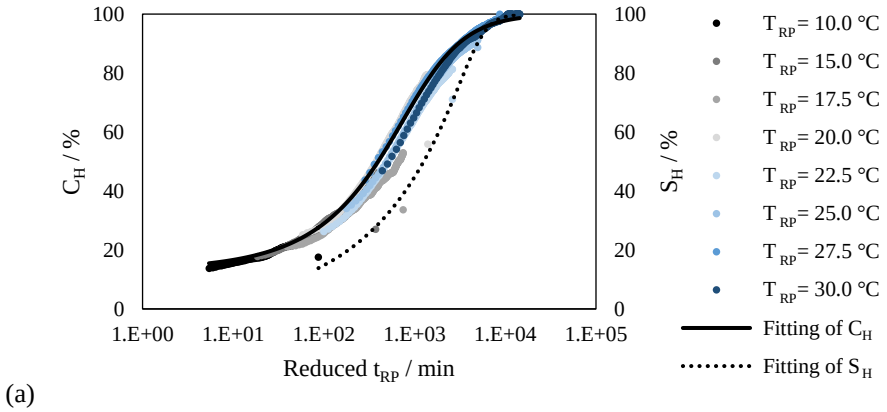

(a)

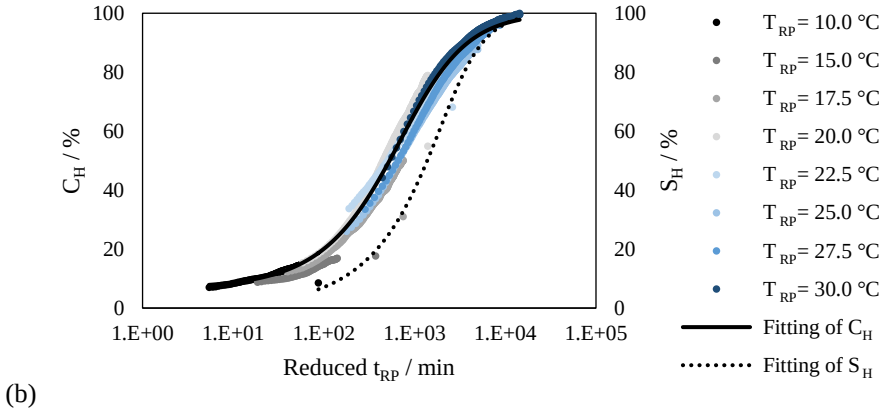

(b)

Figure 4.46 – Self-healing master curves of C_H and S_H at the reference T_{RP} of 10 °C in the case of $\Delta|G^*|$ equal to 35 % (a) and 50 % (b).

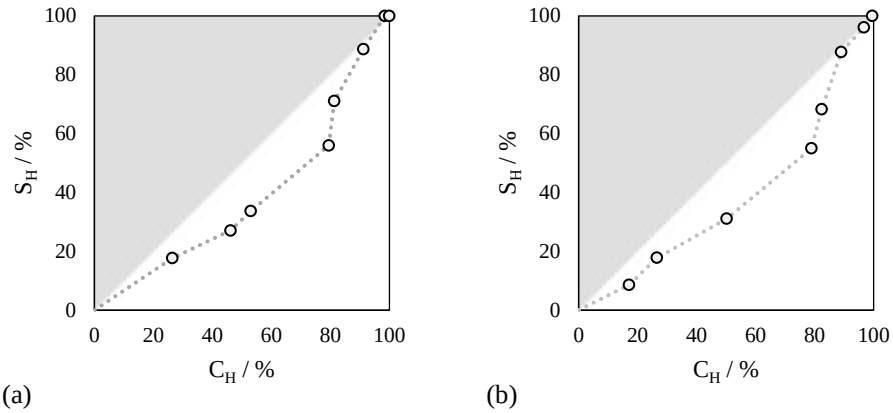

(a) (b)

Figure 4.47 – S_H versus C_H for the binder N1 in the case of $\Delta|G^*|$ equal to 35 % (a) and 50 % (b).

Figure 4.48 and Figure 4.49 extend the results presented above to all the binders: N1 (a), N2 (b), S1 (c) and S2 (d), in the case of $\Delta|G^*|$ equal to 35 % (Figure 4.48) and 50 % (Figure 4.49). As expected, each binder exhibits a different self-healing potential, which is higher in the case of binder N1, as suggested by the greater slope of the self-healing master curve in the reduced time domain. This is consistent with the findings synthesized in Figure 4.21, 4.22 and 4.28, according to which binder N1 is characterized by the highest temperature sensitivity of its self-healing properties.

Generally talking, based on the obtained results, the methodology presented is able to capture the self-healing at any rest period and rest temperature, thus allowing to predict the self-healing potential of bituminous materials.

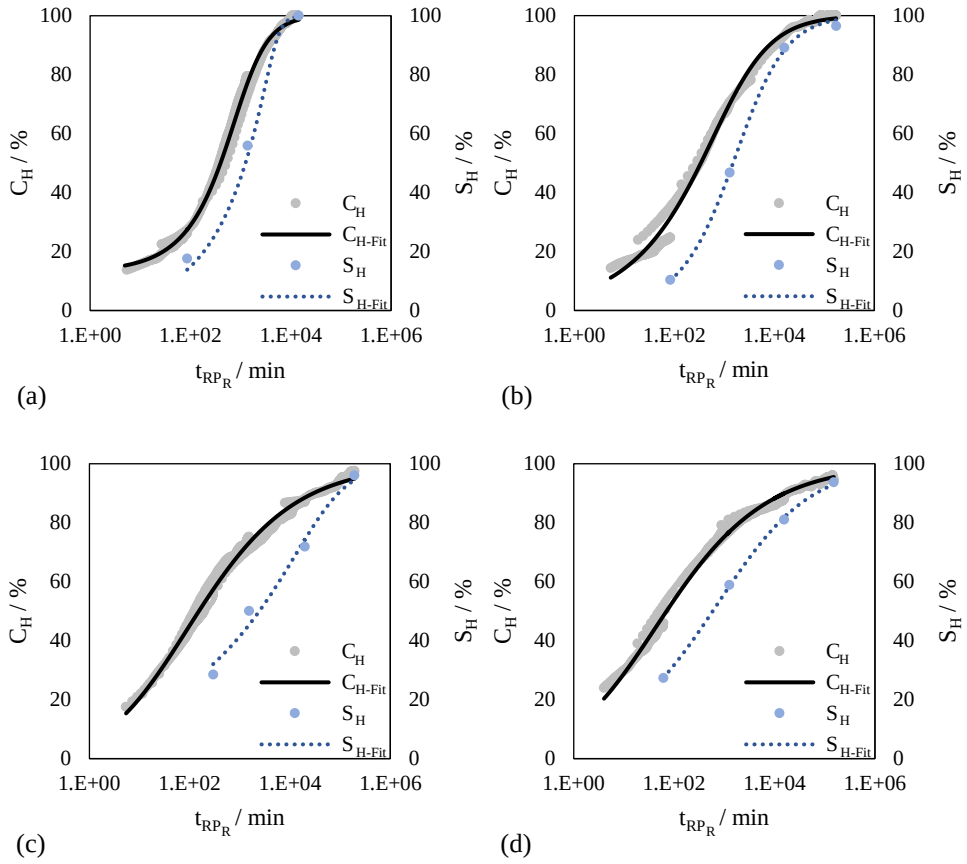

Figure 4.48 – Self-healing master curves of C_H and S_H at the reference T_{RP} of 10 °C in the case of to $\Delta|G^*|$ equal to 35 %, for binder N1 (a), N2 (b), S1 (c) and S2 (d).

Table 4.8 – Regression coefficients of self-healing master curves of C_H obtained at the reference T_{RP} of 10 °C.

Binders	N1		N2		S1		S2	
$\Delta\|G^*\|$ / %	35	50	35	50	35	50	35	50
δ_C / -	3.22	2.82	1.89	1.60	0.89	1.08	0.86	1.30
η_C / min^{-1}	2.87	2.85	2.77	2.66	1.95	1.91	1.63	2.40
$\log \vartheta_C$ / min	2.09	1.46	2.14	1.23	0.49	0.19	0.49	1.39

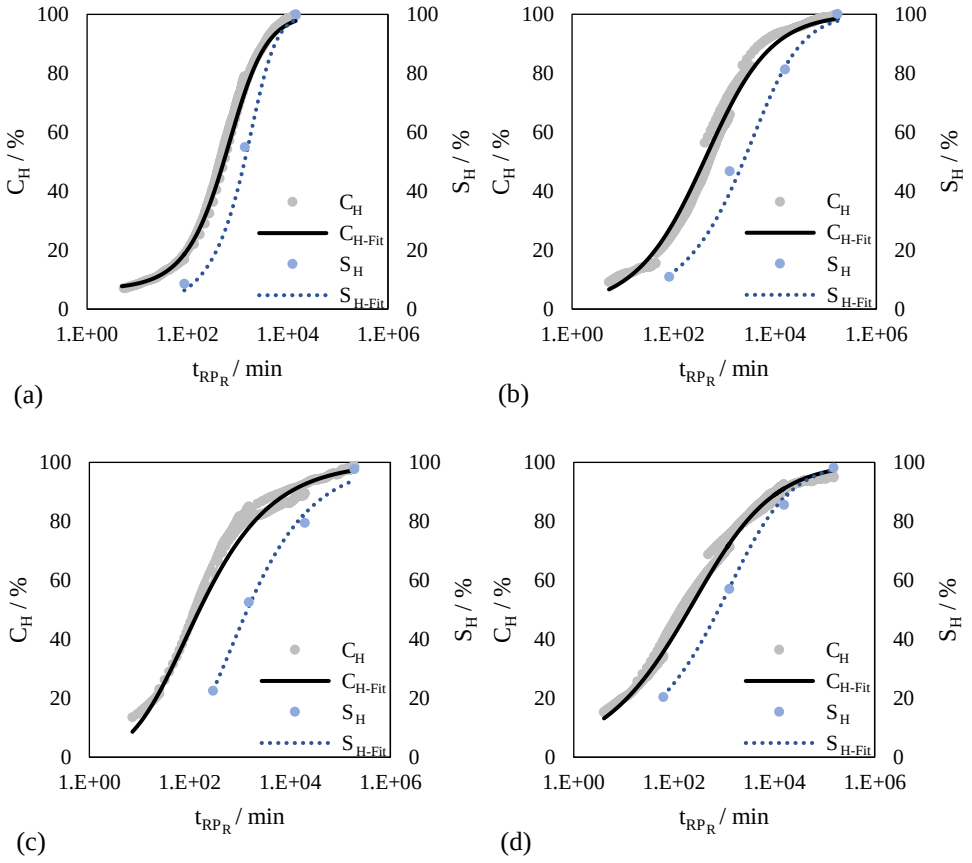

Figure 4.49 – Self-healing master curves of C_H and S_H at the reference T_{RP} of 10 °C in the case of to $\Delta|G^*|$ equal to 50 %, for binder N1 (a), N2 (b), S1 (c) and S2 (d).

Table 4.9 – Regression coefficients of self-healing master curves of S_H obtained at the reference T_{RP} of 10 °C.

Binders	N1		N2		S1		S2	
$\Delta\|G^*\|$ / %	35	50	35	50	35	50	35	50
δ_S / -	8.22	2.57	1.36	2.03	4.77	0.05	1.31	1.94
η_S / min^{-1}	9.06	4.54	2.08	2.23	2.35	1.14	1.12	1.77
$\log \vartheta_S$ / min	3.50	3.28	3.25	3.56	4.11	2.84	2.88	3.10

4.5 Highlights

The application of the different testing protocols selected in this investigation have led to different self-healing potentials of materials, based on the indices introduced by each method. The differences found in the rankings of materials have brought the light on the need of having a unique standardized protocol for the self-healing assessment. Based on such an outcome, a deeper investigation was performed by adopting a single protocol. The generalized logistic function was proposed to describe self-healing based on the fatigue endurance gain (I_N), by incorporating the variables of rest time and rest temperature. Moreover, the S-VECD model was successfully implemented to investigate the self-healing potential. Self-healing mater curves were constructed by applying t-TS principle. Thus, the t-TS principle was proven to hold even in the case of self-healing occurring during rest period performed at different temperatures. The self-healing mater curves of material integrity and damage parameter, represented in the domain of reduced rest time, were fitted to the generalized logistic function. Such master curves can be used as a straightforward tool to obtain the percentage of healing at any rest period and rest temperature, thus allowing to predict the self-healing potential. Moreover, time-dependent and non-linear biasing effects, that can occur during the rest periods and the fatigue loading phases were quantified and removed. The overall results obtained with the application of the S-VECD modeling were found to be consistent with the analysis based on the more traditional approach. In fact, as in the case of fatigue endurance gain, I_N, the parameter S_H was found to be more conservative than C_H (which may correspond to stiffness gain, I_G). Thus, C_H was found to be more prone to reflect partial healing stages, thus leading to an overestimation of the real healing performance of binders. Instead, S_H is found to be more sensitive to the degree of molecular interdiffusion and entanglement, which represent the conclusive phases of the healing phenomenon.

FINAL REMARKS

The experimental study presented in this thesis focused on a methodological approach to evaluate the self-healing potential of bituminous binders. With this purpose, experimental testing was performed, and advanced modeling was developed to interpret the results. In this context, the doctoral research was divided into three main objectives: firstly, three different testing protocols were implemented on neat and SBS-modified binders; based on the obtained results deeper investigations were focused on a single protocol by imposing several testing scenarios in terms of rest time and rest temperature; lastly, the simplified viscoelastic continuum damage approach was adopted and properly implemented to account for self-healing. The main conclusions are discussed as follows.

- The application of three different testing protocols was found to lead to different results in terms of indices introduced to quantitatively assess self-healing capabilities. The differences found in the rankings of materials stand out the urgent need of having a unique standardized protocol for the self-healing assessment. The role played by the adoption of different testing conditions and diverse analytical manipulations was found to be extremely relevant and non-negligible. Based on the results, such a universal protocol needs to account for a wide range of testing conditions, in order to be the most simulative of in-field conditions, in terms of environment and vehicular loading characteristics. In this way, the healing response of materials could be univocally established in representative scenarios, which could allow a more appropriate material selection during the design procedures of road pavements.
- Rest time and rest temperature effect on self-healing was evaluated by introducing two self-healing indices, defined to quantitatively assess the stiffness and fatigue endurance gain, respectively. Obtained results indicated that the proposed indices provide consistent information with the kinetics of the self-healing phenomenon.
- The relevance of temperature conditions which occur during rest periods was highlighted in the case of both neat and polymer-modified binders. Moreover, the flow properties of binders were found to play a crucial role in the achievement of a full healing state, that was shown to correspond to values of the flow behavior index lower than that corresponding to Newtonian behavior.

- Direct comparison of the healing potential of the binders showed that SBS modification, which is known to reduce crack accumulation rate, does not necessarily lead to an enhanced healing capability. On the other hand, when allowed to rest at sufficiently high temperatures, neat bitumen can exhibit remarkable self-healing, which leads to mechanical properties like those of the undamaged state. However, it must be underlined that the evaluation of the overall fatigue performance may lead to results that change the relative ranking of binders based exclusively on the relative assessment of self-healing. For such a reason, a comprehensive approach to the evaluation of the performance properties of bituminous binders must be based on the combined assessment of self-healing capability and fatigue resistance.
- The ranking order among the binders was found to be dependent on testing conditions considered during testing, specifically referred in this thesis to rest temperatures and rest times. Such factors need to be appropriately combined for a reliable evaluation of material self-healing performance. Thus, a single healing index is not capable of conveying a reliable ranking between materials, since it is found to be valid only for the specific condition adopted during testing.
- A new model relying on generalized logistic function was proposed to incorporate the variables of rest time and rest temperature by implementing a rest time-temperature shifting, which allowed derivation of self-healing charts for each material. Such charts can be employed as an easy and effective tool to estimate the self-healing response of a bituminous binder for any specific combination of rest time and temperature. Based on the results, it is suggested that self-healing charts can be constructed by performing a selected set of tests with specific testing conditions in terms of rest times and rest temperatures.
- The S-VECD model was successfully applied to study the self-healing potential of considered binders. In particular, the t-TS principle was applied to combine the variables of rest temperature and rest time within the reduced rest time domain, thus allowing the construction of self-healing master curves. Such curves were referred to the material integrity and damage parameter. Results have proven that the t-TS principle holds even in the case of self-healing occurring during rest period performed at different temperatures. Moreover, time-dependent and non-linear biasing effects, that can occur during rest periods and fatigue loading phases, respectively, were properly quantified and removed by combining the self-healing testing with time sweeps conducted in no-damage conditions and non-linearity testing. The self-healing master curves were fitted to generalized logistic function adopted for different damage levels. Obtained results can be used to gather the percentage

of healing at any rest period and rest temperature, thus allowing to predict the self-healing potential of bituminous binders.

Further experimental studies are certainly needed to corroborate the findings of this dissertation, by considering a wider array of materials and testing conditions to verify the proposed healing models.

- With respect to the healing curve $I_N(T_{RP})$, it would be worth investigating the effect of different temperature conditions on the damage process, thus generalizing the healing function also to fatigue phase temperatures.
- By referring to the S-VECD model, additional computational effort is certainly required to corroborate the validity of the t-TS principle by constructing self-healing master curves at different reference temperatures.
- The effect of damage level deserves to be investigated with a more comprehensive approach in order to further generalize the healing modeling.
- The prediction of healing was based on material integrity and damage parameter. However, a most rigorous approach would require the prediction of the number of loading cycles that the material is capable to endure until failure.
- With respect to the loading path between the beginning of the second loading phase and the point in which the modulus reaches same stiffness conditions of that prior to the rest period, it is specified that the analysis would deserve a more rigorous approach. This is basically due to the fact that the partially healed material behaves differently from the undamaged material if the self-healing phenomenon is not fully developed. Therefore, the governing function $C(S)$ of the partially healed material is different than that viable in the undamaged specimen.
- Application of the proposed models to bituminous binders subjected to aging also deserves consideration in future studies.

REFERENCES

[1] Al-Qadi, I. L., & Nassar, W. N. (2003). Fatigue shift factors to predict HMA performance. International Journal of Pavement Engineering, 4(2), 69-76. https://doi.org/10.1080/10298430310001593254.

[2] Lytton, R. L., Uzan, J., Fernando, E. G., Roque, R., Hiltunen, D., & Stoffels, S. M. (1993). Development and validation of performance prediction models and specifications for asphalt binders and paving mixes (Vol. 357). Washington, DC: Strategic Highway Research Program.

[3] Ayar, P., Moreno-Navarro, F., & Rubio-Gámez, M. C. (2016). The healing capability of asphalt pavements: a state of the art review. Journal of Cleaner Production, 113, 28-40. https://doi.org/10.1016/j.jclepro.2015.12.034

[4] Bazin, P., & Saunier, J. (1967, January). Deformability, fatigue and healing properties of asphalt mixes. In International Conference on the Structural Design of Asphalt Pavements.

[5] García, Á. (2012). Self-healing of open cracks in asphalt mastic. Fuel, 93, 264-272. https://doi.org/10.1016/j.fuel.2011.09.009.

[6] Lytton, R. L., Zhang, Y., Luo, X., & Luo, R. (2015). The fatigue cracking of asphalt mixtures in tension and compression. In Advances in Asphalt Materials (pp. 243-272). Woodhead Publishing. https://doi.org/10.1016/B978-0-08-100269-8.00008-8.

[7] Leegwater, G., Taboković, A., Baglieri, O., Hammoum, F., & Baaj, H. (2020, December). Terms and definitions on crack-healing and restoration of mechanical properties in bituminous materials. In RILEM International Symposium on Bituminous Materials (pp. 47-53). Springer, Cham. https://doi.org/10.1007/978-3-030-46455-4_6

[8] Van den Bergh, W., Van de Ven, M. F. C. (2012). The influence of ageing on the fatigue and healing properties of bituminous mortars. Procedia-Social and Behavioral Sciences, 53, 256-265. https://doi.org/10.1016/j.sbspro.2012.09.878

[9] Baaj, H., Mikhailenko, P., Almutairi, H., & Di Benedetto, H. (2018). Recovery of asphalt mixture stiffness during fatigue loading rest periods. Construction and Building Materials, 158, 591-600. https://doi.org/10.1016/j.conbuildmat.2017.10.016

[10] Bonnaure, F. P., Huibers, A. H. J. J., & Boonders, A. (1982). A laboratory investigation of the influence of rest periods on the fatigue characteristics of bituminous mixes (with discussion). In Association of Asphalt Paving Technologists Proceedings (Vol. 51).

[11] Findley W.N., Lai J.S., Onaran K. (1989). Creep and relaxation of nonlinear viscoelastic materials: with an introduction to linear viscoelasticity. Dover Publications.

[12] Sun, D., Sun, G., Zhu, X., Guarin, A., Li, B., Dai, Z., & Ling, J. (2018). A comprehensive review on self-healing of asphalt materials: Mechanism, model, characterization and enhancement. Advances in Colloid and Interface Science, 256, 65-93. https://doi.org/10.1016/j.cis.2018.05.003

[13] Di Benedetto, H., de La Roche, C., Baaj, H., Pronk, A., & Lundström, R. (2004). Fatigue of bituminous mixtures. Materials and structures, 37(3), 202-216. https://doi.org/10.1007/BF02481620

[14] Bodin, D., Soenen, H., & de La Roche, C. (2004, May). Temperature effects in binder fatigue and healing tests. In Eurasphalt & Eurobitume Congress, Vienna (Vol. 82).

[15] Riahi, E., Allou, F., Botella, R., Dubois, F., Absi, J., & Petit, C. (2017). Quantification of self-heating and its effects under cyclic tests on a bituminous binder. International Journal of Fatigue, 104, 334-341. https://doi.org/10.1016/j.ijfatigue.2017.07.016

[16] Di Benedetto, H., Nguyen, Q. T., & Sauzéat, C. (2011). Nonlinearity, heating, fatigue and thixotropy during cyclic loading of asphalt mixtures. Road Materials and Pavement Design, 12(1), 129-158. https://doi.org/10.1080/14680629.2011.9690356

[17] Qiu, J. (2012). Self healing of asphalt mixtures: towards a better understanding of the mechanism (Doctoral dissertation, Delft University of Technology).

[18] Gaskin, J. (2013). On bitumen microstructure and the effects of crack healing (Doctoral dissertation, University of Nottingham).

[19] Mewis, J., & Wagner, N. J. (2009). Thixotropy. Advances in Colloid and Interface Science, 147, 214-227. https://doi.org/10.1016/j.cis.2008.09.005

[20] Shan, L., Tan, Y., Underwood, B. S., & Kim, Y. R. (2011). Thixotropic characteristics of asphalt binder. Journal of Materials in Civil Engineering, 23(12), 1681-1686. https://doi.org/10.1061/(ASCE)MT.1943-5533.0000328

[21] Mouillet, V., de La Roche, C., Chailleux, E., & Coussot, P. (2012). Thixotropic behavior of paving-grade bitumens under dynamic shear. Journal of Materials in Civil Engineering, 24(1), 23-31. https://doi.org/10.1061/(ASCE)MT.1943-5533.0000354

[22] Shan, L., Tan, Y., Underwood, S., & Kim, Y. R. (2010). Application of thixotropy to analyze fatigue and healing characteristics of asphalt binder. Transportation Research Record, 2179(1), 85-92. https://doi.org/10.3141/2179-10

[23] Divya, P. S., & Krishnan, J. M. (2019). How to consistently collect rheological data for bitumen in a Dynamic Shear Rheometer?. SN Applied Sciences, 1(1), 1-5. https://doi.org/10.1007/s42452-018-0088-6

[24] Masson, J. F., Collins, P., & Polomark, G. (2005). Steric hardening and the ordering of asphaltenes in bitumen. Energy & Fuels, 19(1), 120-122. https://doi.org/10.1021/ef0498667

[25] Traxler, R. N. (1947). A review of the rheology of bituminous materials. Journal of Colloid Science, 2(1), 49-68. https://doi.org/10.1016/0095-8522(47)90009-3

[26] Traxler, R. N., & Schweyer, H. E. (1936). Increase in viscosity of asphalts with time. Proceedings - American Society for Testing Materials, 36, 544-51.

[27] Little, D. N., Allen, D. H., & Bhasin, A. (2018). Modeling and design of flexible pavements and materials. Berlin: Springer. https://doi.org/10.1007/978-3-319-58443-0

[28] Collins, P., Masson, J. F., & Polomark, G. (2006). Ordering and steric-hardening in SBS-modified bitumen. Energy & Fuels, 20(3), 1266-1268. https://doi.org/10.1021/ef050403q

[29] Soenen, H., Ekblad, J., Lu, X., & Redelius, P. (2004, May). Isothermal hardening in bitumen and in asphalt mix. In Eurasphalt & Eurobitume Congress Vienna (pp. 1364-1375).

[30] Santagata, E., Baglieri, O., Tsantilis, L., & Dalmazzo, D. (2013). Evaluation of self healing properties of bituminous binders taking into account steric hardening effects. Construction and Building Materials, 41, 60-67. https://doi.org/10.1016/j.conbuildmat.2012.11.118

[31] Canestrari, F., Virgili, A., Graziani, A., & Stimilli, A. (2015). Modeling and assessment of self-healing and thixotropy properties for modified binders. International Journal of Fatigue, 70, 351-360. https://doi.org/10.1016/j.ijfatigue.2014.08.004

[32] Prager, S., & Tirrell, M. (1981). The healing process at polymer-polymer interfaces. The journal of chemical physics, 75(10), 5194-5198. https://doi.org/10.1063/1.441871

[33] Wool R.P. (1995). Polymer interfaces: structure and strength. Hanser Pub Inc. https://doi.org/10.1002/pi.1995.210380314

[34] Wool, R., & O'connor, K. M. (1981). A theory crack healing in polymers. Journal of Applied Physics, 52(10), 5953-5963. https://doi.org/10.1063/1.328526

[35] De Gennes, P. G. (1971). Reptation of a polymer chain in the presence of fixed obstacles. The Journal of Chemical Physics, 55(2), 572-579. https://doi.org/10.1063/1.1675789

[36] Kausch, H. H., Nguyen, T. Q., & Petrovska-Delacrétaz, D. (1991). Chain interdiffusion: macromolecules between Rouse and de Gennes. Physica Scripta, 1991(T35), 57. https://doi.org/10.1088/0031-8949/1991/T35/012

[37] Barber, P., & Atkinson, J. R. (1972). Some microstructural features of the welds in butt-welded polyethylene and polybutene-1 pipes. Journal of Materials Science, 7(10), 1131-1136. https://doi.org/10.1007/BF00550195

[38] Wool, R. P. (1983). Crack Healing in Polymers. Illinois University at Urbana Dept of Metallurgy and Mining Engineering.

[39] Kim, Y. H., & Wool, R. P. (1983). A theory of healing at a polymer-polymer interface. Macromolecules, 16(7), 1115-1120. https://doi.org/10.1021/ma00241a013

[40] Bucknall, C. B., Drinkwater, I. C., & Smith, G. R. (1980). Hot plate welding of plastics: factors affecting weld strength. Polymer Engineering & Science, 20(6), 432-440. https://doi.org/10.1002/pen.760200609

[41] DiMarzio, E. A., Guttman, C. M., & Hoffman, J. D. (1979). Is crystallization from the melt controlled by melt viscosity and entanglement effects?. Faraday Discussions of the Chemical Society, 68, 210-217. https://doi.org/10.1039/DC9796800210

[42] Phillips, M. C. (1998, May). Multi-step models for fatigue and healing, and binder properties involved in healing. In Eurobitume workshop on performance related properties for bituminous binders, Luxembourg.

[43] Bhasin, A., Little, D. N., Bommavaram, R., & Vasconcelos, K. (2008). A framework to quantify the effect of healing in bituminous materials using material properties. Road Materials and Pavement Design, 9(sup1), 219-242. https://doi.org/10.1080/14680629.2008.9690167

[44] Bommavaram, R. R., Bhasin, A., & Little, D. N. (2009). Determining intrinsic healing properties of asphalt binders: role of dynamic shear rheometer. Transportation Research Record, 2126(1), 47-54. https://doi.org/10.3141/2126-06

[45] Schapery, R. A. (1984). Correspondence principles and a generalized J integral for large deformation and fracture analysis of viscoelastic media. International Journal of Fracture, 25(3), 195-223. https://doi.org/10.1007/BF01140837

[46] Lytton, R. L., Masad, E. A., Zollinger, C., Bulut, R., & Little, D. N. (2005). Measurements of surface energy and its relationship to moisture damage (No. FHWA/TX-05/0-4524-2).

[47] Robertson, R. E., Branthaver, J. F., Harnsberger, P. M., Petersen, J. C., Dorrence, S. M., McKay, J. F., ... & Williams, T. (2001). Fundamental properties of asphalts and modified asphalts, volume I: Interpretive report (No. FHWA-RD-99-212,). https://trid.trb.org/view/690788

[48] Little, D. N., Prapnnachari, S., Letton, A., & Kim, Y. R. (1993). Investigation of the microstructural mechanism of relaxation and fracture healing in asphalt. Texas Transportation Inst College Station.

[49] Hefer, A. W. (2004). Adhesion in bitumen-aggregate systems and quantification of the effects of water on the adhesive bond (Doctoral dissertation, Texas A&M University).

[50] Lytton, R. L. (2000). Characterizing asphalt pavements for performance. Transportation Research Record, 1723(1), 5-16. https://doi.org/10.3141/1723-02

[51] Fowkes, F. M. (1964). Attractive forces at interfaces. Industrial & Engineering Chemistry, 56(12), 40-52. https://doi.org/10.1021/ie50660a008

[52] Fowkes, F. M. (1966). The relation of the attractive forces at interfaces to wetting, spreading, adsorption, and long-range attractive forces. In Fundamental Phenomena in the Materials Sciences (pp. 139-164). Springer, Boston, MA. https://doi.org/10.1007/978-1-4684-8703-9_8

[53] Si, Z., Little, D. N., & Lytton, R. L. (2002). Characterization of microdamage and healing of asphalt concrete mixtures. Journal of Materials in Civil Engineering, 14(6), 461-470. https://doi.org/10.1061/(ASCE)0899-1561(2002)14:6(461)

[54] Lesueur, D. (2009). The colloidal structure of bitumen: Consequences on the rheology and on the mechanisms of bitumen modification. Advances in Colloid and Interface Science, 145(1-2), 42-82. https://doi.org/10.1016/j.cis.2008.08.011

[55] Hamraoui, A., & Nylander, T. (2002). Analytical approach for the Lucas-Washburn equation. Journal of Colloid and Interface Science, 250(2), 415-421. https://doi.org/10.1006/jcis.2002.8288

[56] García, A., Bueno, M., Norambuena-Contreras, J., & Partl, M. N. (2013). Induction healing of dense asphalt concrete. Construction and Building Materials, 49, 1-7. https://doi.org/10.1016/j.conbuildmat.2013.07.105

[57] Kim, Y. R., Little, D. N., & Lytton, R. L. (2003). Fatigue and healing characterization of asphalt mixtures. Journal of Materials in Civil Engineering, 15(1), 75-83. https://doi.org/10.1061/(ASCE)0899-1561(2003)15:1(75)

[58] García, A., Norambuena-Contreras, J., Bueno, M., & Partl, M. N. (2015). Single and multiple healing of porous and dense asphalt concrete. Journal of Intelligent Material Systems and Structures, 26(4), 425-433. https://doi.org/10.1177/1045389X14529029

[59] Wang, C., Xie, W., & Underwood, B. S. (2018). Fatigue and healing performance assessment of asphalt binder from rheological and chemical characteristics. Materials and Structures, 51(6), 1-12. https://doi.org/10.1617/s11527-018-1300-2

[60] Santagata, E., Baglieri, O., Dalmazzo, D., & Tsantilis, L. (2009). Rheological and chemical investigation on the damage and healing properties of bituminous binders. Asphalt Paving Technology-Proceedings, 28, 567.

[61] Kim, Y. R., Little, D. N., & Burghardt, R. C. (1991). SEM analysis on fracture and healing of sand-asphalt mixtures. Journal of Materials in Civil Engineering, 3(2), 140-153. https://doi.org/10.1061/(ASCE)0899-1561(1991)3:2(140)

[62] Qiu, J., Van de Ven, M. F. C., Wu, S., Yu, J., & Molenaar, A. A. A. (2009). Investigating the self healing capability of bituminous binders. Road Materials and Pavement Design, 10(sup1), 81-94. https://doi.org/10.1080/14680629.2009.9690237

[63] Bhasin, A., Bommavaram, R., Greenfield, M. L., & Little, D. N. (2011). Use of molecular dynamics to investigate self-healing mechanisms in asphalt binders. Journal of Materials in Civil Engineering, 23(4), 485-492. https://doi.org/10.1061/(ASCE)MT.1943-5533.0000200

[64] Kim, Y. R., Little, D. N., & Benson, F. C. (1990). Chemical and mechanical evaluation on healing mechanism of asphalt concrete (with discussion). Journal of the Association of Asphalt Paving Technologists, 59. https://trid.trb.org/view/487368

[65] Little, D. N., Lytton, R. L., Williams, D., & Chen, C. W. (2001). Microdamage healing in asphalt and asphalt concrete, Volume 1: microdamage and microdamage

healing, project summary report (No. FHWA-RD-98-141; Research report 7229). Turner-Fairbank Highway Research Center. https://trid.trb.org/view/690454

[66] Carpenter, S. H., & Shen, S. (2006). Dissipated energy approach to study hot-mix asphalt healing in fatigue. Transportation Research Record, 1970(1), 178-185. https://doi.org/10.1177/0361198106197000119

[67] Santagata, E., Baglieri, O., Dalmazzo, D., & Tsantilis, L. (2017). Investigating cohesive healing of asphalt binders by means of a dissipated energy approach. International Journal of Pavement Research and Technology, 10(5), 403-409. https://doi.org/10.1016/j.ijprt.2017.06.004

[68] Shen, S., Chiu, H. M., & Huang, H. (2010). Characterization of fatigue and healing in asphalt binders. Journal of Materials in Civil Engineering, 22(9), 846-852. https://doi.org/10.1061/(ASCE)MT.1943-5533.0000080

[69] Sun, D., Sun, G., Zhu, X., Pang, Q., Yu, F., & Lin, T. (2017). Identification of wetting and molecular diffusion stages during self-healing process of asphalt binder via fluorescence microscope. Construction and Building Materials, 132, 230-239. https://doi.org/10.1016/j.conbuildmat.2016.11.137

[70] Santagata, E., Baglieri, O., Dalmazzo, D., & Tsantilis, L. (2012, June). Damage and healing test protocols for the evaluation of bituminous binders. In 5th Eurasphalt & Eurobitume Congress.

[71] Lv, Q., Huang, W., & Xiao, F. (2017). Laboratory evaluation of self-healing properties of various modified asphalt. Construction and Building Materials, 136, 192-201. https://doi.org/10.1016/j.conbuildmat.2017.01.045

[72] Qiu, J., Van de Ven, M., Wu, S., Yu, J., & Molenaar, A. (2012). Evaluating self healing capability of bituminous mastics. Experimental Mechanics, 52(8), 1163-1171. https://doi.org/10.1007/s11340-011-9573-1

[73] Schaur, A., Unterberger, S., & Lackner, R. (2017). Impact of molecular structure of SBS on thermomechanical properties of polymer modified bitumen. European Polymer Journal, 96, 256-265. https://doi.org/10.1016/j.eurpolymj.2017.09.017

[74] Little, D. N., Lytton, R. L., Williams, D., & Kim, Y. R. (1999). An analysis of the mechanism of microdamage healing based on the application of micromechanics first principles of fracture and healing. Journal of the Association of Asphalt Paving Technologists, 68. https://trid.trb.org/view/639721

[75] Shen, S., & Sutharsan, T. (2011). Quantification of cohesive healing of asphalt binder and its impact factors based on dissipated energy analysis. Road Materials

and Pavement Design, 12(3), 525-546. https://doi.org/10.1080/14680629.2011.9695259

[76] Bhasin, A., Palvadi, S., & Little, D. N. (2011). Influence of aging and temperature on intrinsic healing of asphalt binders. Transportation Research Record, 2207(1), 70-78. https://doi.org/10.3141/2207-10

[77] Luo, X. (2012). Characterization of fatigue cracking and healing of asphalt mixtures (Doctoral dissertation, Texas A&M University).

[78] Ashouri, M. (2014). Modeling Microdamage Healing in Asphalt Pavements Using Continuum Damage Theory (Doctoral dissertation, North Carolina State University).

[79] Shan, L., Tan, Y., & Kim, Y. R. (2013). Establishment of a universal healing evaluation index for asphalt binder. Construction and Building Materials, 48, 74-79. https://doi.org/10.1016/j.conbuildmat.2013.06.039

[80] Tan, Y., Shan, L., Kim, Y. R., & Underwood, B. S. (2012). Healing characteristics of asphalt binder. Construction and Building Materials, 27(1), 570-577. https://doi.org/10.1016/j.conbuildmat.2011.07.006

[81] Stimilli, A., Hintz, C., Li, Z., Velasquez, R., & Bahia, H. U. (2012). Effect of healing on fatigue law parameters of asphalt binders. Transportation Research Record, 2293(1), 96-105. https://doi.org/10.3141/2293-12

[82] Lu, X., Soenen, H., & Redelius, P. (2003, April). Fatigue and healing characteristics of bitumens studied using dynamic shear rheometer. In 6th RILEM Symposium PTEBM (Vol. 3).

[83] Castro, M., & Sánchez, J. A. (2006). Fatigue and healing of asphalt mixtures: discriminate analysis of fatigue curves. Journal of Transportation Engineering, 132(2), 168-174. https://doi.org/10.1061/(ASCE)0733-947X(2006)132:2(168)

[84] Sun, G., Sun, D., Guarin, A., Ma, J., Chen, F., & Ghafooriroozbahany, E. (2019). Low temperature self-healing character of asphalt mixtures under different fatigue damage degrees. Construction and Building Materials, 223, 870-882. https://doi.org/10.1016/j.conbuildmat.2019.07.040

[85] Zhang, L., Liu, Q., Wu, S., Rao, Y., Sun, Y., Xie, J., & Pan, P. (2018). Investigation of the flow and self-healing properties of UV aged asphalt binders. Construction and Building Materials, 174, 401-409. https://doi.org/10.1016/j.conbuildmat.2018.04.109

[86] Qiu, J., Van de Ven, M. F. C., Wu, S. P., Yu, J. Y., & Molenaar, A. A. A. (2011). Investigating self healing behaviour of pure bitumen using dynamic shear rheometer. Fuel, 90(8), 2710-2720. https://doi.org/10.1016/j.fuel.2011.03.016

[87] Tang, J., Liu, Q., Wu, S., Ye, Q., Sun, Y., & Schlangen, E. (2016). Investigation of the optimal self-healing temperatures and healing time of asphalt binders. Construction and Building Materials, 113, 1029-1033. https://doi.org/10.1016/j.conbuildmat.2016.03.145

[88] Sun, G., Hu, M., Sun, D., Deng, Y., Ma, J., & Lu, T. (2020). Temperature induced self-healing capability transition phenomenon of bitumens. Fuel, 263, 116698. https://doi.org/10.1016/j.fuel.2019.116698

[89] Sun, D., Sun, G., Zhu, X., Ye, F., & Xu, J. (2018). Intrinsic temperature sensitive self-healing character of asphalt binders based on molecular dynamics simulations. Fuel, 211, 609-620. https://doi.org/10.1016/j.fuel.2017.09.089

[90] Sun, Y., Wu, S., Liu, Q., Li, B., Fang, H., & Ye, Q. (2016). The healing properties of asphalt mixtures suffered moisture damage. Construction and Building Materials, 127, 418-424. https://doi.org/10.1016/j.conbuildmat.2016.10.048

[91] Riara, M., Tang, P., Mo, L., Hong, W., Chen, M., & Wu, S. (2018). Evaluation of moisture and temperature effect on crack healing of asphalt mortar and mixtures using healing agents. Construction and Building Materials, 177, 388-394. https://doi.org/10.1016/j.conbuildmat.2018.05.020

[92] Caro, S., Masad, E., Bhasin, A., & Little, D. N. (2008). Moisture susceptibility of asphalt mixtures, Part 1: mechanisms. International Journal of Pavement Engineering, 9(2), 81-98. https://doi.org/10.1080/10298430701792128

[93] Mannan, U. A., Ahmad, M., & Tarefder, R. A. (2017). Influence of moisture conditioning on healing of asphalt binders. Construction and Building Materials, 146, 360-369. https://doi.org/10.1016/j.conbuildmat.2017.04.087

[94] Lv, Q., Huang, W., Zhu, X., & Xiao, F. (2017). On the investigation of self-healing behavior of bitumen and its influencing factors. Materials & Design, 117, 7-17. https://doi.org/10.1016/j.matdes.2016.12.072

[95] Hammoum, F., de La Roche, C., Piau, J. M., & Stefani, C. (2002, August). Experimental investigation of fracture and healing of bitumen at pseudo-contact of two aggregates. In 9th international conference on asphalt pavements.

[96] Baglieri, O., Tsantilis, L., & Santagata, E. (2018). Evaluation of healing potential of bituminous binders using a viscoelastic continuum damage approach. Construction

and Building Materials, 184, 344-350. https://doi.org/10.1016/j.conbuildmat.2018.05.228

[97] Pang, L., Jiang, H., Wu, S., & Wu, S. (2012). Self healing capacity of asphalt binders. Journal of Wuhan University of Technology-Mater. Sci. Ed., 27(4), 794-796. https://doi.org/10.1007/s11595-012-0550-z

[98] Baglieri, O., Baaj, H., Canestrari, F., Wang, C., Hammoum, F., Tsantilis, L., & Cardone, F. (2020, December). Testing methods to assess healing potential of bituminous binders. In RILEM International Symposium on Bituminous Materials (pp. 55-62). Springer, Cham. https://doi.org/10.1007/978-3-030-46455-4_7

[99] Safaei, F., Castorena, C., & Kim, Y. R. (2016). Linking asphalt binder fatigue to asphalt mixture fatigue performance using viscoelastic continuum damage modeling. Mechanics of Time-Dependent Materials, 20(3), 299-323. https://doi.org/10.1007/s11043-016-9304-1

[100] Bahia, H. U., Hanson, D. I., Zeng, M., Zhai, H., Khatri, M. A., & Anderson, R. M. (2001). Characterization of modified asphalt binders in superpave mix design (No. Project 9-10 FY'96).

[101] Johnson, C. M. (2010). Estimating asphalt binder fatigue resistance using an accelerated test method (Doctoral dissertation, University of Wisconsin-Madison).

[102] AASHTO, TP 101-12 (2018). Estimating Fatigue Resistance of Asphalt Binders Using the Linear Amplitude Sweep.

[103] Bahia, H. U., Zhai, H., Onnetti, K., & Kose, S. (1999). Non-linear viscoelastic and fatigue properties of asphalt binders. Journal of the Association of Asphalt Paving Technologists, 68. https://trid.trb.org/view/639703

[104] Qiu, X., Cheng, W., Xu, W., Xiao, S., & Yang, Q. (2020). Fatigue evolution characteristic and self-healing behaviour of asphalt binders. International Journal of Pavement Engineering, 1-12. https://doi.org/10.1080/10298436.2020.1806277

[105] de La Roche, C., Hammoum, F., Piau, J., Stéfani, C. (2003). Behavior of a thin film of bitumen at the pseudo-contact between two aggregates. Bulletin des Laboratoires des Ponts et Chaussbees.

[106] Maillard, S., de La Roche, C., Hammoum, F., Such, C., & Piau, J. M. (2004). Bitumen healing investigation using a specific fracture test. Road Materials and Pavement Design, 5(sup1), 45-63. https://doi.org/10.1080/14680629.2004.9689987

[107] Huang P.-T. (2013). Rheological properties and lubrication performance of clay-based drilling fluids for trenchless technologies (Doctoral dissertation, Purdue University).

[108] Macosko, C.W. (1996). Rheology: principles, measurements, and applications. Wiley-VCH.

[109] Speight, J.G. (2014). The chemistry and technology of petroleum, Fifth Edition. CRC Press.

[110] Hunter, R.N., Self, A., Read, J. (2015). The Shell Bitumen handbook, Sixth Edition. Shell Bitumen.

[111] Claine, P. J. (1984). Chemical composition of asphalt as related to asphalt durability: State of the Art. Transp. Res. Rec, 999, 13-30.

[112] Ishai, I., Tuffour, Y. A., & Craus, J. (1993). Some aspects of the effect of asphalt chemical composition on material behavior and pavement performance. Transportation Research Record, (1391). https://trid.trb.org/view/382178

[113] Sultana, S., & Bhasin, A. (2014). Effect of chemical composition on rheology and mechanical properties of asphalt binder. Construction and Building Materials, 72, 293-300. https://doi.org/10.1016/j.conbuildmat.2014.09.022

[114] Saal, R. N. J., & Labout, J. W. A. (1940). Rheological Properties of Asphaltic Bitumen. The Journal of Physical Chemistry, 44(2), 149-165.

[115] Pfeiffer, J. P., & Saal, R. N. J. (1940). Asphaltic bitumen as colloid system. The Journal of Physical Chemistry, 44(2), 139-149.

[116] Corbett, L. W. (1969). Composition of asphalt based on generic fractionation, using solvent deasphaltening, elution-adsorption chromatography, and densimetric characterization. Analytical Chemistry, 41(4), 576-579. https://doi.org/10.1021/ac60273a004

[117] Robertson, R. E., Branthaver, J. F., Plancher, H. E. N. R. Y., Duvall, J. J., Ensley, E. K., Harnsberger, P. M., & Petersen, J. C. (1991). Chemical properties of asphalts and their relationship to pavement performance (No. SHRP-A/UWP-91-510). Washington, DC: Strategic Highway Research Program, National Research Council.

[118] Airey, G. D. (2003). Rheological properties of styrene butadiene styrene polymer modified road bitumens. Fuel, 82(14), 1709-1719. https://doi.org/10.1016/S0016-2361(03)00146-7

[119] Isacsson, U., & Lu, X. (1995). Testing and appraisal of polymer modified road bitumens-state of the art. Materials and Structures, 28(3), 139-159. https://doi.org/10.1007/BF02473221

[120] Adedeji, A., Grünfelder, T., Bates, F. S., Macosko, C. W., Stroup-Gardiner, M., & Newcomb, D. E. (1996). Asphalt modified by SBS triblock copolymer: structures and properties. Polymer Engineering & Science, 36(12), 1707-1723. https://doi.org/10.1002/pen.10567

[121] Dong, F., Zhao, W., Zhang, Y., Wei, J., Fan, W., Yu, Y., & Wang, Z. (2014). Influence of SBS and asphalt on SBS dispersion and the performance of modified asphalt. Construction and Building Materials, 62, 1-7. https://doi.org/10.1016/j.conbuildmat.2014.03.018

[122] Collins, J. H., Bouldin, M. G., Gelles, R., & Berker, A. (1991). Improved performance of paving asphalts by polymer modification (with discussion). Journal of the Association of Asphalt Paving Technologists, 60. https://trid.trb.org/view/486823

[123] Lu, X., & Isacsson, U. (2000). Modification of road bitumens with thermoplastic polymers. Polymer Testing, 20(1), 77-86. https://doi.org/10.1016/S0142-9418(00)00004-0

[124] Elwardany, M. D., Planche, J. P., & Adams, J. J. (2019). Determination of binder glass transition and crossover temperatures using 4-mm plates on a dynamic shear rheometer. Transportation Research Record, 2673(10), 247-260. https://doi.org/10.1177/0361198119849571

[125] Santagata, E., Tozzi, C., Baglieri, O., & Dalmazzo, D. (2020, December). Comparative evaluation of different methods for assessing the glass transition temperature of bituminous binders. In RILEM International Symposium on Bituminous Materials (pp. 405-411). Springer, Cham. https://doi.org/10.1007/978-3-030-46455-4_51

[126] AASHTO, T 312-12 (2012). Determining the rheological properties of asphalt binder using a Dynamic Shear Rheometer (DSR).

[127] Underwood, B. S., & Kim, Y. R. (2015). Nonlinear viscoelastic analysis of asphalt cement and asphalt mastics. International Journal of Pavement Engineering, 16(6), 510-529. https://doi.org/10.1080/10298436.2014.943133

[128] Petersen, J. C., Robertson, R. E., Branthaver, J. F., Harnsberger, P. M., Duvall, J. J., Kim, S. S., ... & Bahia, H. U. (1994). Binder characterization and evaluation: Volume 1. Rep. No. SHRP-A-367, Strategic Highway Research Program, National Research Council, Washington, DC.

[129] Tsantilis, L., Underwood, S. B., Miglietta, F., Riviera, P. P., Baglieri, O., & Santagata, E. (2021). Ageing effects on the linear and nonlinear viscoelasticity of bituminous binders. Road Materials and Pavement Design, 22(sup1), S37-S50. https://doi.org/10.1080/14680629.2021.1908406

[130] Xie, W., Castorena, C., Wang, C., & Kim, Y. R. (2017). A framework to characterize the healing potential of asphalt binder using the linear amplitude sweep test. Construction and Building Materials, 154, 771-779. https://doi.org/10.1016/j.conbuildmat.2017.08.021

[131] Ferry, J.D. (1980). Viscoelastic properties of polymers, Third Edition. Wiley.

[132] Santagata, E., Baglieri, O., Tsantilis, L., Dalmazzo, D., & Chiappinelli, G. (2016). Fatigue and healing properties of bituminous mastics reinforced with nano-sized additives. Mechanics of Time-Dependent Materials, 20(3), 367-387. https://doi.org/10.1007/s11043-016-9301-4

[133] Wang, C., Castorena, C., Zhang, J., & Richard Kim, Y. (2015). Unified failure criterion for asphalt binder under cyclic fatigue loading. Road Materials and Pavement Design, 16(sup2), 125-148. https://doi.org/10.1080/14680629.2015.1077010

[134] Tschegg, E. K., Ritchie, R. O., & McClintock, F. A. (1983). On the influence of rubbing fracture surfaces on fatigue crack propagation in mode III. International Journal of Fatigue, 5(1), 29-35. https://doi.org/10.1016/0142-1123(83)90005-1

[135] Hintz, C., & Bahia, H. (2013). Understanding mechanisms leading to asphalt binder fatigue in the dynamic shear rheometer. Road Materials and Pavement Design, 14(sup2), 231-251. https://doi.org/10.1080/14680629.2013.818818

[136] Santagata, E., Miglietta, F., Baglieri, O., & Tsantilis, L. (2020, December). Effect of temperature on self-healing properties of bituminous binders. In RILEM International Symposium on Bituminous Materials (pp. 623-629). Springer, Cham. https://doi.org/10.1007/978-3-030-46455-4_79

[137] Shen, S., Lu, X., Liu, L., & Zhang, C. (2016). Investigation of the influence of crack width on healing properties of asphalt binders at multi-scale levels. Construction and Building Materials, 126, 197-205. https://doi.org/10.1016/j.conbuildmat.2016.08.107

[138] Miglietta, F., Tsantilis, L., Baglieri, O., & Santagata, E. (2021). A new approach for the evaluation of time-temperature superposition effects on the self-healing of bituminous binders. Construction and Building Materials, 287, 122987. https://doi.org/10.1016/j.conbuildmat.2021.122987

[139] Miglietta, F., Tsantilis, L., Baglieri, O., & Santagata, E. (2021). Investigating the effect of temperature on self-healing properties of neat and polymer-modified bituminous binders. Road Materials and Pavement Design, 1-14. https://doi.org/10.1080/14680629.2021.1982752

[140] Lee, H. J., & Kim, Y. R. (1998). Viscoelastic continuum damage model of asphalt concrete with healing. Journal of Engineering Mechanics, 124(11), 1224-1232. https://doi.org/10.1061/(ASCE)0733-9399(1998)124:11(1224)

[141] Cao, W., Norouzi, A., & Kim, Y. R. (2016). Application of viscoelastic continuum damage approach to predict fatigue performance of Binzhou perpetual pavements. Journal of Traffic and Transportation Engineering (English Edition), 3(2), 104-115. https://doi.org/10.1016/j.jtte.2016.03.002

[142] Kim, R., Chehab, G., Schapery, R., Witczak, M., & Bonaquist, R. (2003). Characterization of asphalt concrete in uniaxial tension using a viscoelastoplastic continuum damage model. Journal of the Association of Asphalt Paving Technologists, 72, 315-355.

[143] Underwood, B. S., Kim, Y. R., & Guddati, M. N. (2010). Improved calculation method of damage parameter in viscoelastic continuum damage model. International Journal of Pavement Engineering, 11(6), 459-476. https://doi.org/10.1080/10298430903398088

[144] Schapery, R. A. (1987). Deformation and fracture characterization of inelastic composite materials using potentials. Polymer Engineering & Science, 27(1), 63-76. https://doi.org/10.1002/pen.760270110

[145] Kim, Y. R., & Little, D. N. (1990). One-dimensional constitutive modeling of asphalt concrete. Journal of Engineering Mechanics, 116(4), 751-772. https://doi.org/10.1061/(ASCE)0733-9399(1990)116:4(751)

[146] Lee, H. J., Daniel, J. S., & Kim, Y. R. (2000). Continuum damage mechanics-based fatigue model of asphalt concrete. Journal of materials in Civil Engineering, 12(2), 105-112. https://doi.org/10.1061/(ASCE)0899-1561(2000)12:2(105)

[147] Kim, Y. R., Lee, Y. C., & Lee, H. J. (1995). Correspondence principle for characterization of asphalt concrete. Journal of Materials in Civil Engineering, 7(1), 59-68. https://doi.org/10.1061/(ASCE)0899-1561(1995)7:1(59)

[148] Chehab, G. R., Kim, Y. R., Schapery, R. A., Witczak, M. W., & Bonaquist, R. (2002). Time-temperature superposition principle for asphalt concrete with growing damage in tension state. Journal of the Association of Asphalt Paving Technologists, 71.

[149] Underwood, B. S., Baek, C., & Kim, Y. R. (2012). Simplified viscoelastic continuum damage model as platform for asphalt concrete fatigue analysis. Transportation research record, 2296(1), 36-45. https://doi.org/10.3141/2296-04

[150] AASHTO, TP 107-14 (2018). Determining the damage characteristic curve of asphalt mixtures from direct tension cyclic fatigue tests.

[151] Wen, H., & Bahia, H. (2009). Characterizing fatigue of asphalt binders with viscoelastic continuum damage mechanics. Transportation Research Record, 2126(1), 55-62. https://doi.org/10.3141/2126-07

[152] Johnson, C., Bahia, H., & Wen, H. (2009). Practical application of viscoelastic continuum damage theory to asphalt binder fatigue characterization. Asphalt Paving Technology-Proceedings, 28, 597.

[153] AASHTO, TP 123-16 (2018). Measuring Asphalt Binder Yield Energy and Elastic Recovery Using the Dynamic Shear Rheometer.

[154] Wang, Y., Wang, C., & Bahia, H. (2017). Comparison of the fatigue failure behaviour for asphalt binder using both cyclic and monotonic loading modes. Construction and Building Materials, 151, 767-774. https://doi.org/10.1016/j.conbuildmat.2017.06.144

[155] Hintz, C., & Bahia, H. (2013). Simplification of linear amplitude sweep test and specification parameter. Transportation Research Record, 2370(1), 10-16. https://trid.trb.org/view/1240744

[156] Safaei, F., & Castorena, C. (2016). Temperature effects of linear amplitude sweep testing and analysis. Transportation Research Record, 2574(1), 92-100. https://doi.org/10.3141/2574-10

[157] Safaei, F., & Hintz, C. (2014, June). Investigation of the effect of temperature on asphalt binder fatigue. In Asphalt Pavements, Proceedings of the International Conference on Asphalt Pavements (Rayleigh) (Vol. 1, No. 2014, pp. 1491-1500). https://doi.org/10.1201/B17219-181

[158] Daniel, J. S., & Kim, Y. R. (2002). Development of a simplified fatigue test and analysis procedure using a viscoelastic, continuum damage model (with discussion). Journal of the Association of Asphalt Paving Technologists, 71.

[159] Schapery, R. A. (1990). A theory of mechanical behavior of elastic media with growing damage and other changes in structure. Journal of the Mechanics and Physics of Solids, 38(2), 215-253. https://doi.org/10.1016/0022-5096(90)90035-3

[160] Park, S. W., Kim, Y. R., & Schapery, R. A. (1996). A viscoelastic continuum damage model and its application to uniaxial behavior of asphalt concrete. Mechanics of Materials, 24(4), 241-255. https://doi.org/10.1016/S0167-6636(96)00042-7

[161] Underwood, B. S., Kim, Y. R., Guddati, M., Pellinen, T., Rongzong, W., King, G., ... & Gibson, N. (2006). Characterization and performance prediction of ALF mixtures using a viscoelastoplastic continuum damage model. In Association of Asphalt Paving Technologists-Proceedings of the Technical Sessions 2006 Annual Meeting (pp. 577-636).

[162] Morland, L. W., & Lee, E. H. (1960). Stress analysis for linear viscoelastic materials with temperature variation. Transactions of the Society of Rheology, 4(1), 233-263. https://doi.org/10.1122/1.548856

[163] Williams, M. L., Landel, R. F., & Ferry, J. D. (1955). The temperature dependence of relaxation mechanisms in amorphous polymers and other glass-forming liquids. Journal of the American Chemical Society, 77(14), 3701-3707. https://doi.org/10.1021/ja01619a008

[164] Palvadi, S., Bhasin, A., & Little, D. N. (2012). Method to quantify healing in asphalt composites by continuum damage approach. Transportation Research Record, 2296(1), 86-96. https://doi.org/10.3141/2296-09

[165] Su, Y., Asadi, H., & Nikraz, H. (2020). VECD investigation and quantification of rest period healing within pulse-rest loading. International Journal of Pavement Engineering, 21(14), 1729-1745. https://doi.org/10.1080/10298436.2019.1566543

[166] Roque, R., Zou, J., Kim, Y. R., Baek, C., Thirunavukkarasu, S., Underwood, B. S., & Guddati, M. N. (2010). Top-down cracking of hot-mix asphalt layers: Models for initiation and propagation (No. NCHRP Project 1-42A). https://doi.org/10.17226/22935

[167] Ashouri, M., Wang, Y., Choi, Y. T., & Kim, Y. (2021). Development of healing model and simplified characterization test procedure for asphalt concrete. Construction and Building Materials, 271, 121515. https://doi.org/10.1016/j.conbuildmat.2020.121515